Open-File Report 82-458

Open-File Report 82-458

UNITED STATES
DEPARTMENT OF THE INTERIOR
GEOLOGICAL SURVEY

DETERMINATION OF THE IN SITU STATE OF STRESS AT THE SPENT FUEL TEST--CLIMAX SITE, CLIMAX STOCK, NEVADA TEST SITE

BY
W. L. Ellis and J. E. Magner

Open-File Report 82-458
1982

Prepared by the U.S. Geological Survey
for the
Nevada Operations Office
U.S. Department of Energy
(Interagency Agreement DE-AI08-76DP00474)

Copies of this Open-file Report
may be purchased from

Open-File Services Section
Branch of Distribution
U.S. Geological Survey
Box 25425, Federal Center
Denver, Colorado 80225

PREPAYMENT IS REQUIRED

Price information will be published
in the monthly listing
"New Publications of the Geological Survey"

FOR ADDITIONAL INFORMATION
CALL: Commercial: (303)234-5888
FTS: 234-5888

CONTENTS

ILLUSTRATIONS

TABLES

DETERMINATION OF THE IN SITU STATE OF STRESS AT THE SPENT FUEL TEST--CLIMAX SITE, CLIMAX STOCK, NEVADA TEST SITE

By

W. L. Ellis and J. E. Magner

ABSTRACT

Determination of the in situ state of stress at the site of the Spent Fuel Test--Climax, using the U.S. Bureau of Mines overcore method, indicates principal stress magnitudes of 11.6 MPa, 7.1 MPa, and 2.8 MPa. The bearing and plunge of the maximum and minimum principal stress components are, respectively: N. 56° E., 29° NE; and N. 42° W., 14° NW. The vertical stress magnitude of 7.9 MPa calculated from the overcore data is significantly less than expected from overburden pressure, suggesting the stress field is influenced by local or areal geologic factors. Results from this investigation indicate (1) the stress state at the Spent Fuel Test--Climax site deviates significantly from a gravitational stress field, both in relative stress magnitudes and in orientation; (2) numerical modeling will not realistically simulate the near-field response of the Spent Fuel Test--Climax site if gravitational and (or) horizontal and vertical applied stress boundary conditions are assumed; and (3) substantial stress variations may occur spatially within the stock.

INTRODUCTION

During March 1979, the U.S. Geological Survey conducted an investigation of the in situ state of stress at the site of the Lawrence Livermore National Laboratory (LLNL) Spent Fuel Test Facility (SFT-C) in the Climax stock at the Nevada Test Site (NTS) (Ramspott and others, 1979). The SFT-C is an LLNL field test to demonstrate the handling, storage, and retrieval of spent reactor fuel in hard crystalline rock, and to assess the thermomechanical response of the rock to heat generated by the waste and auxiliary electrical heaters. The SFT-C site is located at a vertical depth of 418 m within the Climax stock, a granitic intrusive located at the northern end of Yucca Flat at the NTS (fig. 1).

The investigation consisted of a determination of the complete three-dimensional stress field and a determination of a secondary principal stress profile for a distance of about 1.4 drift diameters into the left rib of the south heater drift (fig. 2). Field data for determining the complete state of stress and the secondary principal stress profile were obtained using the U.S. Bureau of Mines (USBM) overcore method (Hooker and Bickel, 1974). The elastic moduli of the overcore samples, used for converting borehole-deformation data to stress values, were determined with a biaxial pressure chamber and the three-component borehole deformation gage (Fitzpatrick, 1962).

This study was initiated at the request of LLNL, which provided for drilling and logistical support. Mr. Lynn Parish of Fenix & Scisson, Inc., assisted with the collection of field data and Mr. Dale Wilder of LLNL provided geologic information pertinent to the investigation.

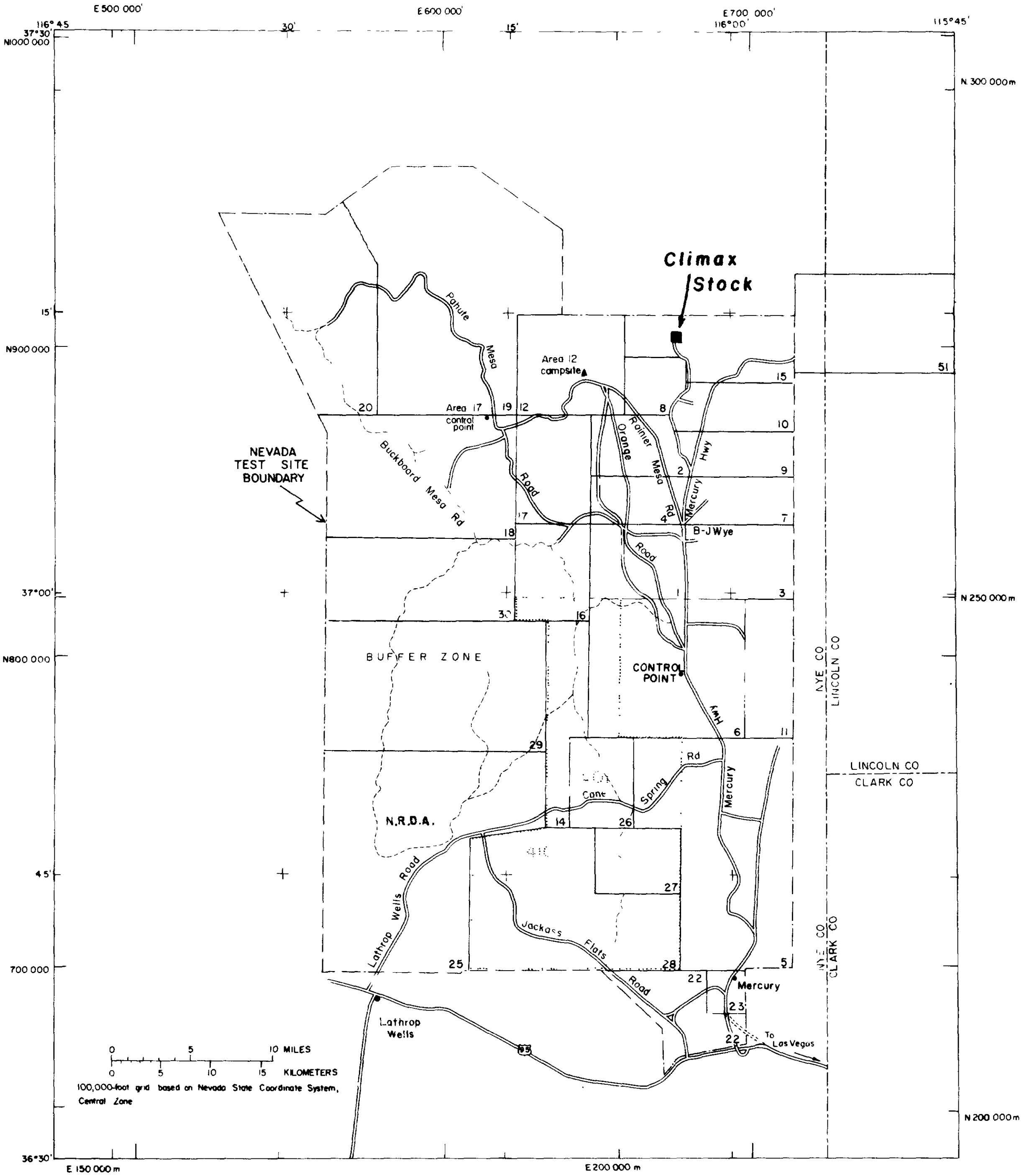

Figure 1.--Index map of Nevada Test Site showing location of Climax stock.

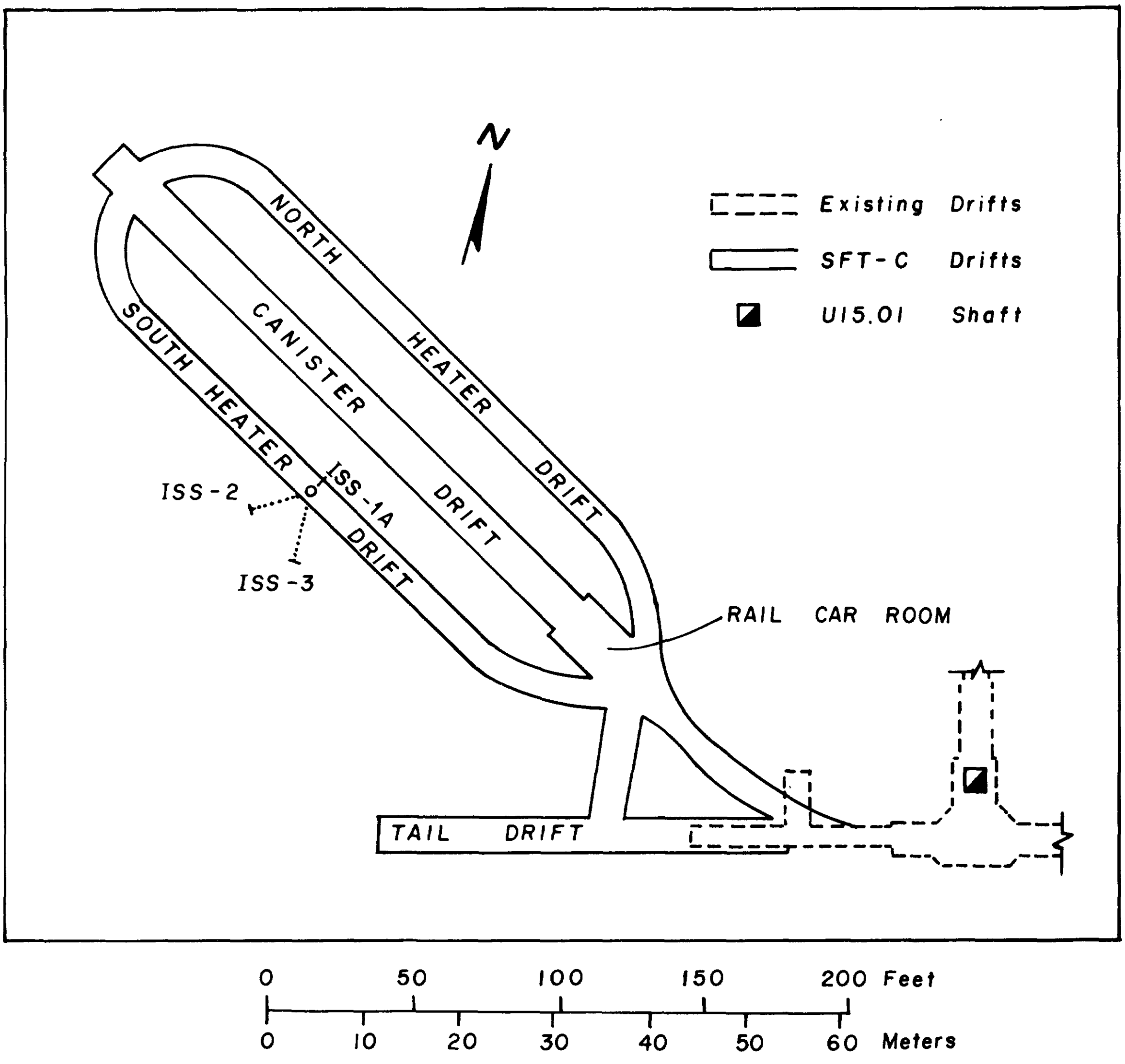

Figure 2.--SFT-C workings showing location of overcore stress determination (ISS) drill holes. Mining of upper heading of Canister drift was in progress during time period of overcore measurements.

GEOLOGY

The Climax stock is a composite stock composed of quartz monzonite and granodiorite of Cretaceous age which intrudes sedimentary rocks of Paleozoic and Precambrian age. The stock and sedimentary rocks are overlain by Tertiary rocks consisting of tuff, welded tuff, and breccia. The stock has a surface exposure of approximately 2.4 km in the north-south direction and 1.6 km in the east-west direction. The geology of the Climax stock area is shown on figure 3. A comprehensive summary of the geology and physical properties of the Climax stock has been presented by Maldonado (1977).

STRESS INVESTIGATION SITE

Location

The SFT-C workings are located approximately 50 m northwest of the Area 15 (U15.01) shaft at a vertical depth of 418 m below the surface (fig. 4). Two tunnel complexes associated with underground nuclear tests, the Pile Driver and Hard Hat complexes, have been driven in the stock and are also shown on figure 4. The SFT-C and Pile Driver tunnels are at the same level in the stock; the Hard Hat tunnel is at a depth of about 260 m below the surface. Access to the SFT-C workings and the Pile Driver/Hard Hat tunnels is through the Area 15 (U15.01) shaft, sometimes referred to as the Pile Driver shaft (fig. 3).

The location of the stress determination site in the SFT-C workings is approximately midway along the south heater drift. Overcoring borehole deformation data were obtained in drill holes ISS-1A, 2, and 3 (fig. 2). The secondary principal stress profile was obtained in the ISS-2 hole. Specific information concerning these overcore drill holes is listed in table 1. At the time the field measurements were made, only the north and south heater drifts had been completely mined. During the overcoring measurements, mining of the upper heading of the canister drift proceeded from a point near the rail car room (fig. 2) to a point approximately 13 m past the stress-determination site.

Local Geology

The SFT-C workings are located entirely in the quartz monzonite of the stock. Maldonado (1977) summarized data by W. L. Emerick (USGS, unpub. data, 1966) on fault and joint occurrences in the Pile Driver tunnel. Four dominant fault systems occur in the quartz monzonite. In order of occurrence these are: N. 46° W., 78° NE dip; N. 50° W., 82° SW dip; N. 49° W., 90° dip; and N. 44° E., 68° SE dip. Three definite sets of joints were found by Emerick in the Pile Driver tunnel and summarized by Maldonado as follows:

Table 1.--Orientation and depth of overcore drill holes in south heater drift, SFT-C

Hole designation	Bearing	Inclination	Total depth
SFT-C ISS-1A	N. 29° E.	76.5° below horizontal	6.1 m
SFT-C ISS-2	S. 59° W.	3° above horizontal	5.5 m
SFT-C ISS-3	S. 01° E.	3° above horizontal	7.5 m

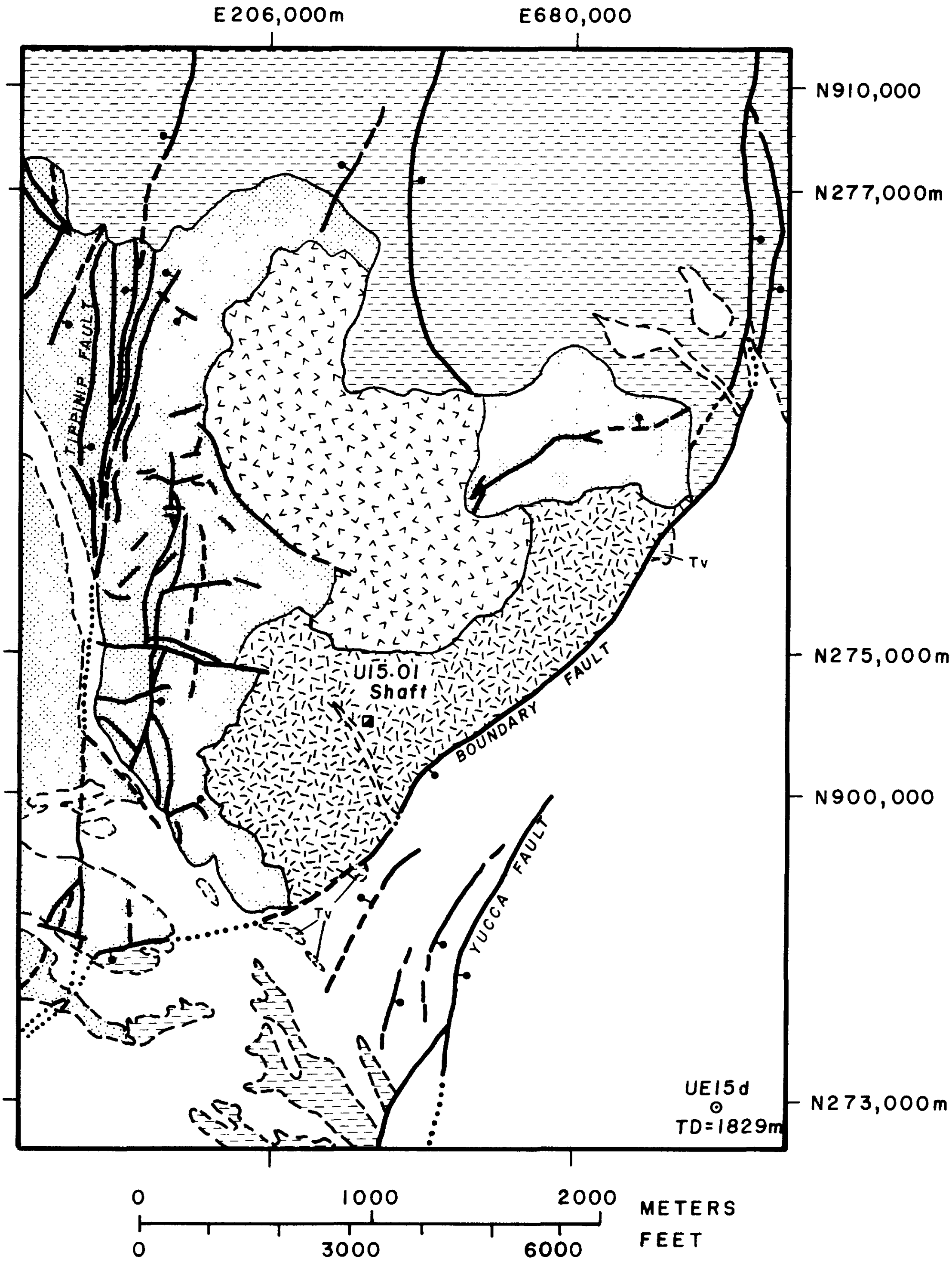

Figure 3.--Geologic map of Climax stock. (Modified from Barnes and others, 1963.)

EXPLANATION

Qal	ALLUVIUM (QUATERNARY)
Tv	VOLCANIC TUFF, UNDIFFERENTIATED (TERTIARY)
Kqm	QUARTZ MONZONITE, CLIMAX STOCK (CRETACEOUS)
Kgd	GRANODIORITE, CLIMAX STOCK (CRETACEOUS)
Pz	LIMESTONE, DOLOMITE, SHALE, AND QUARTZITE, UNDIVIDED (PALEOZOIC)

CONTACT -- *Dashed where approximately located*

FAULT -- *Dashed where approximately located. Dotted where concealed. Bar and ball on downthrown side*

U15.01 — SHAFT

UE15d, TD=1829m — DRILL HOLE -- *Showing total depth in meters*

Figure 3.--Continued

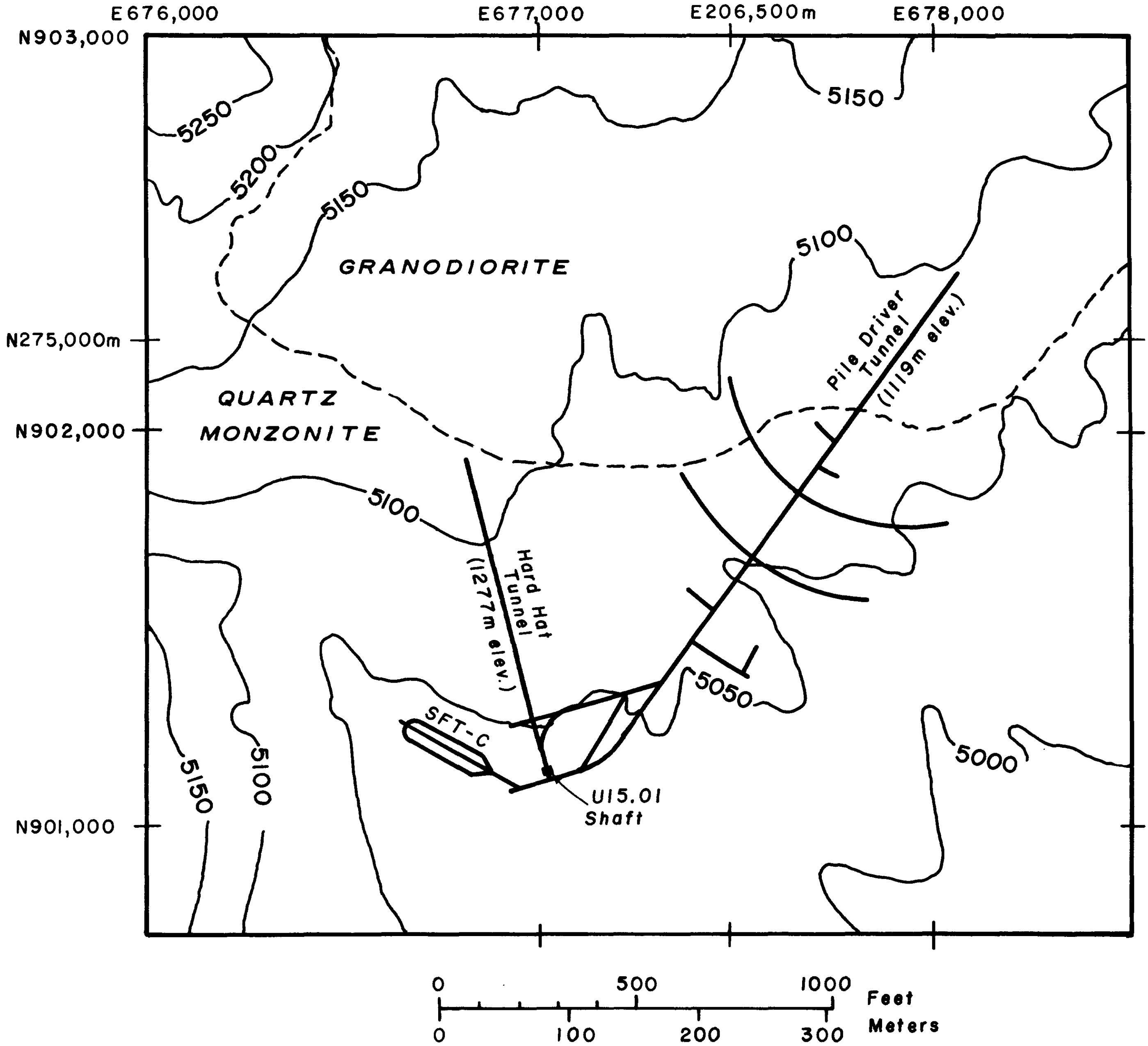

Figure 4.--Map of Climax stock area showing SFT-C, Pile Driver, and Hard Hat tunnels (topographic contours in feet, dashed line is contact between quartz monzonite and granodiorite).

1. Most prominent: from N. 30° W. to N. 75° W., with greatest concentration from N. 30° W. to N. 45° W.

2. Less prominent: striking northeast and dipping 45°-80° SE.

3. Least prominent: due north or due west and dipping 15°-40° NE.

As reported by Maldonado, Emerick concluded that the difference in rock composition between quartz monzonite and granodiorite had little effect on the orientation and density of the observed joints.

A major normal fault intersects the Area 15 shaft at the Pile Driver tunnel level, and at closest approach is approximately 75 m southeast of the stress determination site. At this location the fault has a N. 20° E. trend and dips about 65° SE. The southeast (hanging wall) side of the fault is downthrown relative to the northeast (footwall) side, which contains the SFT-C workings. No estimate is given for the displacement across the fault. Whether or not the fault has any significance with respect to stress distribution in the vicinity of the SFT-C is not known.

LLNL personnel mapped and reported the major geologic features found in the SFT-C workings (Carlson and others, 1980). These features, shown on figure 5, consist of two faults and several major joints or discontinuties. Carlson and others (1980) described some of these discontinuities as zones containing crushed mineral grains and altered feldspars, with a few containing clay layers about 1-3 mm thick. The most significant feature is the fault located at the receiving room end of the cannister drift, described as "a zone approximately 1.8 m wide, consisting of about 1.5 m of intensely fractured rock and a 0.3 m thickness of clay gouge" (Carlson and others, 1980). The zone strikes N. 45° E. and dips 65°-70° SE. No estimate of relative displacement is available.

Carlson and others do not specifically address joint sets in the actual SFT-C workings, although, they do report results of joint mapping in the tail drift. Two dominant sets of joints were observed. One set, consisting of low-angle joints (<45° dip) strikes about N. 45° W. with northeasterly dips. The other set consists of high-angle joints (>45° dip) striking N. 30° E.-N. 50° E. and dipping to the southeast. These two joint sets seem to be generally consistent with the two most prominent joint sets reported by Maldonado (1977) for the Pile Driver tunnel.

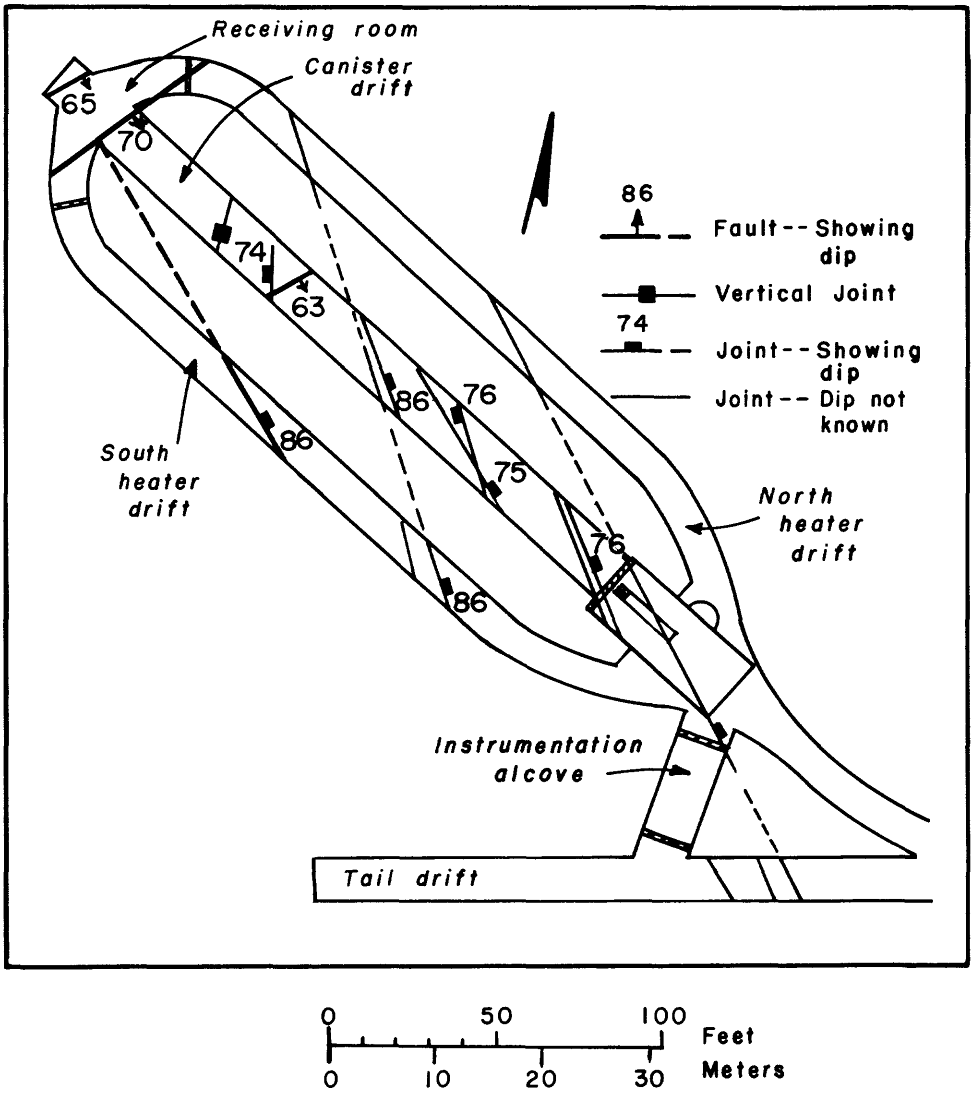

Figure 5.--Major geologic features mapped in SFT-C workings. (Modified from Carlson and others, 1980.)

INSTRUMENTATION AND METHOD

USBM Overcore Method

The USBM overcore method of stress determination has been previously described (Hooker and Bickel, 1974; Hooker and others, 1974) and will not be discussed in detail. Briefly, the method consists of emplacing a three-component borehole deformation gage in a 3.8-cm diameter pilot hole. The pilot hole containing the gage is then overcored using a 15-cm diameter core barrel. The overcoring process relieves the applied stress on the rock, resulting in a deformation of the pilot hole. The borehole-deformation gage measures the deformation of the pilot hole across three diameters spaced 60° apart. The deformations of the borehole are continually monitored during the overcoring process such that a plot of borehole deformation versus overcore depth (position of cutting edge of overcore barrel with respect to gage) can be obtained (app. A). The diametral deformations, designated U_1, U_2, and U_3, along with the elastic modulus (app. B) and Poisson's ratio of the rock, are used to calculate the secondary principal stresses normal to the axis of the borehole, assuming either plane stress or plane strain conditions. In determination of the three-dimensional state of stress, overcoring measurements are made in three noncoplanar drill holes, in which case the assumption of plane stress or plane strain is not necessary in the stress calculations (Panek, 1966).

Biaxial Tests

The elastic moduli of the overcore samples are determined by use of a biaxial pressure chamber and the three-component borehole deformation gage (Fitzpatrick, 1962). In this procedure, the overcore sample is emplaced in the biaxial pressure cell and subjected to a uniform radial pressure. The corresponding deformations of the 3.8-cm-diameter pilot hole are then measured using the three-component borehole-deformation gage. The pressure-deformation relationship is then used to calculate the elastic modulus of the overcore samples using equations for a thick-walled cylinder.

In conducting a biaxial test for overcoring data, the sample is first subjected to some predetermined radial pressure and the borehole deformation recorded. The pressure is then released in increments back to zero pressure, and the borehole deformations recorded for each pressure increment. The data are then used to construct a plot of borehole deformation versus radial pressure during the unloading cycle (app. B). The elastic modulus used in the stress calculations is the secant modulus from the loaded to the unloaded state, because this modulus best represents the conditions present during the in situ overcoring process. Because three diameters are recorded during the tests, three elastic modulus values are calculated. If the rock is not significantly anisotropic, then the three modulus values are averaged for use in the stress calculations. If the rock is significantly anisotropic, more sophisticated testing procedures are required to properly adjust for the anisotropy (Becker and Hooker, 1967).

For this work the majority of overcore samples were subjected to radial pressures of 6.9 MPa, with a few samples tested to 10.3 MPa. The elastic moduli used in the calculations were determined from the 6.9 MPa unloading cycle. Tests indicated the samples to be essentially linearly elastic in the pressure ranges tested, and no significant anisotropy was observed in any of the overcore samples.

The largest ratio of elastic modulus anisotropy (Emaximum/Eminimum normal to the axis of the overcore) for any of the overcores tested was 1.36, as calculated from the three diametral deformations recorded during the biaxial tests. For most of the overcore samples tested, this ratio was less than 1.20. Using equations presented by Becker and Hooker (1967) for an orthotropic solid, the error due to neglecting this minor degree of anisotropy can be estimated. For an anisotropic ratio of 1.4 and secondary principal stress ratios (maximum/minimum) between 1.5 and 5, the greatest error in stress magnitude would be about 12 percent, and the greatest error in orientation would be about 10°. The maximum magnitude error occurs for the special case when the maximum secondary principal stress is coincident with the minimum elastic modulus axis, and the greatest orientation error occurs when the maximum principal stress is at 45° to the elastic axes. For all other alinements the error is less. It is estimated that for the SFT-C the error due to ignoring anisotropy is less than 10 percent in stress magnitude and less than 5° in orientation. Isotropic conditions were therefore assumed in the data analysis.

Borehole-Deformation Gage Calibrations

The borehole deformation gage is calibrated by first securing the gage in a calibration device. Two micrometers, with resolution of 2.54 µm (0.0001 in.) are then used to displace each pair of diametral sensors by a known amount. The ratio of measured displacement to gage readout provides the calibration factor for each pair of diametral sensors. The gage is calibrated between 0 and 813 µm (0.032 in.) displacement for each diametral component; however, the calibration factor is determined for the range 203 µm (0.008 in.) to 813 µm (0.032 in.) deformation. This is the working range of the gage and eliminates the unwanted effects of O-ring friction on the sensing elements at small displacement.

The borehole deformation gage used in this work was calibrated prior to field measurements and again immediately after completion of the field measurements. The first calibration yielded calibration factors of 0.84, 0.87, and 0.85 for the U_1, U_2, U_3 components, respectively. The second calibration indicated no change in the U_1 and U_3 calibration factors, and only a 3 percent decrease in the U_2 calibration factor.

FIELD MEASUREMENTS AND RESULTS

A total of 18 overcoring measurements were obtained in the three overcore holes; 4 in hole ISS-1A, 3 in hole ISS-3, and 11 in hole ISS-2. Hole ISS-2 was also used to obtain the secondary principal stress profile. Data from 15 of the overcore measurements were used in the stress calculations (app. A). Biaxial tests for elastic modulus determination (app. B) were made on 17 of the overcore samples (overcore No. 4 from the ISS-3 hole was not recovered). The drill-hole number, drill-hole depth, elastic modulus, and borehole deformations for each overcore used in stress calculations are listed in table 2. The borehole-deformation plots for each overcore are included in appendix A and the plots of borehole deformation versus radial pressure from the biaxial tests are given in appendix B.

The borehole-deformation plots shown in appendix A represent the data as recorded in the field. Some of the plots show offsets caused by "settling in" of the gage shortly after commencement of the overcore drilling, or occasionally a spurious reading caused by some disturbance of the gage during the overcoring operation. These factors have been corrected for the final borehole deformations listed in table 2.

Three-Dimensional Stress Determination

Data from the two deepest overcores from each drill hole were used to calculate the complete three-dimensional state of stress. Because these overcores were farthest from the drift opening (greater than one drift diameter), calculated stresses should be representative of the free-field stress conditions. The six overcores provided 18 borehole-deformation measurements which, along with the elastic moduli values, were used to calculate the complete state of stress using a computer program developed by the USBM. A Poisson's ratio of 0.20 was assumed in the calculations.

The computer program treats the input data statistically to yield the least-squares estimates of the stress components and their standard deviations. Results of the calculations are shown in table 3. Figure 6 is a graphical representation of the principal stress components S_1, S_2, and S_3 of table 3. Note that the calculated standard deviations of the principal stress components (table 3) indicate a good statistical fit of the field data, implying that the overcores used in the calculations were obtained in a reasonably uniform stress field.

The northeast-southwest orientation of the maximum principal stress and the northwest-southeast orientation of the minimum principal stress is generally consistent with the stress pattern observed in Rainier Mesa at the NTS (Ellis and Magner, 1980) and with estimates of the regional stress orientation based on geologic and geophysical evidence (Carr, 1974). An obvious feature of the principal stress ellipsoid is its significant deviation from a vertical and horizontal alinement, which is also a common characteristic of stresses determined in Rainier Mesa (Ellis and Magner, 1980). The state of stress determined in the south heater drift, therefore, appears to be generally consistent with the regional stress pattern of the NTS area.

An unusual aspect of the stress field is the apparently low vertical stress magnitude of 7.9 MPa (σ_z in table 3). Given a representative density of 2.65 Mg/m^3 for the granite of the Climax Stock (Maldonado, 1977), the 418 m of overburden would be expected to produce a vertical stress of 10.9 MPa under normal gravity loading. The determined vertical stress magnitude is therefore about 28 percent lower than expected. Considering the excellent quality of the borehole-deformation data and the essentially linear-elastic and isotropic behavior of the granite overcores, this discrepancy is too large to be attributed entirely to measurement uncertainties. Based on the data gathered in this investigation there is no readily apparent explanation for the reduced vertical stress. It may, however, be an indication that geologic factors, possibly including residual stress effects from the cooling history of the stock, are influencing the distribution of stress in the vicinity of the SFT-C.

Table 2.--Hole depth, elastic modulus, and borehole deformations for 15 overcores used in stress calculations

Overcore drill-hole no.	Overcore no.	Hole depth (m)	Elastic modulus (GPa)	Borehole deformations[1] (mircoinch) Component U_1	U_2	U_3	U_1 Orientation
SFT-C ISS-1A	[2]3	5.5	69.0	376	-6	406	Normal to drift centerline.
	[2]4	6.9	74.5	463	-110	310	
SFT-C ISS-2	1	1.5	71.7	541	64	160	Vertical
	2	1.9	75.8	339	70	105	
	3	2.3	76.5	326	12	214	
	4	2.7	76.5	331	93	217	
	5	3.1	79.3	324	85	190	
	6	3.4	77.9	468	78	215	
	7	3.8	79.3	528	-68	325	
	8	4.2	77.9	457	-46	307	
	9	4.6	80.7	431	-185	348	
	[2]10	5.0	80.7	337	55	200	
	[2]11	5.3	80.0	351	80	191	
SFT-C ISS-3	[2]3	6.9	82.7	253	92	355	
	[2]4	7.3	[3]77.0	299	61	365	

[1]Positive indicates borehole expansion, negative indicates borehole contraction. 1 microinch equals 2.54×10^{-2} micrometer.

[2]Denotes overcores used in three-dimensional stress calculations.

[3]Core not recovered. Elastic modulus value is average of 17 overcore samples.

Table 3.--State of stress determined in south heater drift, SFT-C

[---, not applicable]

	Stress magnitude	Standard deviation	Bearing	Inclination
	MPa	MPa		+ degrees above horizontal - degrees below horizontal
Principal stresses				
	(+, compression)			
S_1 (maximum)	+11.56	±1.05	N. 56° E.	-29°
S_2 (intermediate)	+7.13	±0.81	N. 26° E.	+57°
S_3 (minimum)	+2.75	±0.65	N. 42° W.	-14°
Normal stress components in X, Y, Z (east, north, vertical) coordinate system				
	(+, compression)			
σ_x	+7.64	±0.63	East	Horizontal
σ_y	+5.87	±0.81	North	Horizontal
σ_z	+7.92	±0.67	---	Vertical
Shear stress components in X, Y, Z coordinate system[1]				
τ_{xy}	+3.61	±0.50	---	---
τ_{yz}	-0.28	±0.72	---	---
τ_{zx}	-2.24	±0.54	---	---

[1]Positive or negative sign on shear stress magnitude indicates direction of shear stress with respect to X, Y, Z coordinate system.

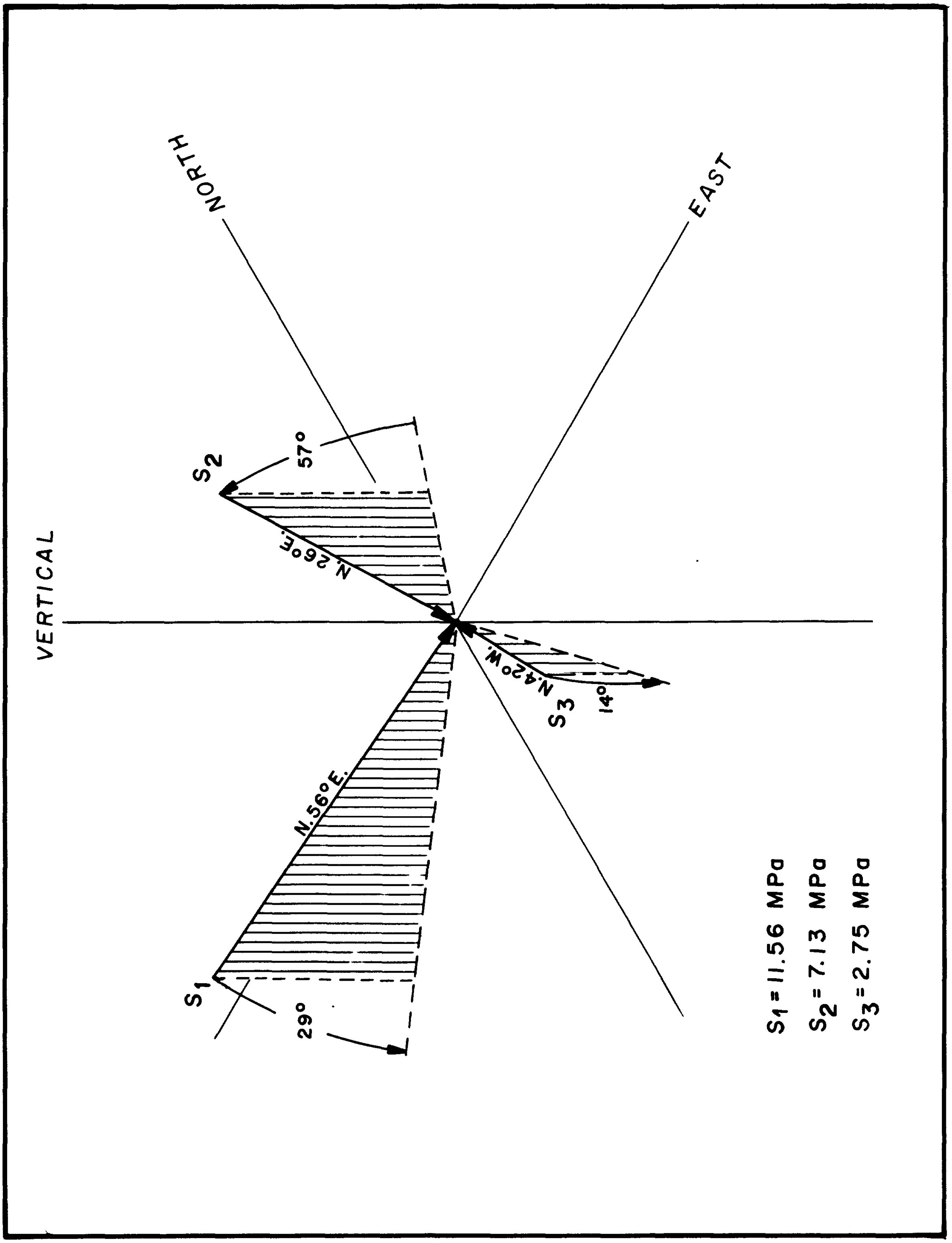

Figure 6.--Graphical representation of principal stresses, SFT-C.

Secondary Principal Stress Profile

A profile of secondary principal stress versus drill-hole depth was obtained in hole ISS-2 penetrating the left rib of the south heater drift (fig. 2). Eleven overcore measurements were made on approximately 0.38-m intervals between drill-hole depths of 1.52 and 5.33 m. This drill-hole interval corresponds to depths of 1.32 to 4.62 m into the rib normal to the drift centerline. Cross-sectional dimensions of the south heater drift are approximately 3.4 by 3.4 m.

The secondary principal stresses calculated from these overcore measurements, assuming plane strain conditions (axial strain = o) are listed in table 4 along with the average elastic modulus of each overcore sample. Figure 7 is a plot of the secondary principal stresses versus drill-hole depth, with a graphical representation of the secondary principal stress components as viewed by looking down the axis of the drill hole.

Given the vertical stress magnitude of 7.9 MPa from the stress ellipsoid calculations, figure 7 indicates the presence of two zones of stress concentration (vertical, or near-vertical component) along the length of the ISS-2 hole. One, located near the rib, is inferred from overcore number 1 (table 4) at 1.52-m hole depth. The other zone of stress concentration occurs between hole depths of about 3.0 and 5.0 m, as indicated by overcores 6-9 (table 4).

The stress distribution observed along the length of the ISS-2 hole is not consistent with expectations based on elastic theory and the assumption of a gravitational stress field. In this specialized case, the maximum vertical stress concentration would occur near the rib and decrease to approximately the free-field vertical stress at a distance of about one drift diameter into the rib. The fact that the stress distribution observed along the ISS-2 drill hole does not behave in this manner is not surprising, considering that the rock is not a perfectly homogeneous material, the in situ principal stresses are not predominantly gravitational, and the alinement of the principal stresses are asymmetrical to the cross-sectional shape of the drift. It is not uncommon in jointed rock for secondary principal stress magnitudes to vary considerably from point to point, although their directions remain quite constant (Obert and Duvall, 1967, p. 477). The presence of the northwest-striking discontinuities, especially the one near the stress determination site (fig. 5), may also exert some influence on the stress distribution.

DISCUSSION OF RESULTS

The state of stress determined at the SFT-C site is generally consistent with the pattern of stress observed in nearby Rainier Mesa and inferred for the NTS area. This pattern is characterized by a relatively high, northeast-southwest bearing principal stress component and a northwest-southeast alinement of the minimum principal stress. An unusual feature of the stress field at the SFT-C is the anomalously low vertical stress magnitude.

Based on this one stress determination, the uniformity of the stress field in the vicinity of the SFT-C workings cannot be verified. Because the area is relatively small, however, it is probably reasonable to assume that the stress field determined in the south heater drift is representative of the

Table 4.--Secondary principal stresses determined in SFT-C ISS-2 drill hole

Overcore no.	Depth in drill hole (m)	Elastic modulus GPA	Secondary principal stress Maximum MPa	Secondary principal stress Minimum MPa	Orientation of maximum[1] Degrees clockwise from vertical
1	1.52	71.7	9.98	2.72	5°
2	1.86	75.8	6.74	2.29	3°
3	2.29	76.5	7.33	2.47	20°
4	2.68	76.5	7.50	3.85	16°
5	3.05	79.3	7.40	3.59	13°
6	3.44	77.9	9.95	3.77	10°
7	3.81	79.3	12.02	2.39	20°
8	4.21	77.9	10.51	2.44	22°
9	4.63	80.7	10.95	0.14	26°
10	5.00	80.7	7.80	3.25	15°
11	5.33	80.0	7.94	3.57	12°

[1]As viewed looking into collar of drill hole.

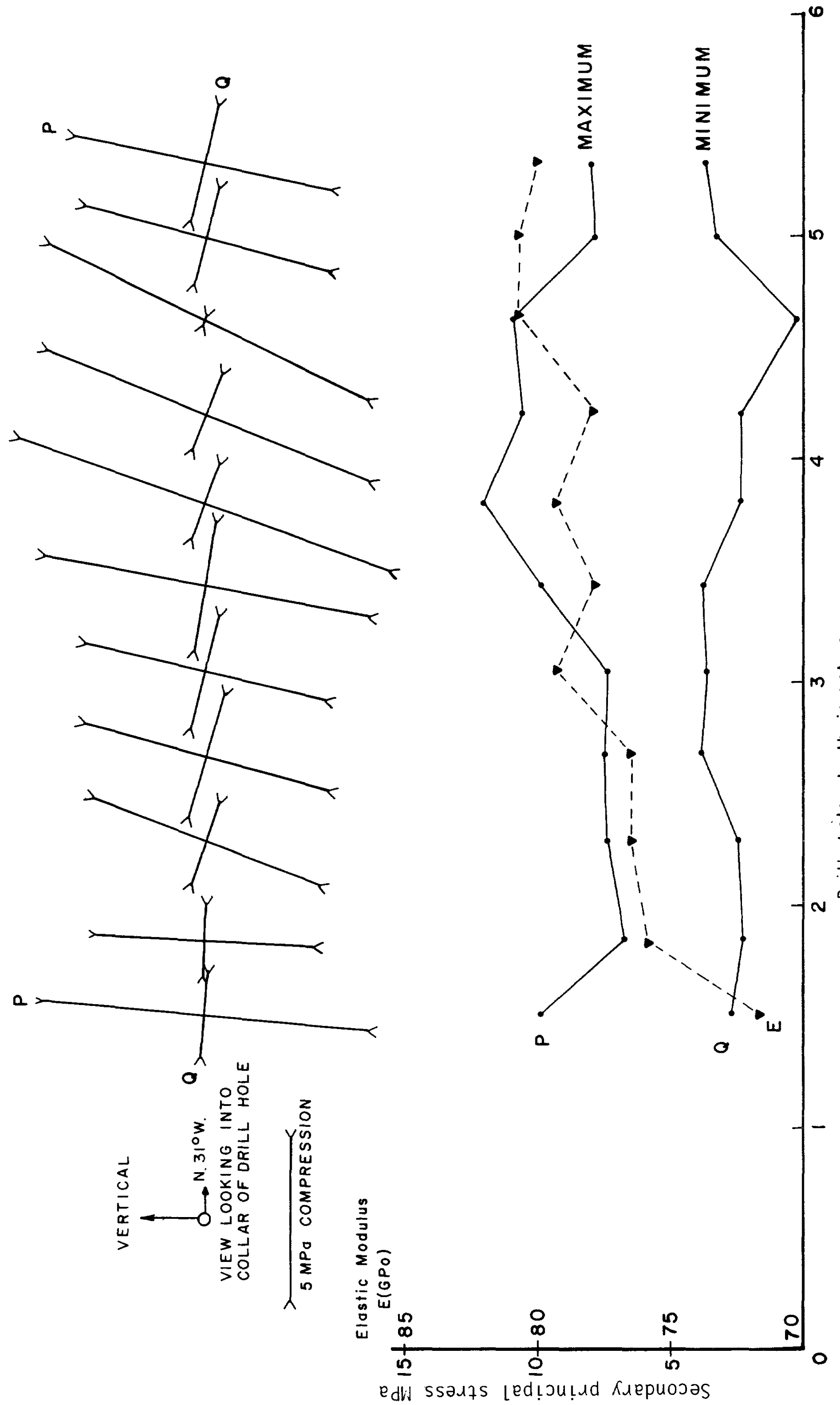

Figure 7.--Graph showing secondary principal stress versus drill-hole depth, ISS-2 drill hole.

entire SFT-C area, although localized variations in the stress field may occur near more significant geologic structure, such as the fault zone crossing the receiving room end of the canister drift (fig. 5). The zone of influence of such geologic structure is, however, uncertain. Because the stress field differs significantly from a simple gravitional field, numerical modeling of the SFT-C for mining and thermomechanical response should incorporate stress boundary conditions closely approximating those determined in situ. The high horizontal component of stress normal to the drifts, and more significantly the nonvertical and nonhorizontal alinement of the stress ellipsoid, will result in a distribution of stress, strain, and displacement in the vicinity of the mined drifts different than what would occur under horizontal and vertical applied stresses. Also, the orientation of the principal stresses may be especially significant with regard to the deformational response of geologic discontinuities within the zone of influence of the SFT-C workings. Numerical models, in which some variation of gravitational loading is assumed (i.e., vertical and horizontal principal stresses) will not realistically simulate the mechanical and thermomechanical response of the rock mass surrounding the SFT-C test.

The anomalously low vertical stress magnitude determined at the SFT-C suggests some geologic influence on stress distribution in the area. This influence could be localized, owing to geologic structure such as the fault through the canister receiving room (fig. 5) or the major discontinuities mapped in the SFT-C workings. The possibility also exists that larger areal stress variations may occur within the stock. Such a possibility is suggested by a comparison of the SFT-C stresses to data collected during an earlier stress investigation in the Hard Hat tunnel (Obert, 1963).

Obert reported the results of stress determinations conducted in the Hard Hat tunnel, which is portaled from the Area 15 shaft at a depth of approximately 260 m (fig. 4). Obert's results were reported as secondary principal stresses and as such did not define the complete state of stress. For one location near the Area 15 shaft, however, the authors have utilized the borehole deformation and elastic moduli data reported by Obert to calculate the complete stress state using the USBM computer program. Results of these calculations are shown in table 5.

Comparison of table 5 with table 3 (the SFT-C stress state) indicates that Obert's data yields somewhat higher magnitudes for the principal stress components, although their relative ratios are very similar. The major difference between the two stress states is in the orientation of the maximum stress component which, at the SFT-C bears northeast-southwest and plunges to the northeast, and at the Hard Hat site bears northwest-southeast and plunges to the southeast. Also, at the Hard Hat site the vertical stress magnitude of 10.8 MPa (σ_z in table 5) is about 1.6 times greater than expected for the 260 m of overburden. As noted earlier, the vertical stress magnitude at the deeper SFT-C site is approximately 28 percent less than expected for overburden.

Whether or not these apparent differences in stress states between the two locations in the stock is an indication of relatively large scale stress variations is uncertain. Certainly, local geologic factors at each site could have contributed to the differences. Also, it is unknown what effects the Hard Hat nuclear test may have had on Obert's data, and similarly, what effect

Table 5.--State of stress calculated for site in Hard Hat tunnel using borehole deformation data of Obert (1963)

	Stress magnitude	Standard deviation	Bearing	Inclination
	MPa	MPa		+ degrees above horizontal - degrees below horizontal
Principal stresses				
	(+, compression)			
S_1 (maximum)	+13.92	±0.77	N. 36° W.	+55°
S_2 (intermediate)	+9.07	±0.74	N. 59° E.	+4°
S_3 (minimum)	+4.28	±0.80	N. 28° W.	-35°
Normal stress components in X, Y, Z (east, north, vertical) coordinate system				
	(+, compression)			
σ_x	+8.89	±0.76	East	Horizontal
σ_y	+7.60	±0.76	North	Horizontal
σ_z	+10.78	±0.68	---	Vertical
Shear stress components in X, Y, Z coordinate system[1]				
τ_{xy}	+0.60	±0.44	---	---
τ_{yz}	+3.81	±0.56	---	---
τ_{zx}	-2.41	±0.56	---	---

[1]Positive or negative sign on shear stress magnitude indicates direction of shear stress with respect to X, Y, Z coordinate system.

both the Hard Hat and Pile Driver nuclear tests may have had on stress distribution in the vicinity of the SFT-C. Nonetheless, the possibility exists that relatively large scale stress variation, induced by such factors as history of cooling and crystallization, may exist within the stock. Because significant stress variations within a granitic intrusive could have important implications with respect to nuclear repository siting and design, the question of the origin of the apparent stress variations in the Climax stock is one that warrants further investigation.

REFERENCES CITED

Barnes, Harley, Houser, F. N., and Poole, F. G., 1963, Geologic map of the Oak Spring quadrangle, Nye County, Nevada: U.S. Geological Survey Geologic Quadrangle Map GQ-214, scale 1:24,000.

Becker, R. M., and Hooker, V. E., 1967, Some anisotropic considerations in rock stress determinations: U.S. Bureau of Mines Report of Investigations 6965, 23 p.

Carlson, R. C., and others, 1980, Spent Fuel Test--Climax: technical measurements interim report, FY 1980: Lawrence Livermore National Laboratory report UCRL-53064, 103 p.

Carr, W. J., 1974, Summary of tectonic and structural evidence for stress orientation at the Nevada Test Site: U.S. Geological Survey Open-File Report 74-176, 53 p.

Ellis, W. L., and Magner, J. E., 1980, Compilation of results of three-dimensional stress determinations made in Rainier and Aqueduct Mesas, Nevada Test Site, Nevada: U.S. Geological Survey Open-File Report 80-1098, 27 p.

Fitzpatrick, John, 1962, Biaxial device for determining the modulus of elasticity of stress-relief cores: U.S. Bureau of Mines Report of Investigations 6128, 13 p.

Hooker, V. E., and Bickel, D. L., 1974, Overcoring equipment and techniques used in rock stress determination: U.S. Bureau of Mines Information Circular 8618, 32 p.

Hooker, V. E., Aggson, J. R., and Bickel, D. L., 1974, Improvements in the three-component borehole deformation gage and overcoring techniques, with appendix on Stress relief by center hole, by W. I. Duvall: U.S. Bureau of Mines Report of Investigations 7894, 29 p.

Maldonado, Florian, 1977, Summary of the geology and physical properties of the Climax stock, Nevada Test Site: U.S. Geological Survey Open-File Report 77-356, 25 p.

Obert, Leonard, 1963, Operation Nougat, shot Hard Hat, project officers report--project 3.6, static stress determinations: Defense Atomic Support Agency, POR-1804, 69 p.

Obert, Leonard, and Duvall, W. I., 1967, Rock mechanics and the design of structures in rock: New York, John Wiley & Sons, Inc., 650 p.

Panek, L. A., 1966, Calculation of the average ground stress components from measurements of the diametral deformation of a drill hole: U.S. Bureau of Mines Report of Investigations 6732, 41 p.

Ramspott, L. D., and others, 1979, Technical concept for a test of geologic storage of spent reactor fuel in the Climax Granite, Nevada Test Site: Lawrence Livermore National Laboratory report UCRL-52796, 47 p.

APPENDIX A
Borehole Deformation Plots

Computer plots of borehole deformation versus overcore depth (relative to start of overcore) for 15 overcores used in the SFT-C stress calculations are shown. Each plot is identified by location (U15SFT-C), hole number (ISS), overcore number (OC), and component of deformation (U_1, U_2, U_3). Units are given in inches for overcore depth and microinches for deformation.

1 inch=2.54 cm
1 microinch=2.54×10^{-2} micrometers

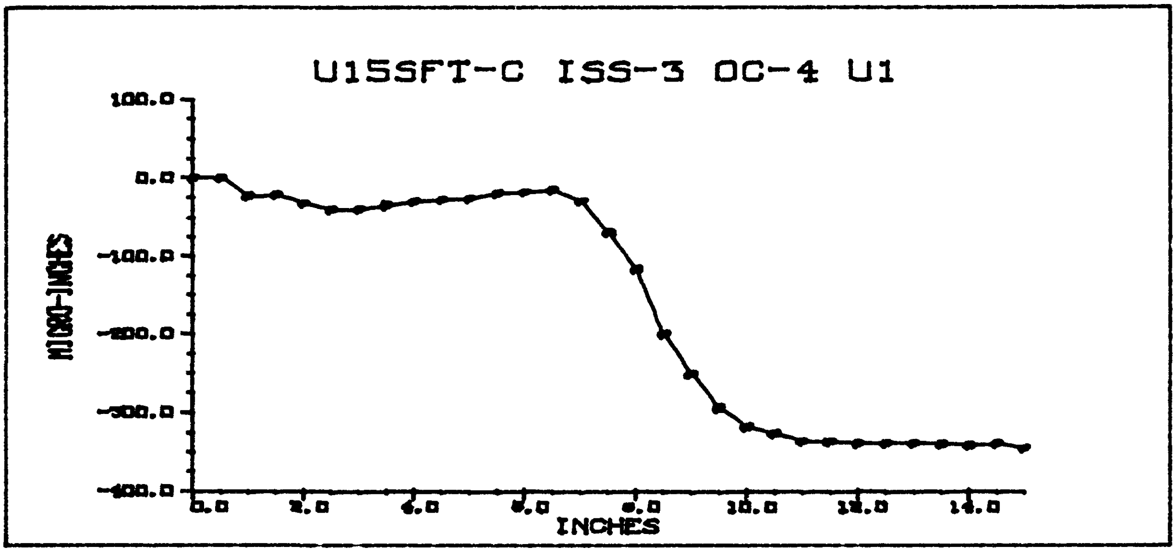
U15SFT-C ISS-3 OC-4 U1
MICRO-INCHES
INCHES
100.0
0.0
-100.0
-200.0
-300.0
-400.0

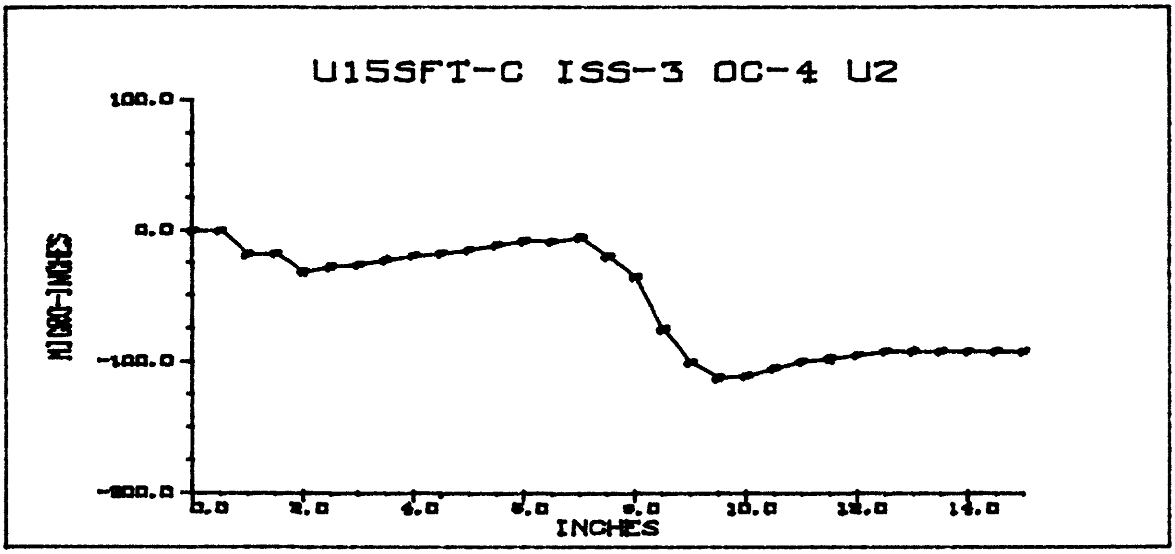
U15SFT-C ISS-3 OC-4 U2
MICRO-INCHES
INCHES
100.0
0.0
-100.0
-200.0

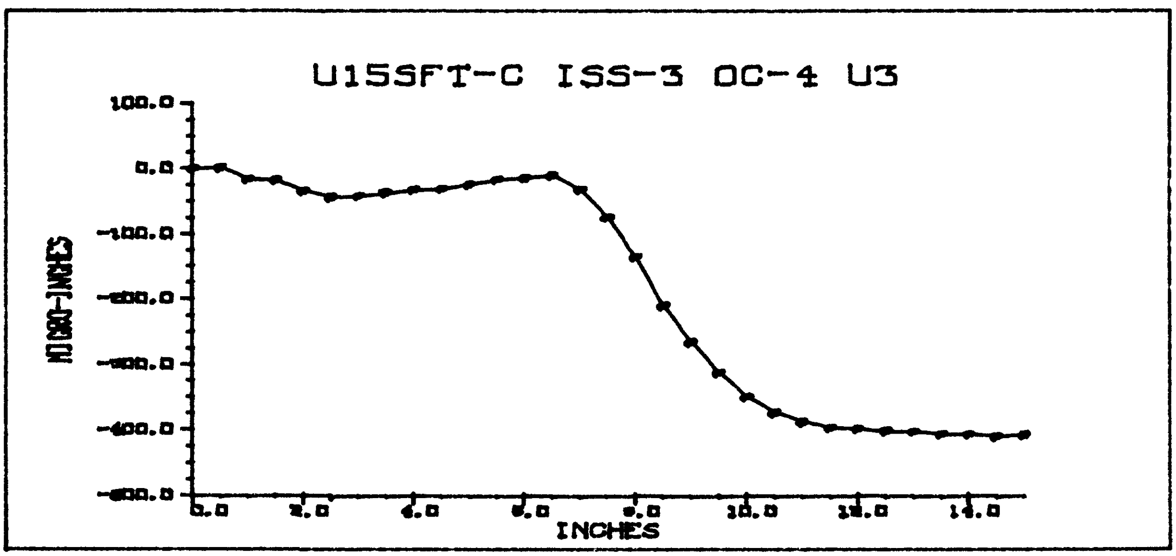
U15SFT-C ISS-3 OC-4 U3
MICRO-INCHES
INCHES
100.0
0.0
-100.0

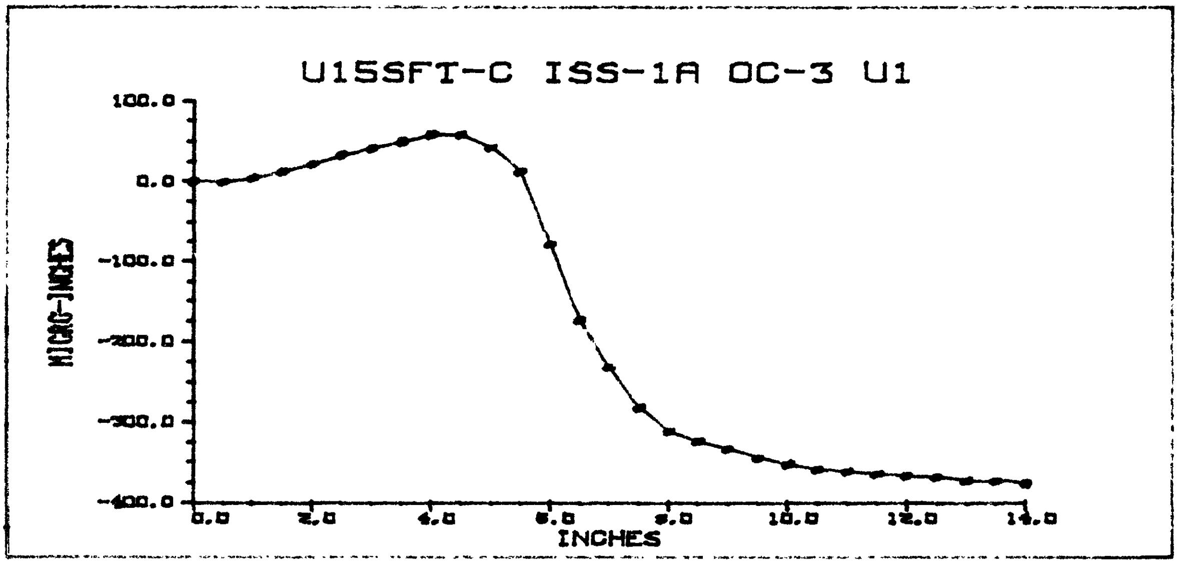
U15SFT-C ISS-1A OC-3 U1
MICRO-INCHES
INCHES

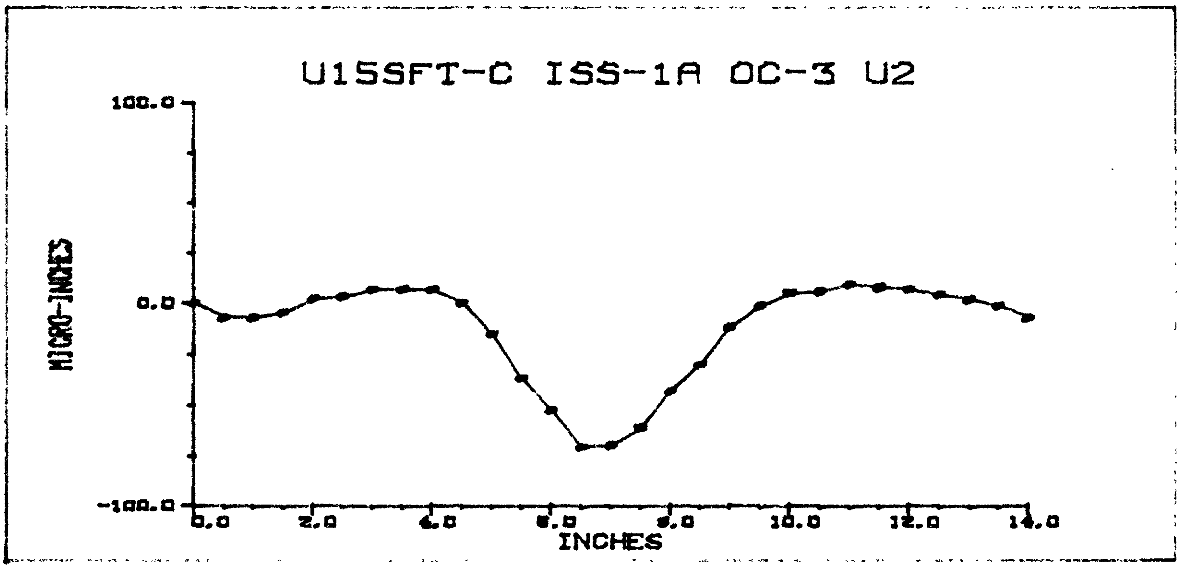
U15SFT-C ISS-1A OC-3 U2
MICRO-INCHES
INCHES

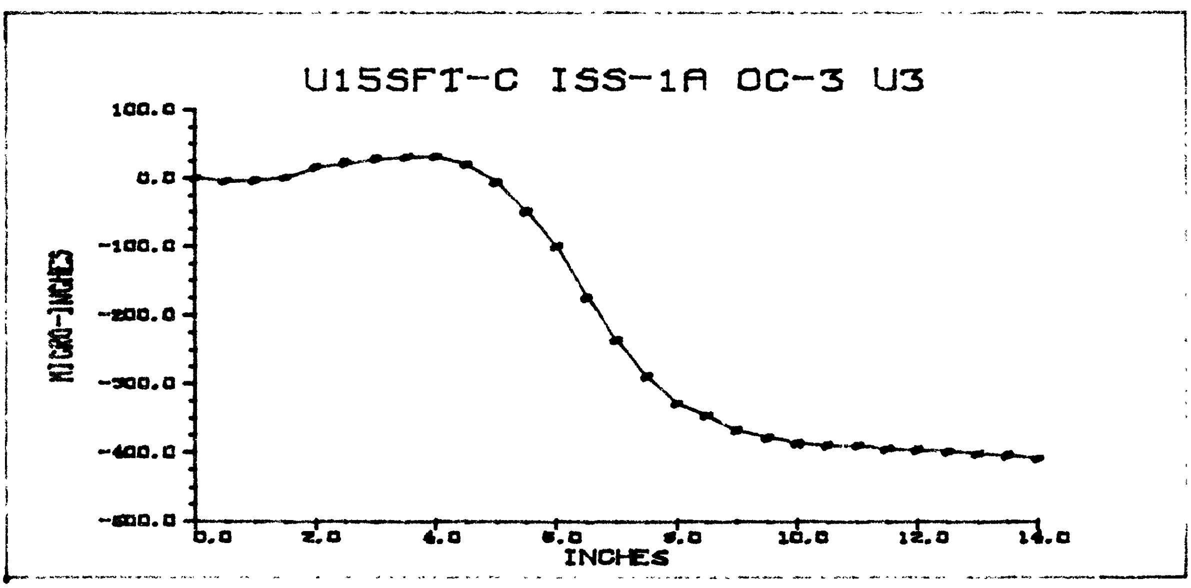
U15SFT-C ISS-1A OC-3 U3
MICRO-INCHES
INCHES

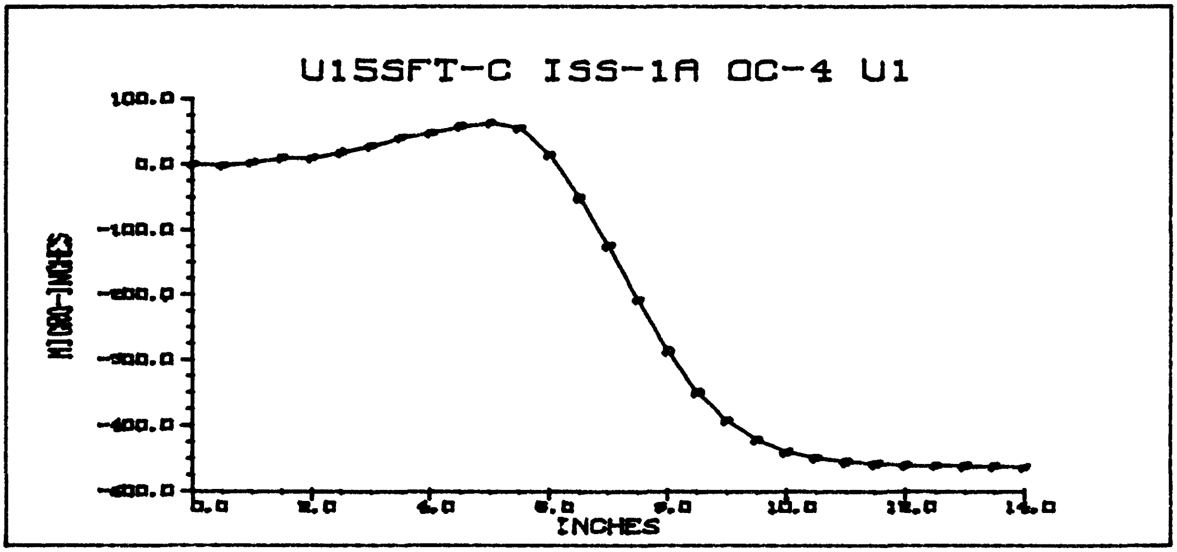
U15SFT-C ISS-1A OC-4 U1
MICRO-INCHES
INCHES

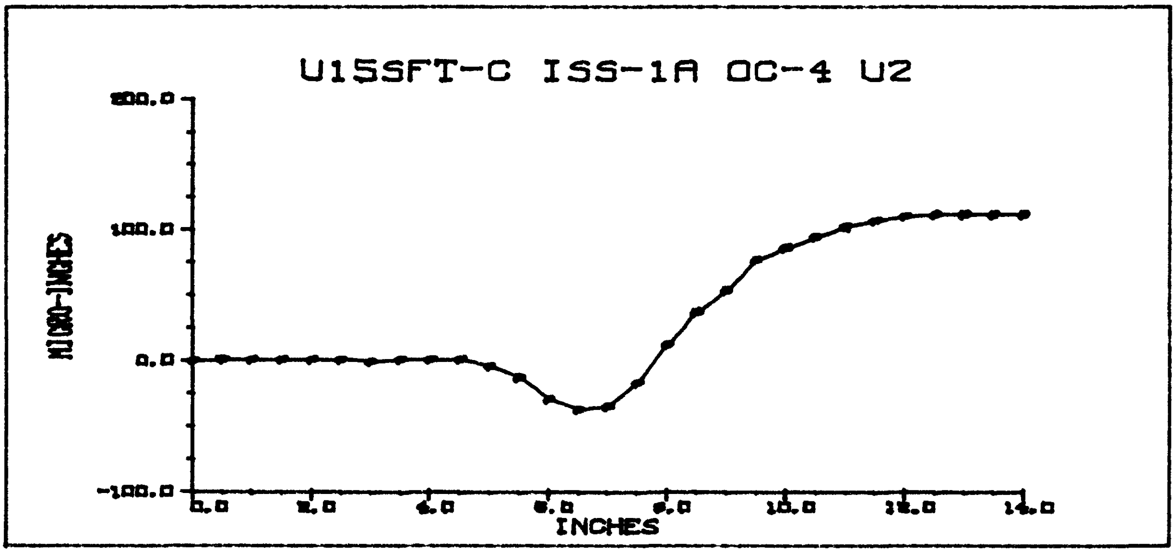
U15SFT-C ISS-1A OC-4 U2
MICRO-INCHES
INCHES

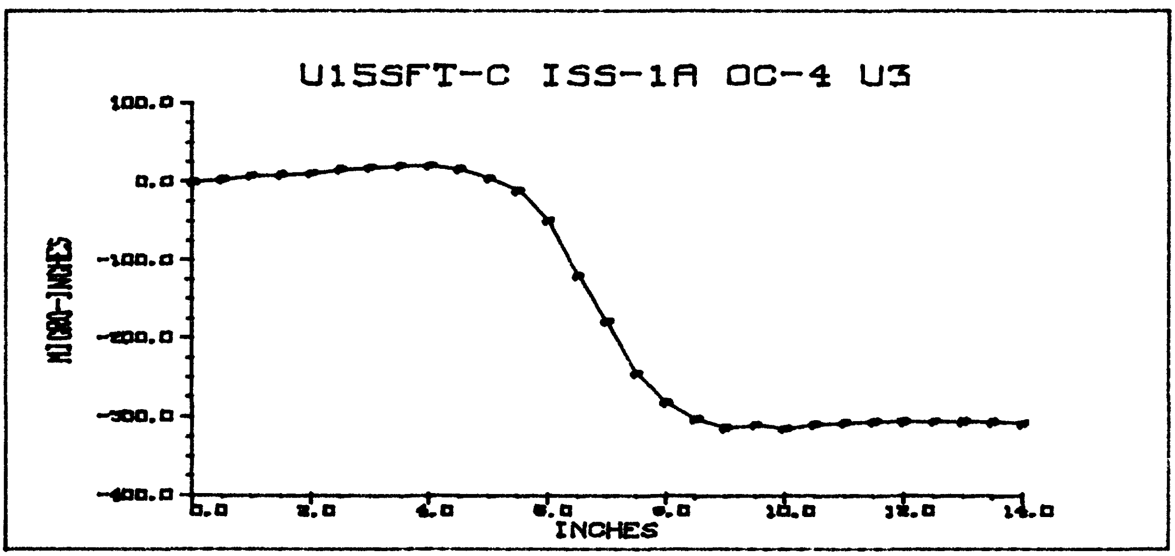
U15SFT-C ISS-1A OC-4 U3
MICRO-INCHES
INCHES

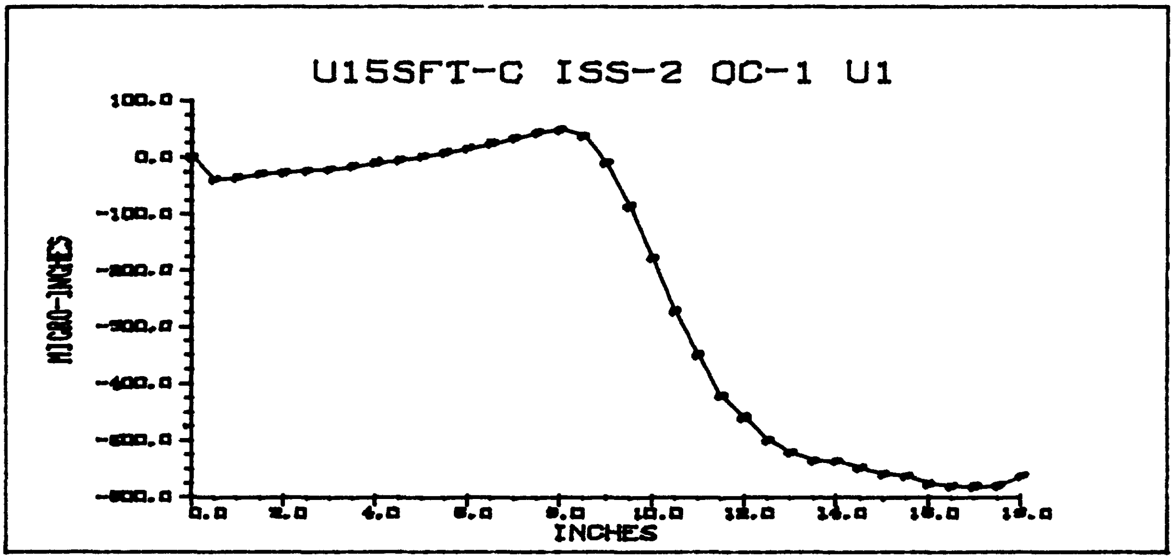
U15SFT-C ISS-2 OC-1 U1
MICRO-INCHES
INCHES

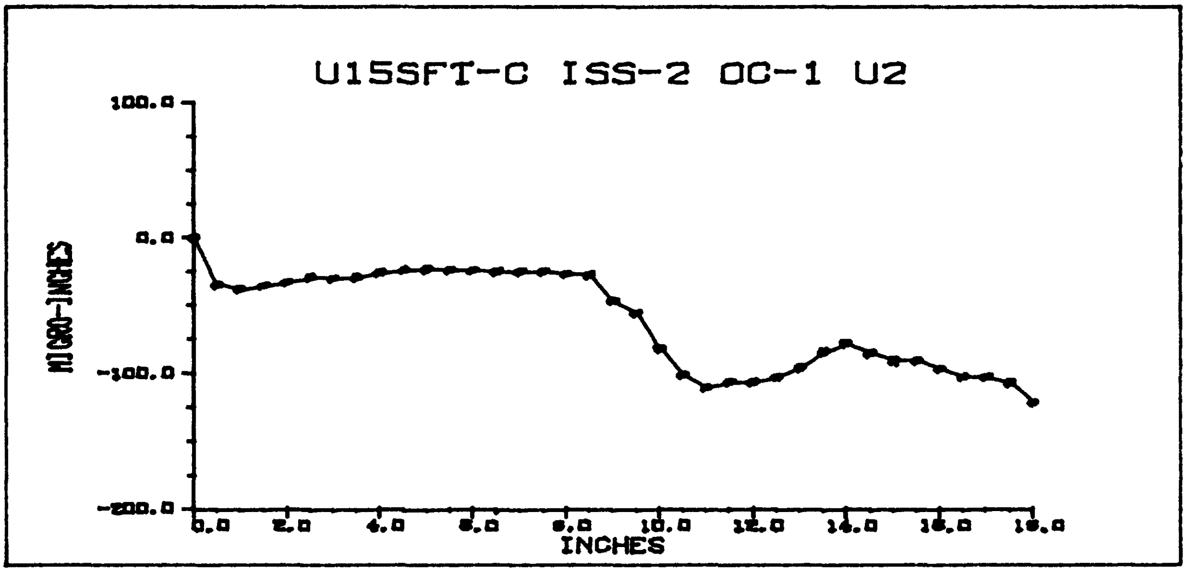
U15SFT-C ISS-2 OC-1 U2
MICRO-INCHES
INCHES

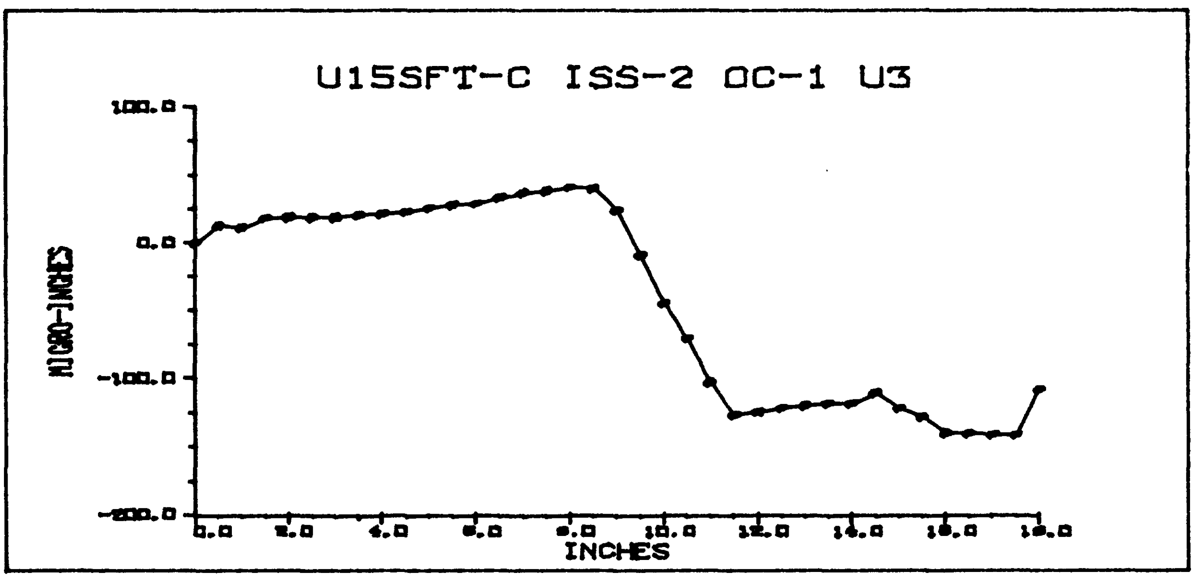
U15SFT-C ISS-2 OC-1 U3
MICRO-INCHES
INCHES

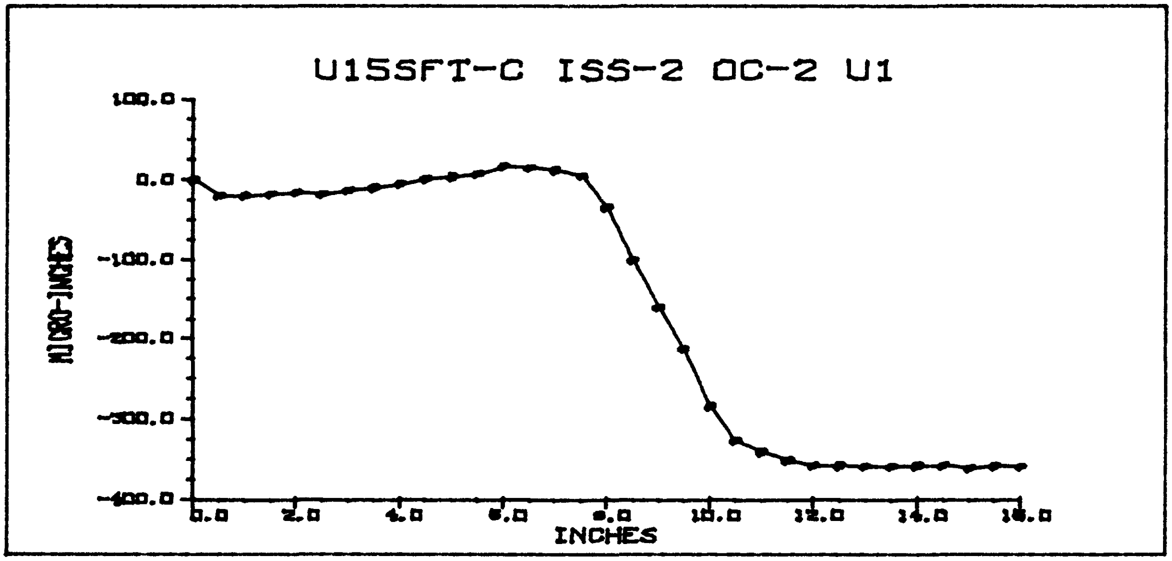
U15SFT-C ISS-2 OC-2 U1
MICRO-INCHES
INCHES

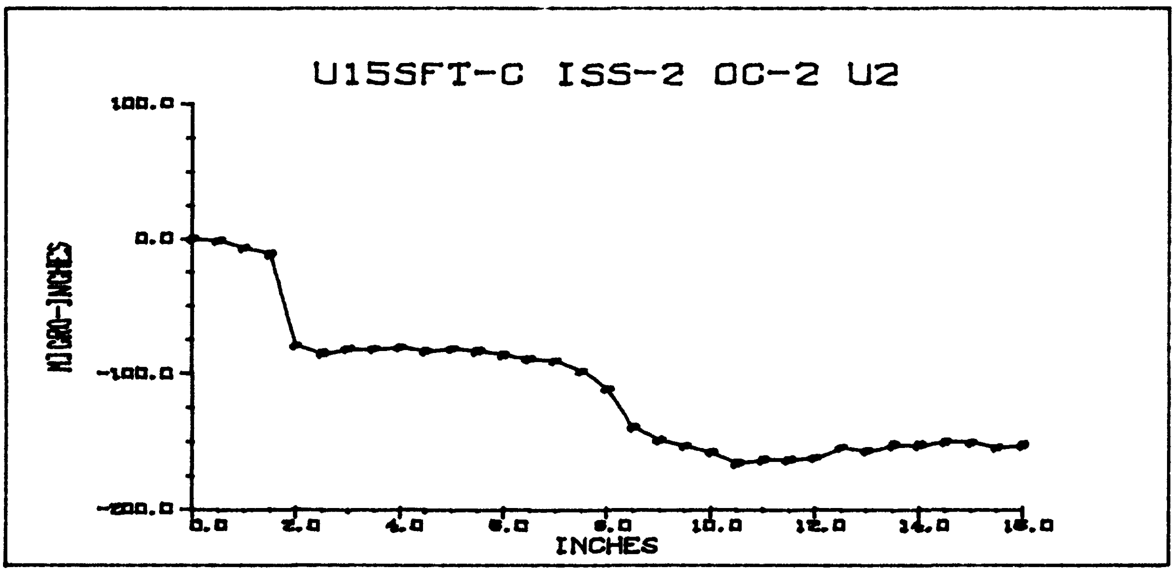
U15SFT-C ISS-2 OC-2 U2
MICRO-INCHES
INCHES

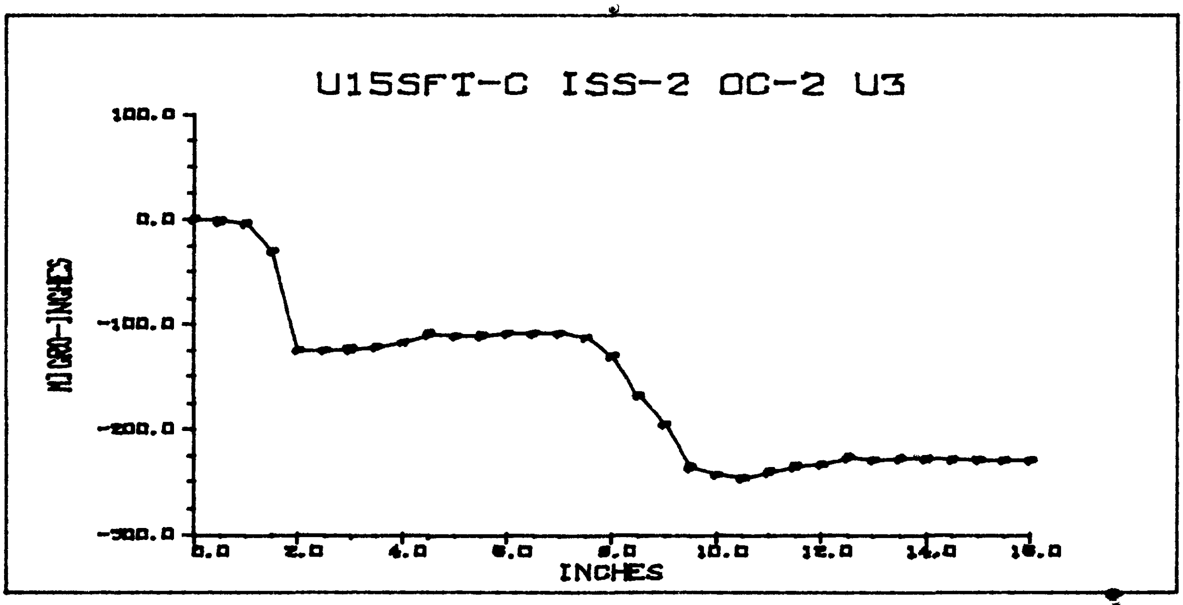
U15SFT-C ISS-2 OC-2 U3
MICRO-INCHES
INCHES

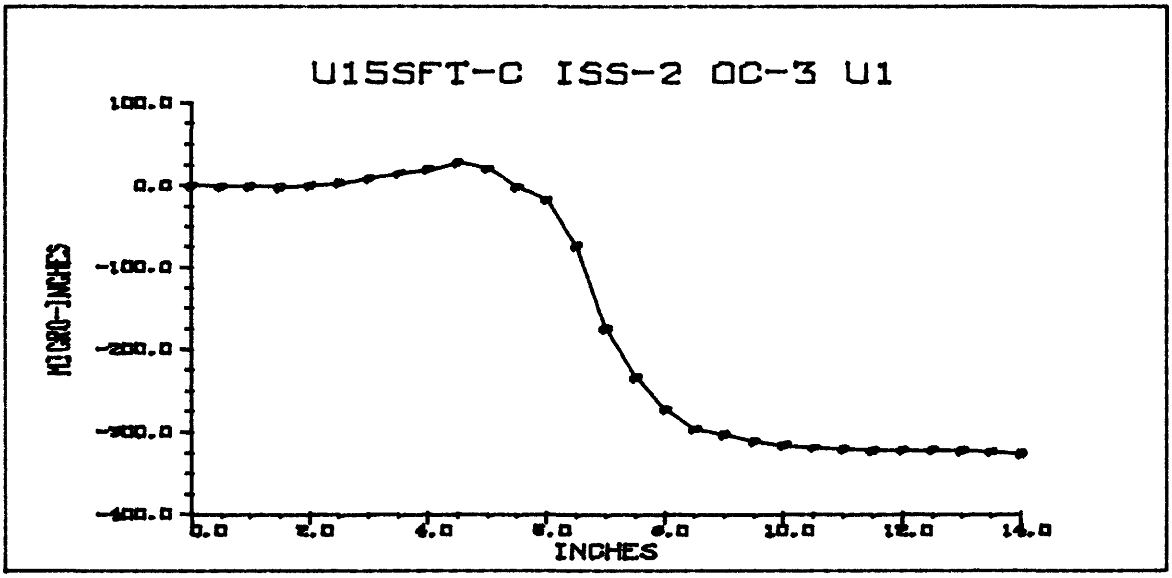
U15SFT-C ISS-2 OC-3 U1
MICRO-INCHES
INCHES

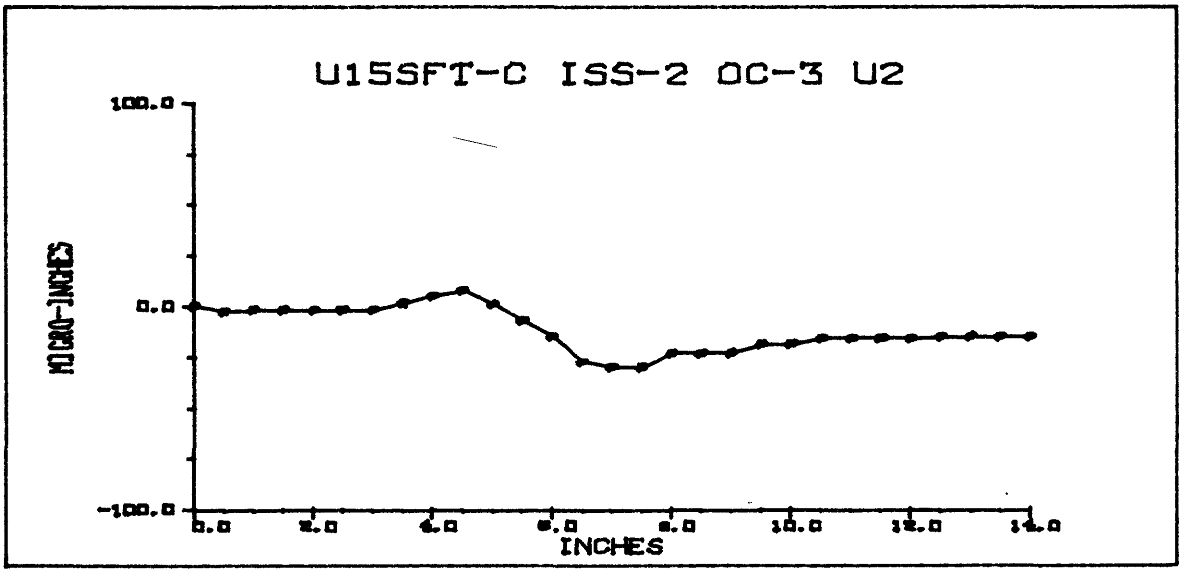
U15SFT-C ISS-2 OC-3 U2
MICRO-INCHES
INCHES

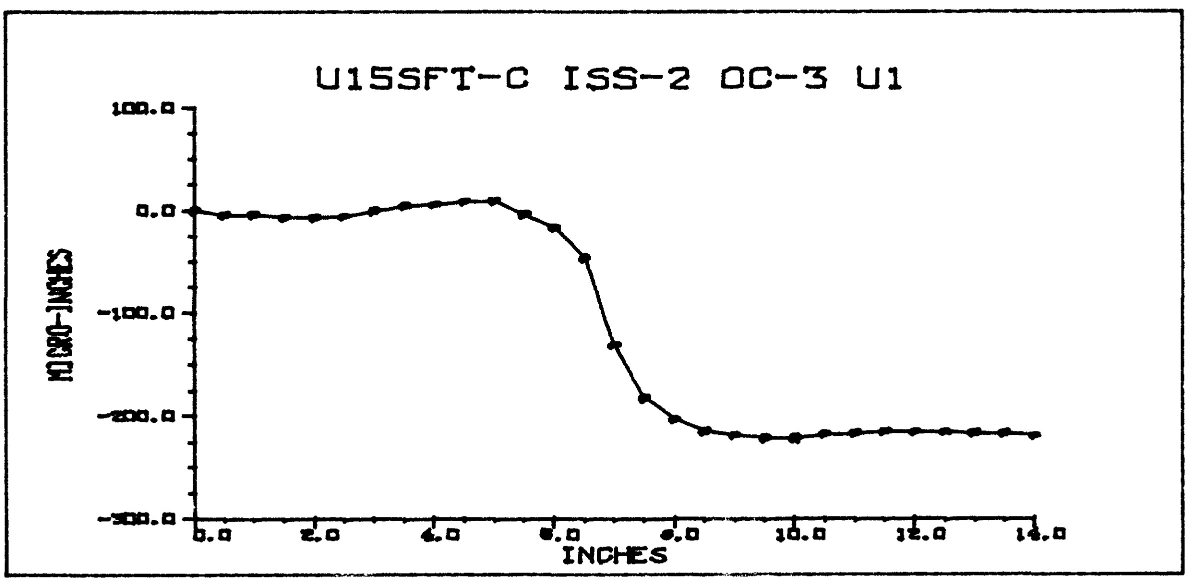
U15SFT-C ISS-2 OC-3 U1
MICRO-INCHES
INCHES

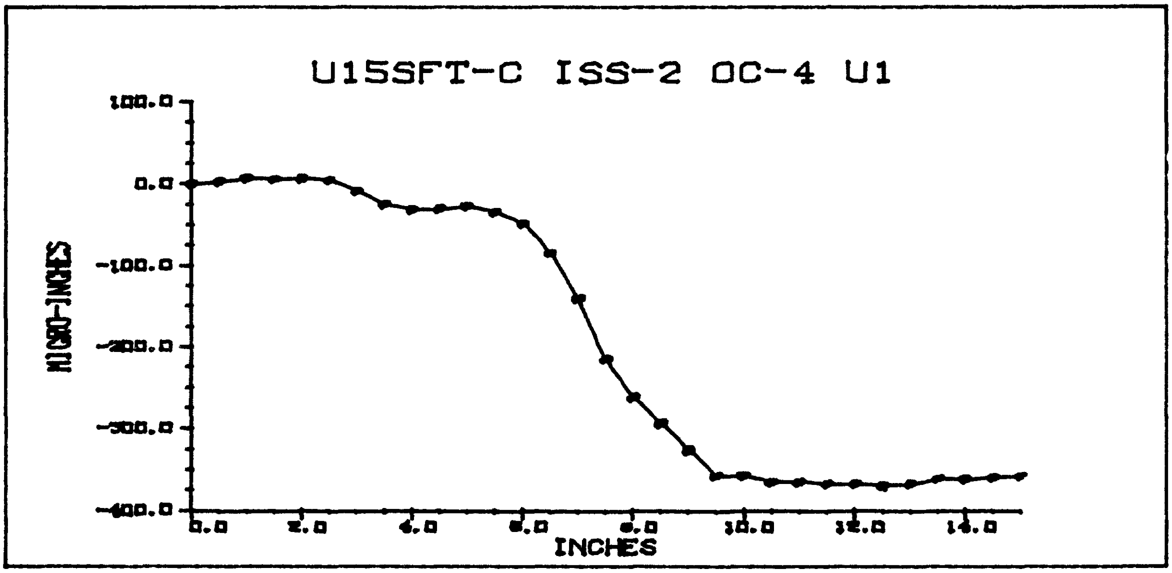
U15SFT-C ISS-2 OC-4 U1
100.0
0.0
-100.0
-200.0
-300.0
-400.0
MICRO-INCHES
0.0
2.0
4.0
6.0
8.0
10.0
12.0
14.0
INCHES

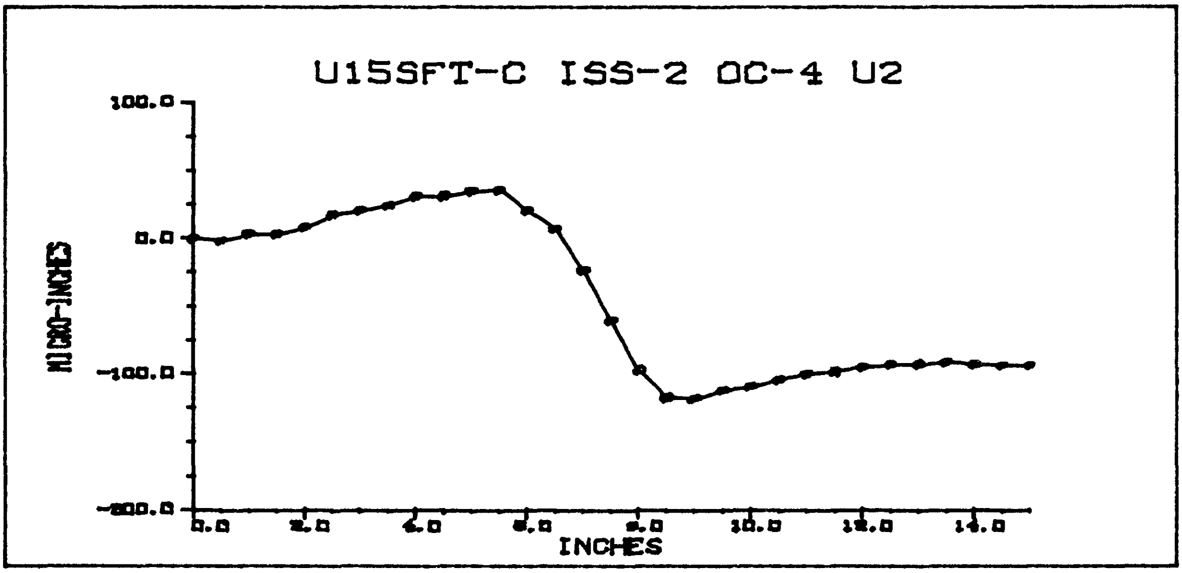
U15SFT-C ISS-2 OC-4 U2
100.0
0.0
-100.0
-200.0
MICRO-INCHES
0.0
2.0
4.0
6.0
8.0
10.0
12.0
14.0
INCHES

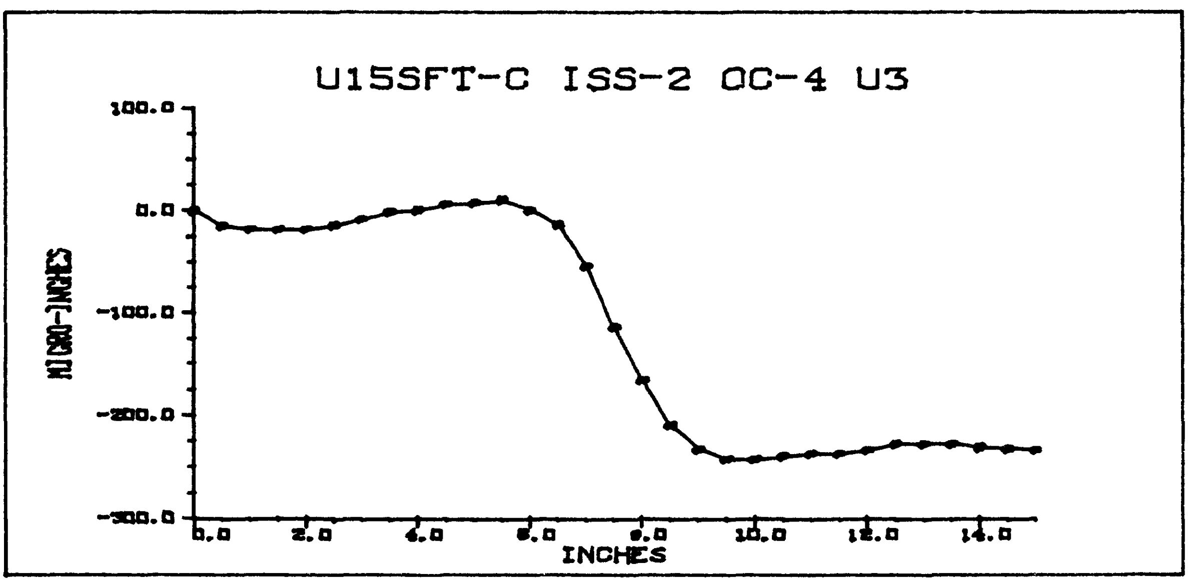
U15SFT-C ISS-2 OC-4 U3
100.0
0.0
-100.0
-200.0
-300.0
MICRO-INCHES
0.0
2.0
4.0
6.0
8.0
10.0
12.0
14.0
INCHES

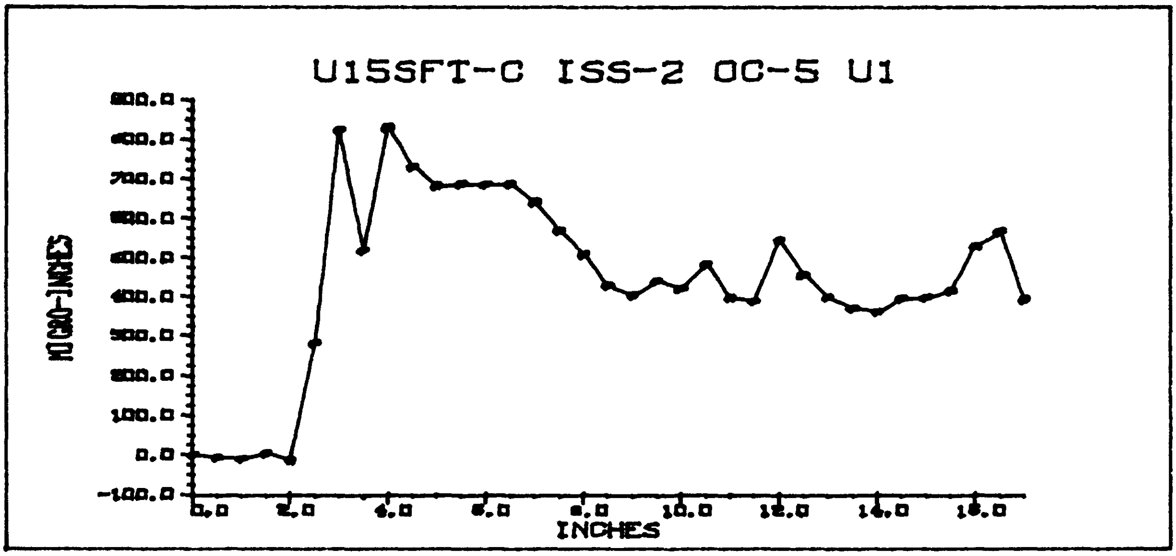
U15SFT-C ISS-2 OC-5 U1
MICRO-INCHES
INCHES

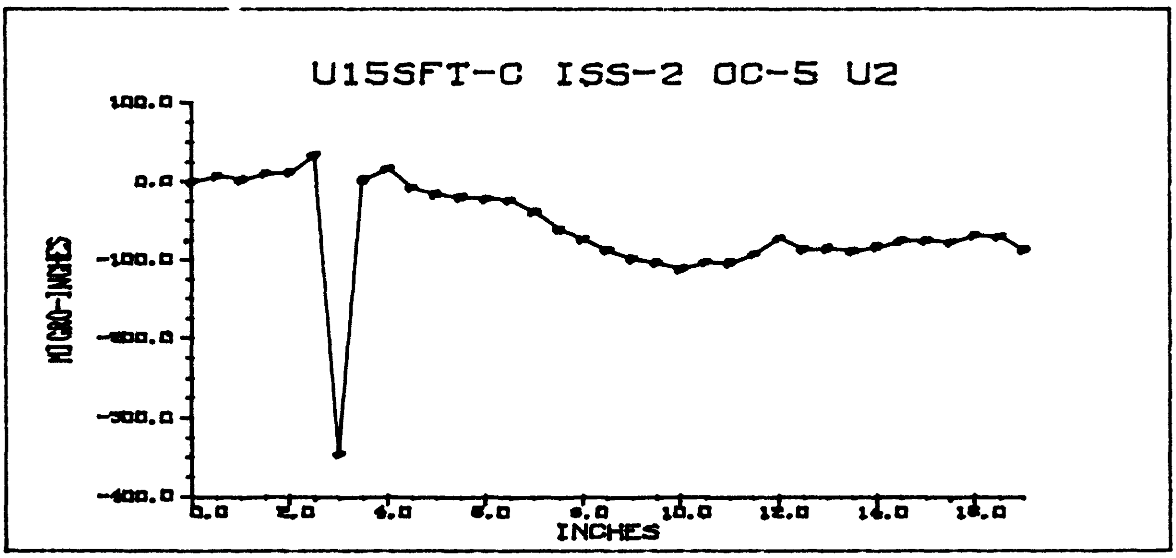
U15SFT-C ISS-2 OC-5 U2
MICRO-INCHES
INCHES

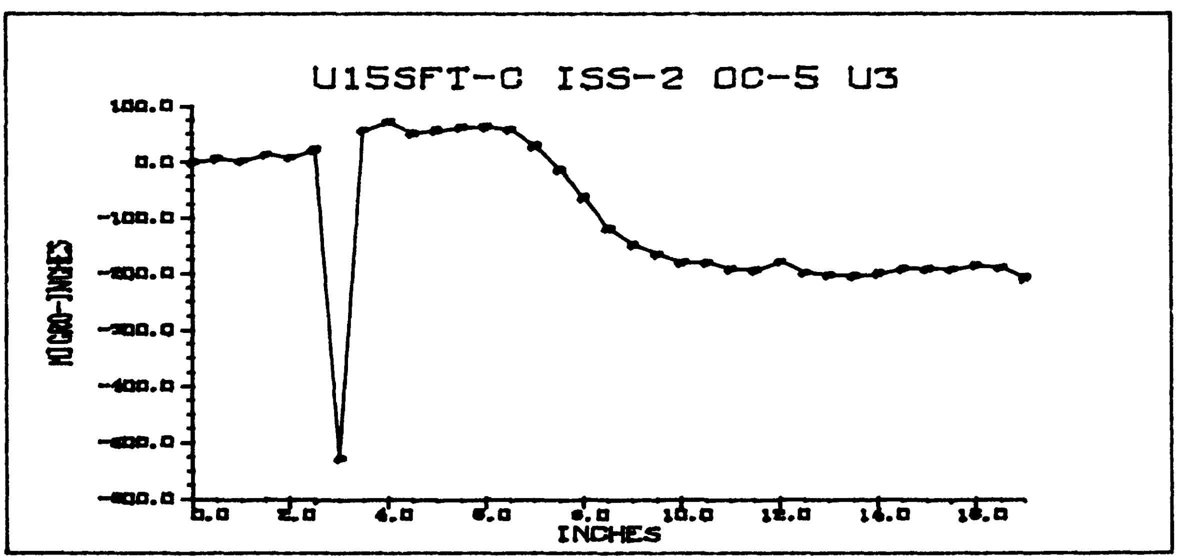
U15SFT-C ISS-2 OC-5 U3
MICRO-INCHES
INCHES

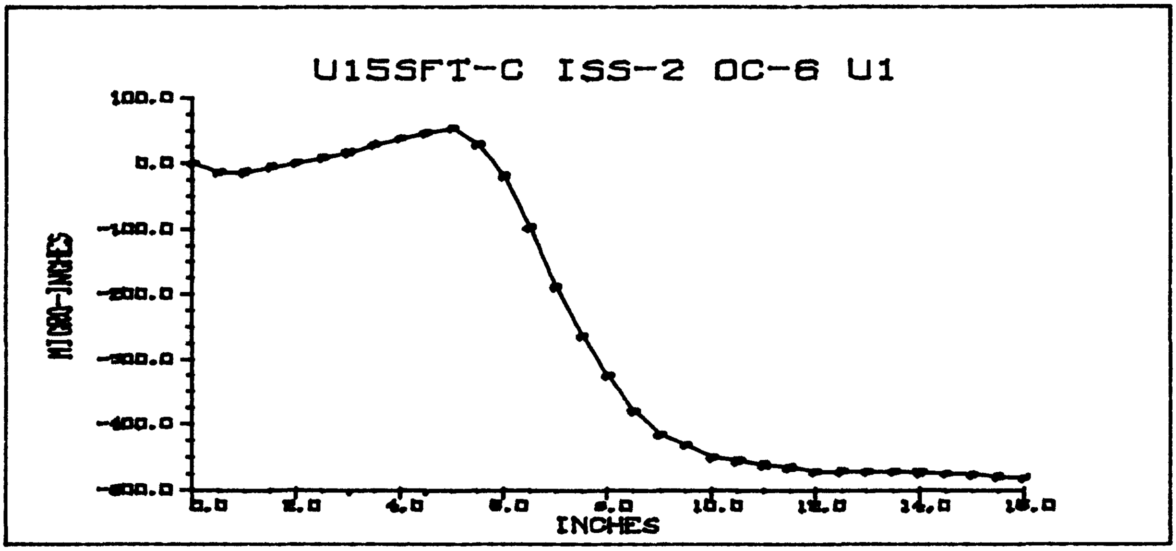
U15SFT-C ISS-2 OC-6 U1
MICRO-INCHES
INCHES
100.0
0.0
-100.0
-200.0
-300.0
-400.0
-500.0

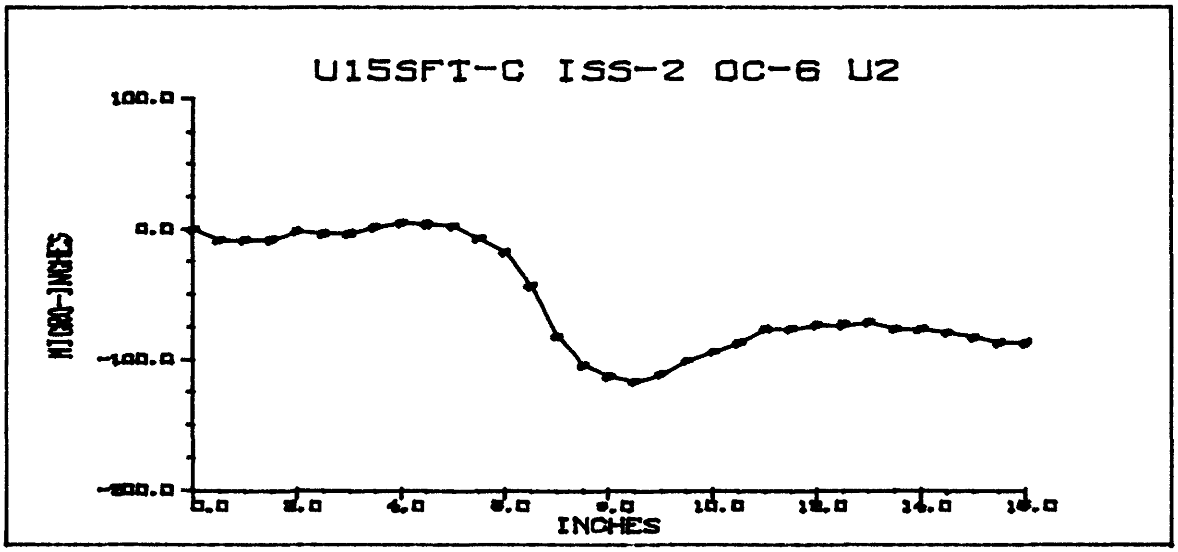
U15SFT-C ISS-2 OC-6 U2
MICRO-INCHES
INCHES
100.0
0.0
-100.0
-200.0

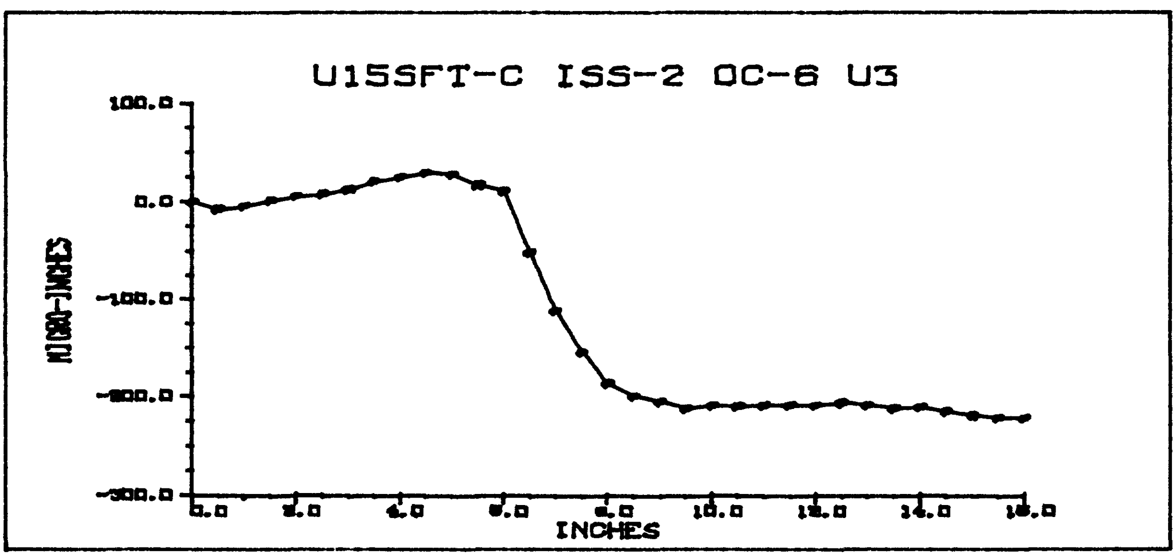
U15SFT-C ISS-2 OC-6 U3
MICRO-INCHES
INCHES
100.0
0.0
-100.0
-200.0
-300.0

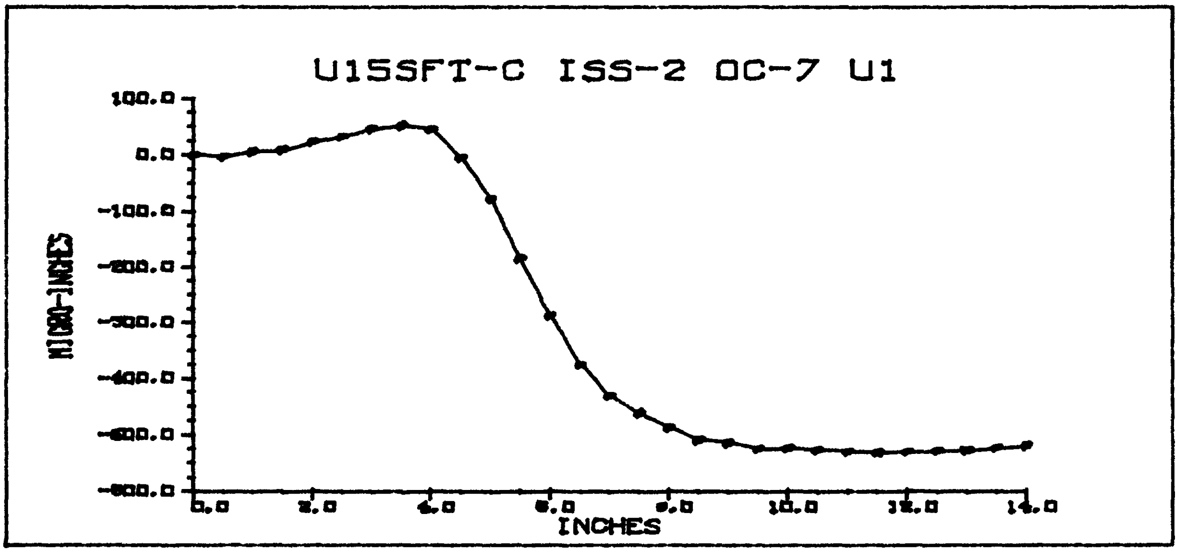
U15SFT-C ISS-2 OC-7 U1
MICRO-INCHES
INCHES

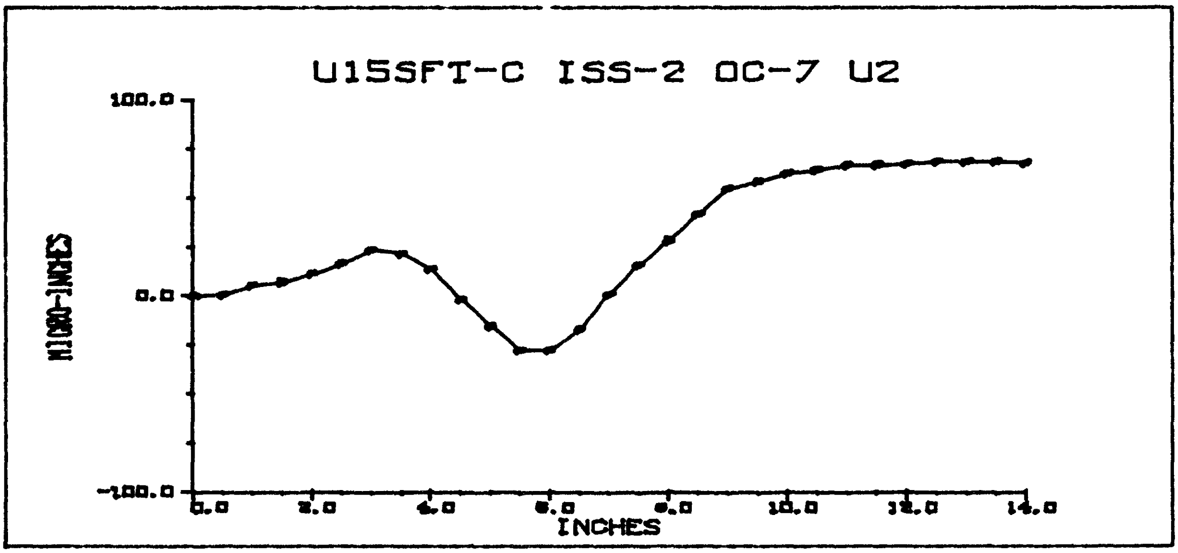
U15SFT-C ISS-2 OC-7 U2
MICRO-INCHES
INCHES

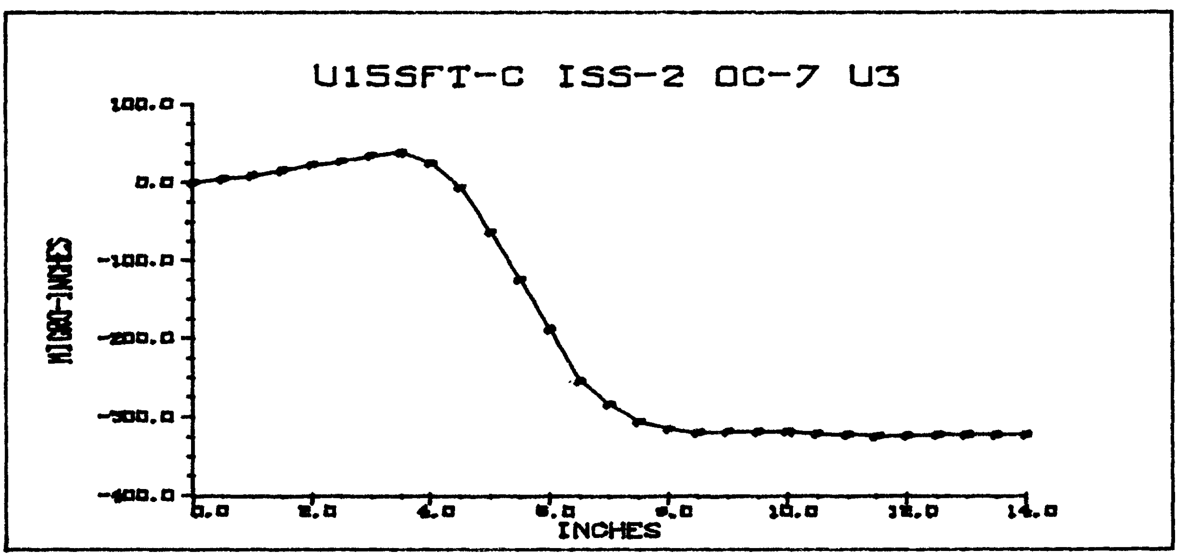
U15SFT-C ISS-2 OC-7 U3
MICRO-INCHES
INCHES

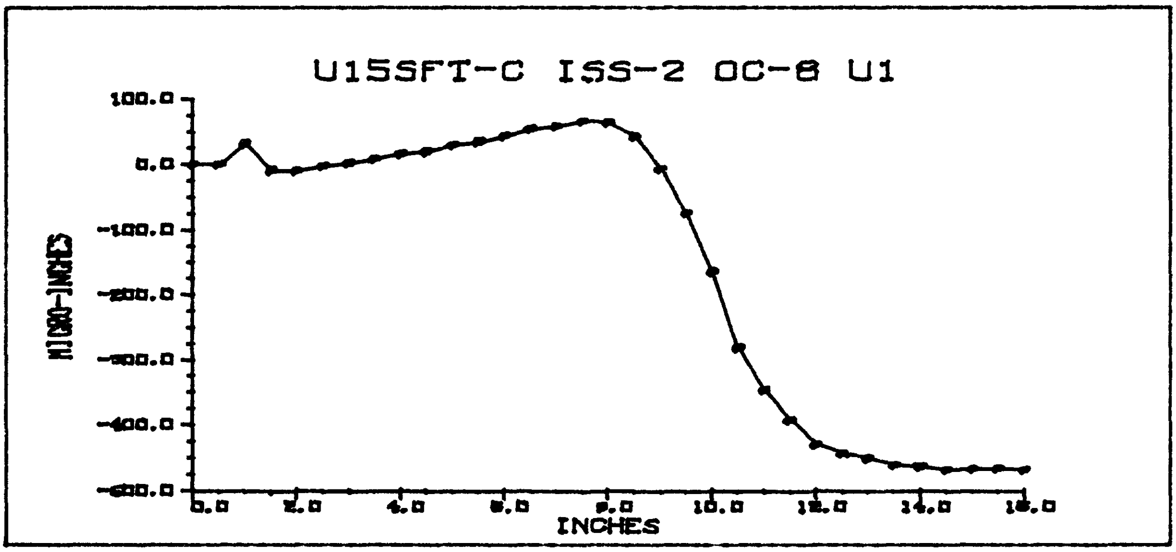
U15SFT-C ISS-2 OC-8 U1
MICRO-INCHES
INCHES

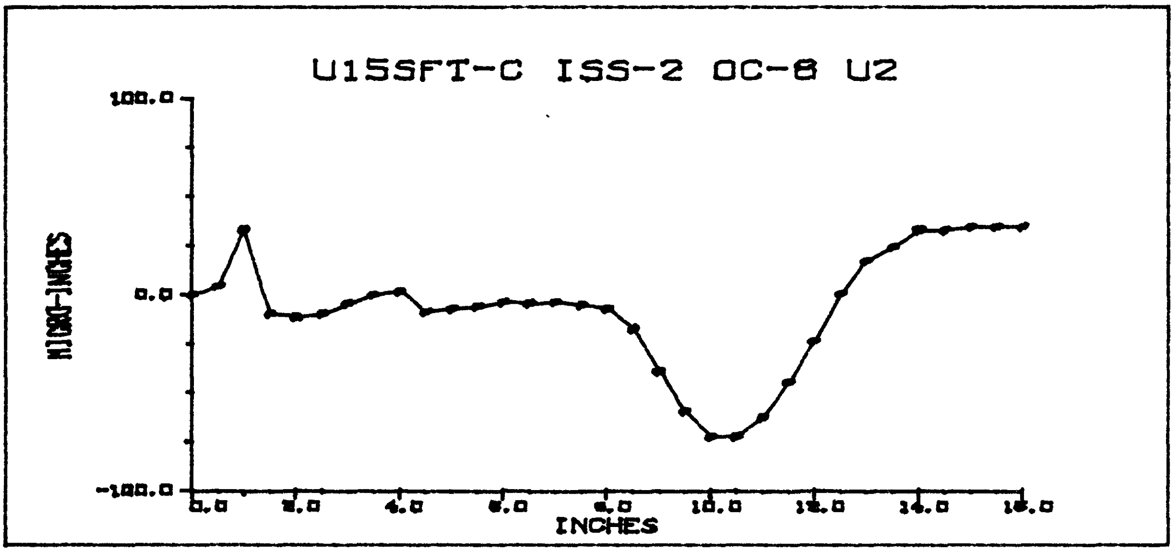
U15SFT-C ISS-2 OC-8 U2
MICRO-INCHES
INCHES

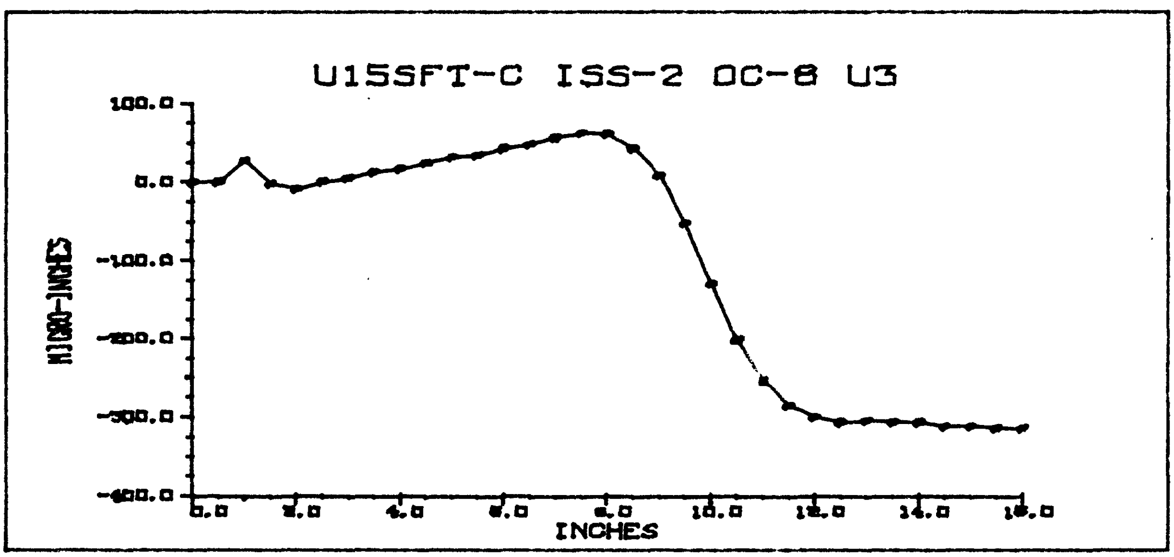
U15SFT-C ISS-2 OC-8 U3
MICRO-INCHES
INCHES

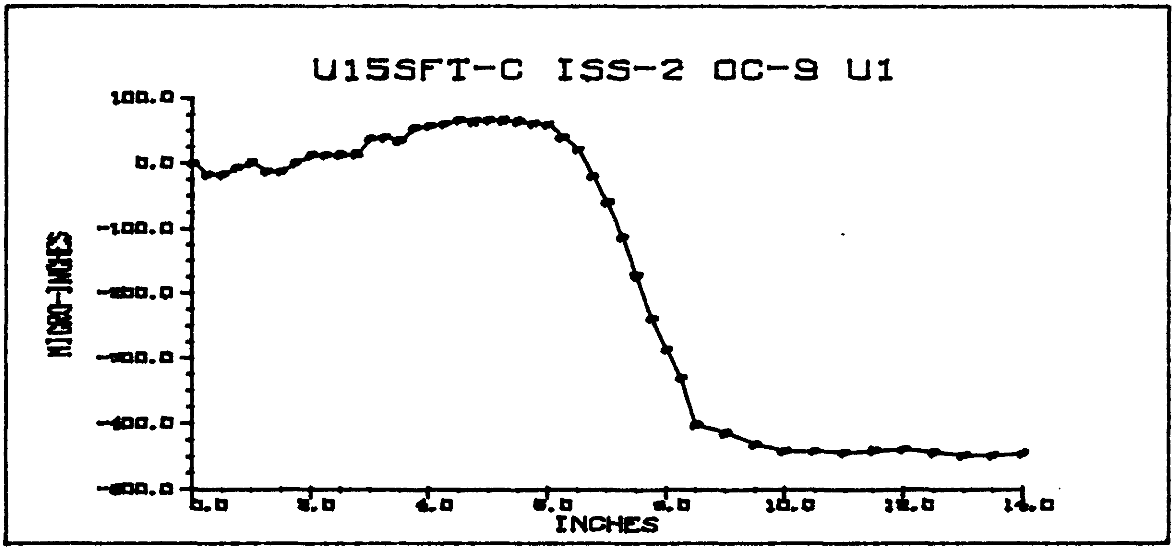
U15SFT-C ISS-2 OC-9 U1
100.0
0.0
-100.0
-400.0
MICRO-INCHES
INCHES
0.0
4.0
10.0
14.0

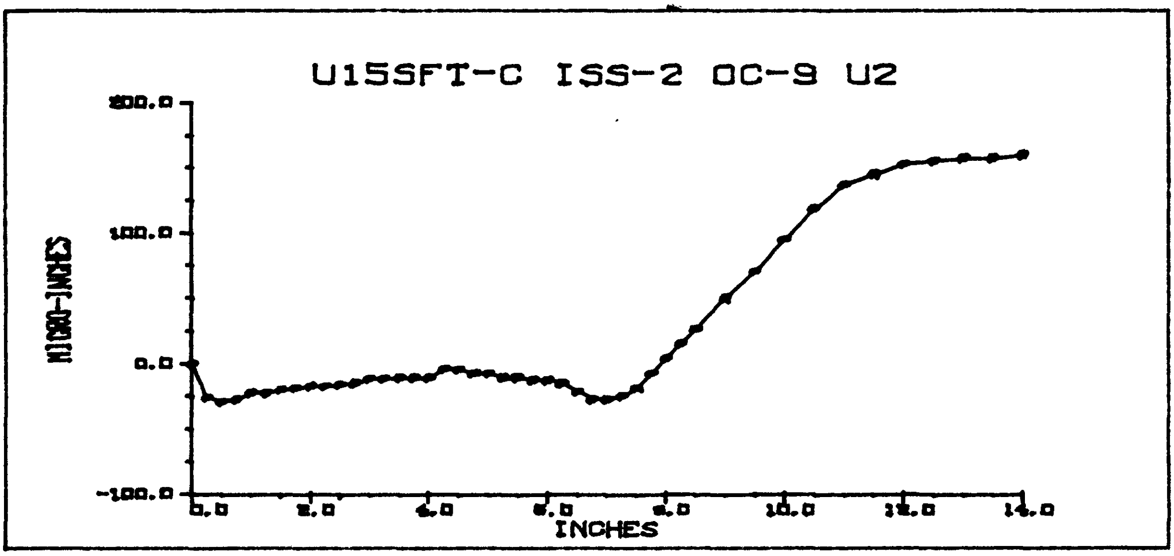
U15SFT-C ISS-2 OC-9 U2
100.0
0.0
-100.0
MICRO-INCHES
INCHES
0.0
2.0
4.0
10.0
14.0

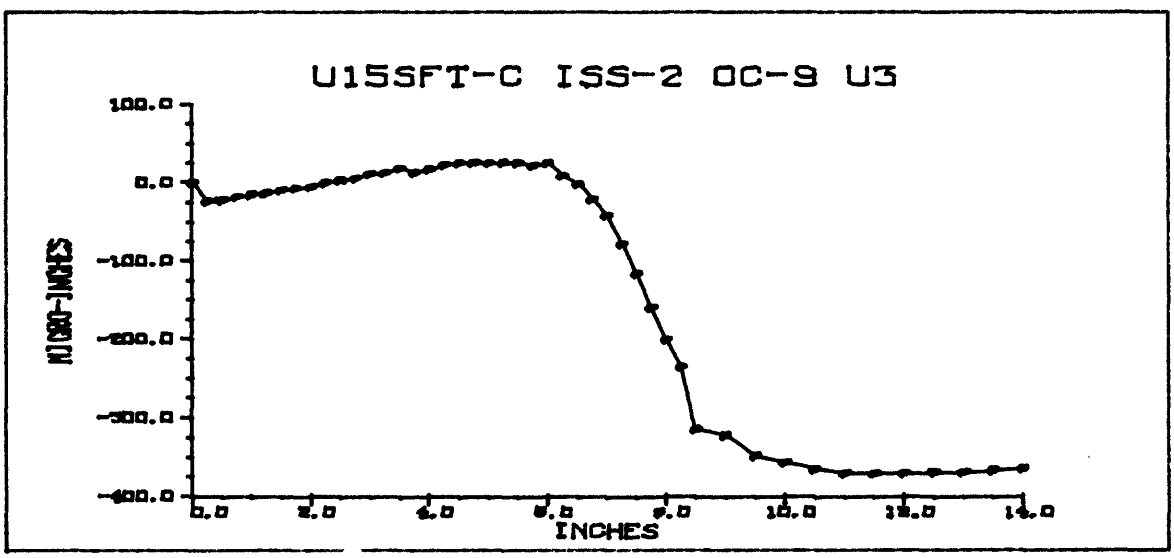
U15SFT-C ISS-2 OC-9 U3
100.0
0.0
-100.0
-200.0
-300.0
MICRO-INCHES
INCHES
0.0
2.0
4.0
10.0
14.0

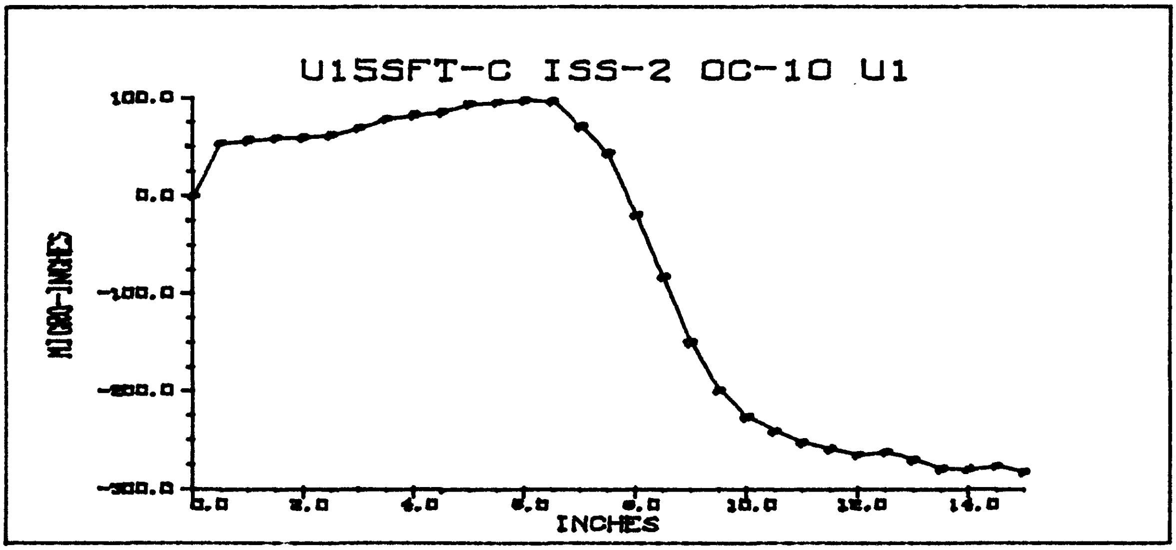
U15SFT-C ISS-2 OC-10 U1
100.0
0.0
-100.0
-200.0
-300.0
MICRO-INCHES
0.0
2.0
4.0
6.0
8.0
10.0
12.0
14.0
INCHES

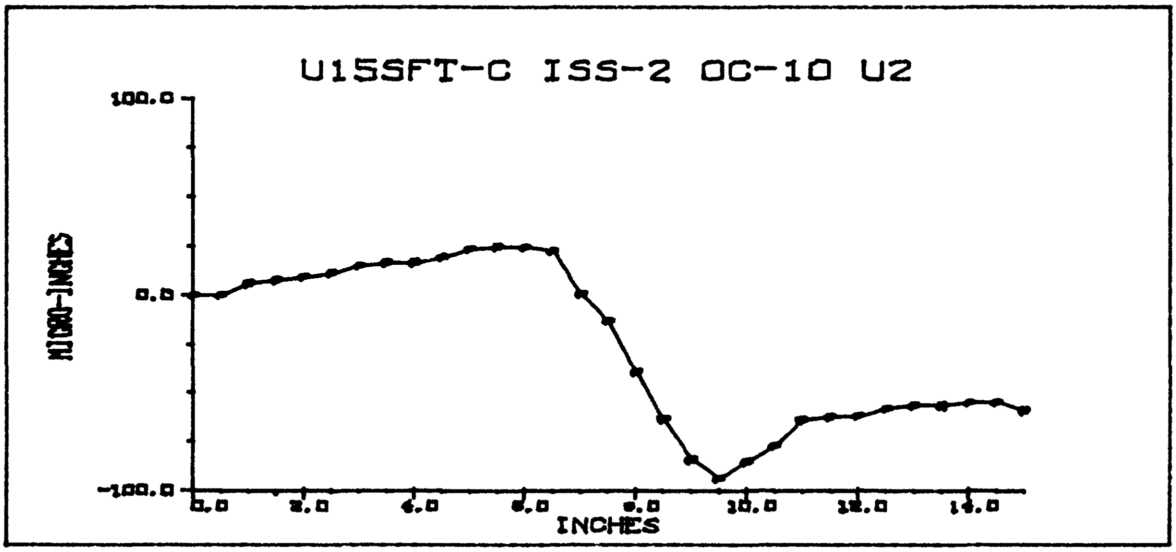
U15SFT-C ISS-2 OC-10 U2
100.0
0.0
-100.0
MICRO-INCHES
0.0
2.0
4.0
6.0
8.0
10.0
12.0
14.0
INCHES

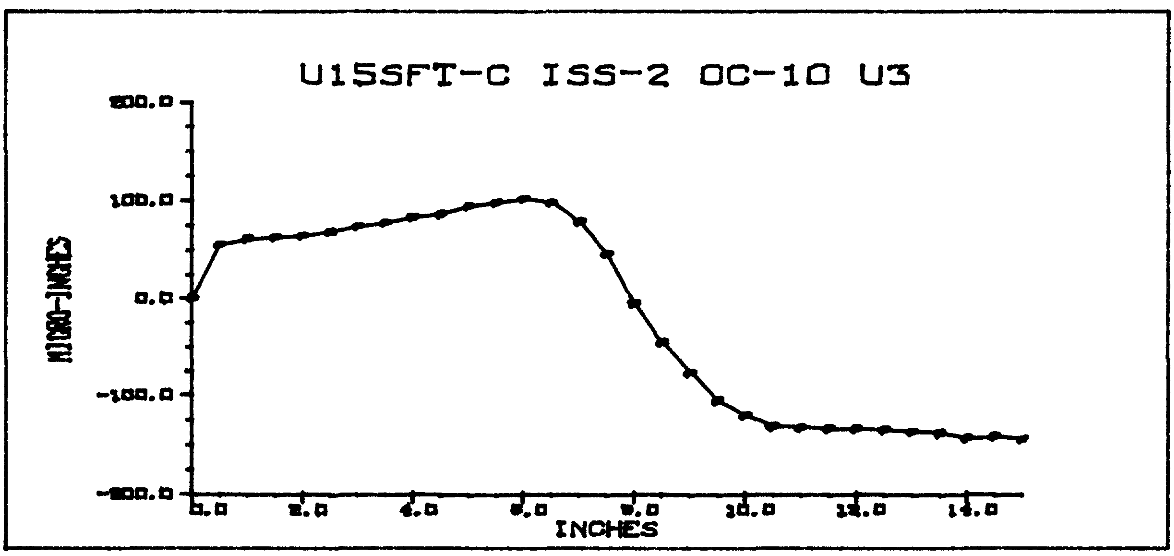
U15SFT-C ISS-2 OC-10 U3
200.0
100.0
0.0
-100.0
-200.0
MICRO-INCHES
0.0
2.0
4.0
6.0
8.0
10.0
12.0
14.0
INCHES

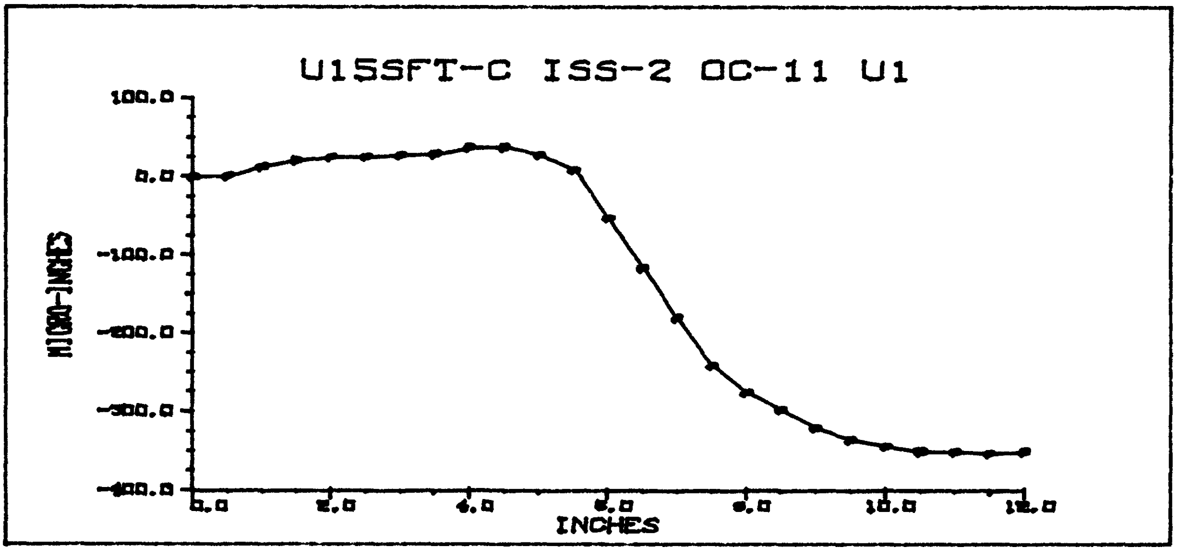
U15SFT-C ISS-2 OC-11 U1
100.0
0.0
-100.0
-200.0
-300.0
-400.0
MICRO-INCHES
0.0
2.0
4.0
6.0
8.0
10.0
12.0
INCHES

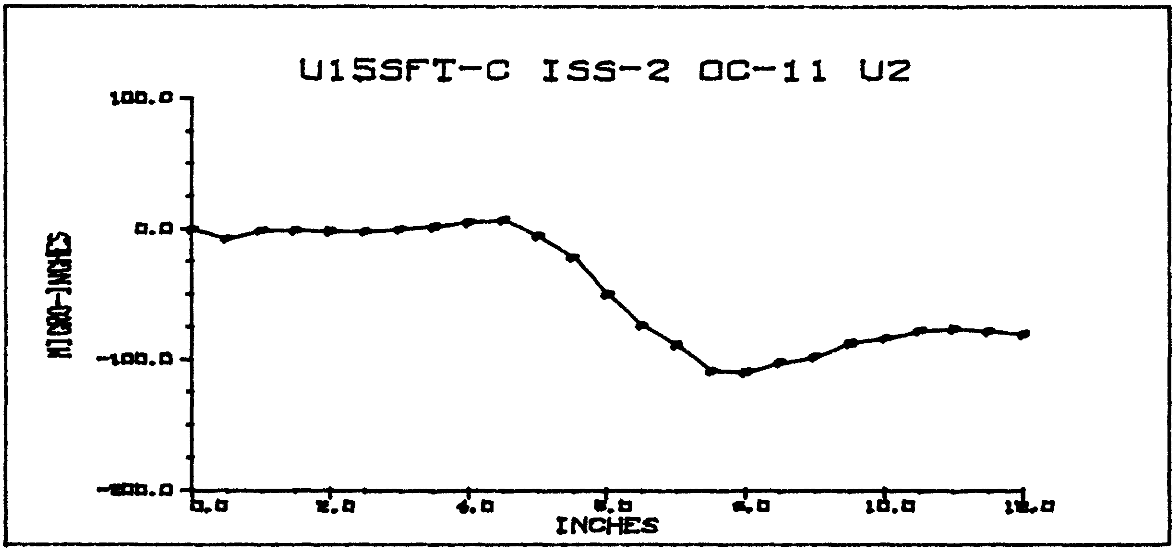
U15SFT-C ISS-2 OC-11 U2
100.0
0.0
-100.0
-200.0
MICRO-INCHES
0.0
2.0
4.0
6.0
8.0
10.0
12.0
INCHES

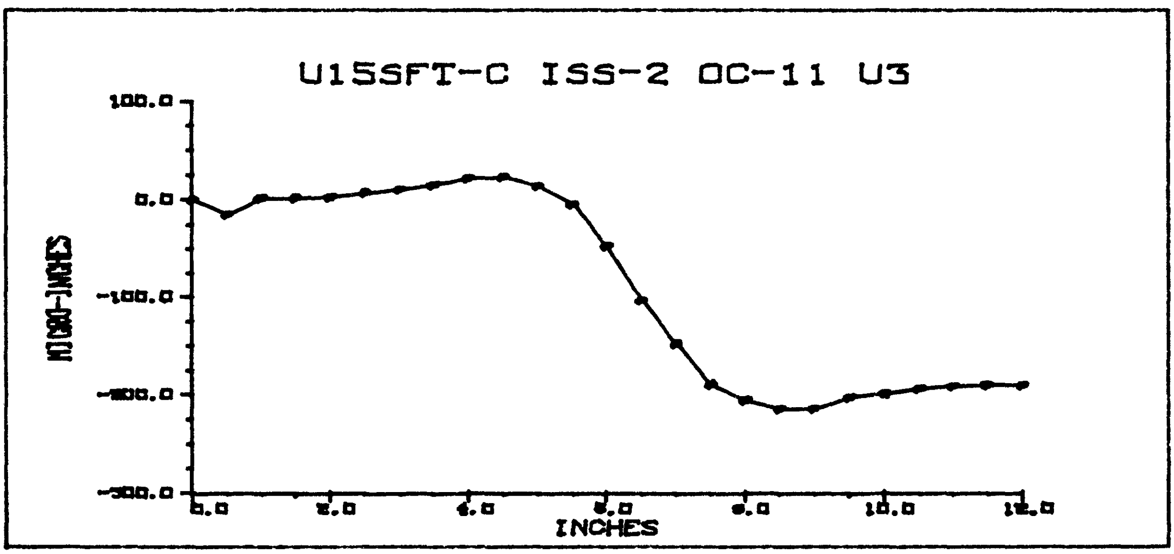
U15SFT-C ISS-2 OC-11 U3
100.0
0.0
-100.0
-200.0
-300.0
MICRO-INCHES
0.0
2.0
4.0
6.0
8.0
10.0
12.0
INCHES

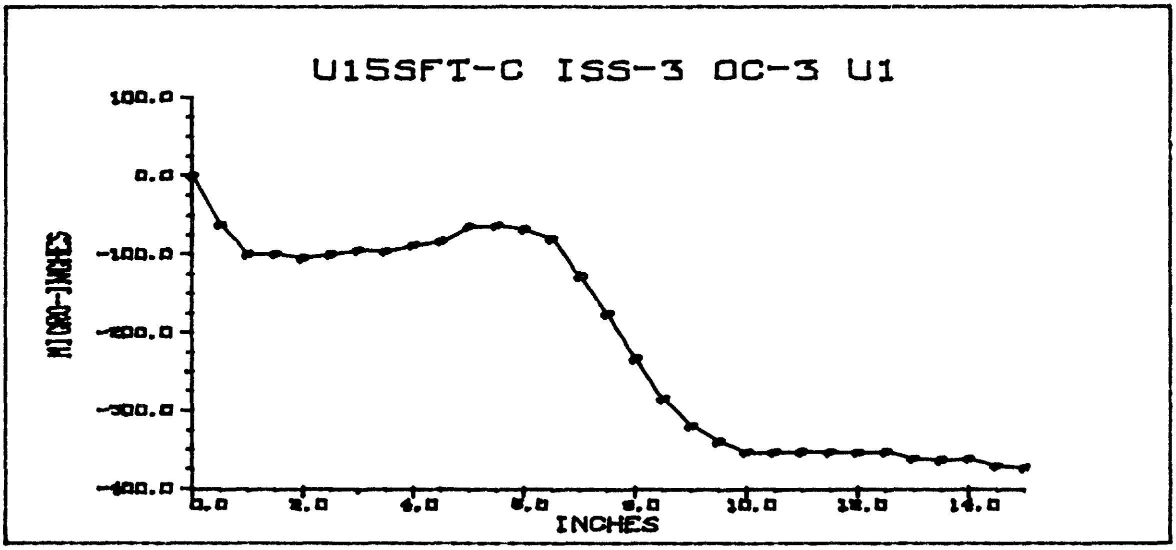
U15SFT-C ISS-3 OC-3 U1
100.0
0.0
-100.0
-200.0
-300.0
-400.0
MICRO-INCHES
0.0
2.0
4.0
6.0
8.0
10.0
12.0
14.0
INCHES

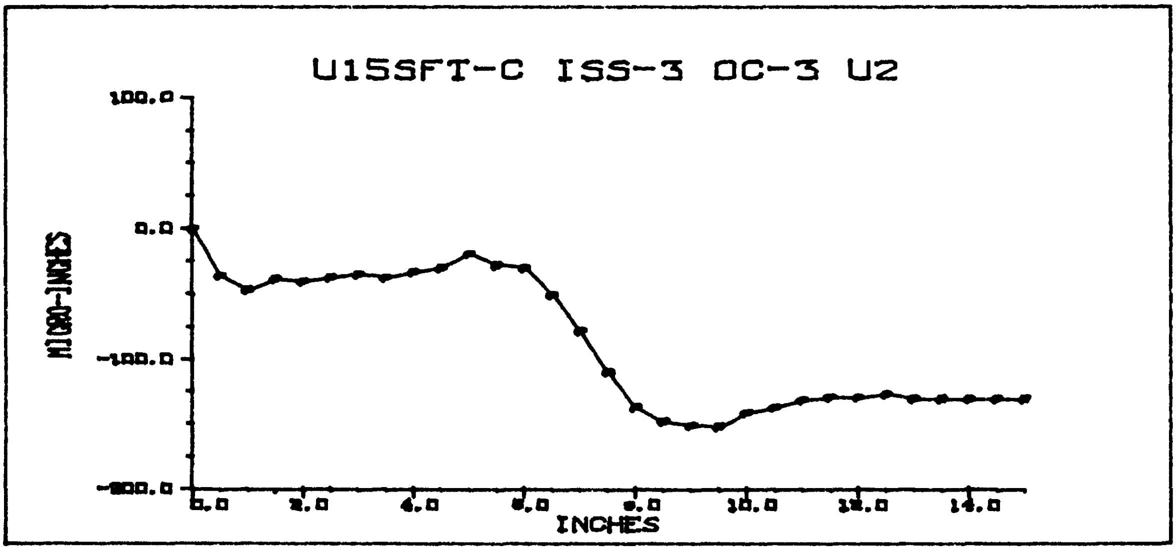
U15SFT-C ISS-3 OC-3 U2
100.0
0.0
-100.0
-200.0
MICRO-INCHES
0.0
2.0
4.0
6.0
8.0
10.0
12.0
14.0
INCHES

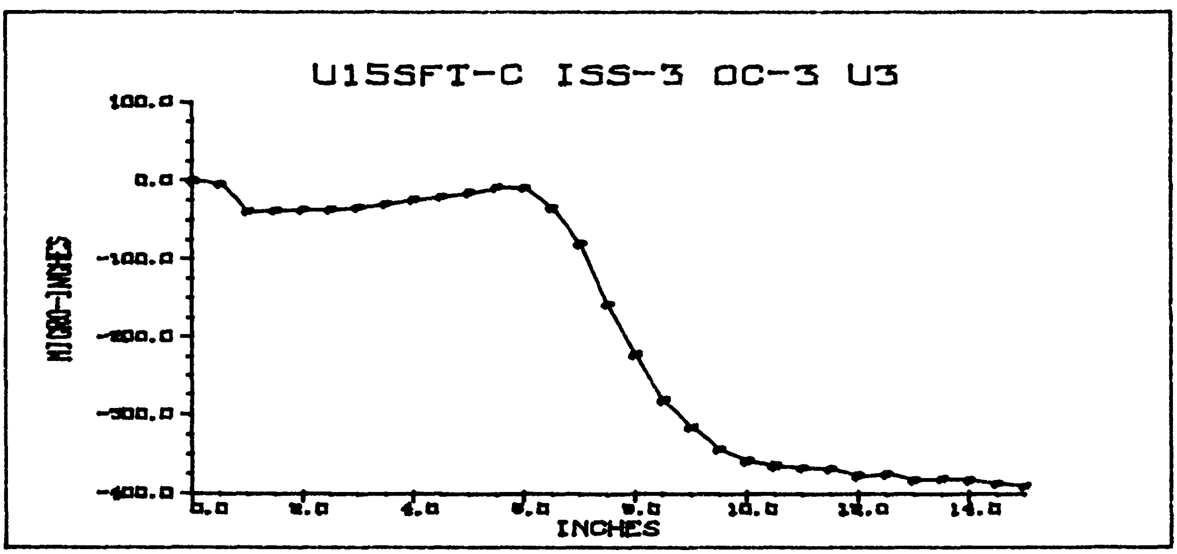
U15SFT-C ISS-3 OC-3 U3
100.0
0.0
-100.0
-200.0
-300.0
-400.0
MICRO-INCHES
0.0
2.0
4.0
6.0
8.0
10.0
12.0
14.0
INCHES

APPENDIX B
Biaxial Test Data

Computer plots of radial pressure versus borehole deformation from biaxial tests on 14 stress-relief overcores used in stress calculations (overcore No. 4 from ISS-3 hole was not recovered) are shown. The elastic modulus of the overcores was determined from the 6.9 MPa (1,000 lb/in^2) unloading cycle, which is set equal to zero deformation at zero pressure on the plots. Each plot is identified by location (U15SFT-C), hole number (ISS), overcore number (OC), and component of deformation (U_1, U_2, U_3). Units are given in lb/in^2 for radial pressure and microinches for deformation.

145.04 lb/in^2=1.0 MPa
1 microinch=$2.54X10^{-2}$ micrometers

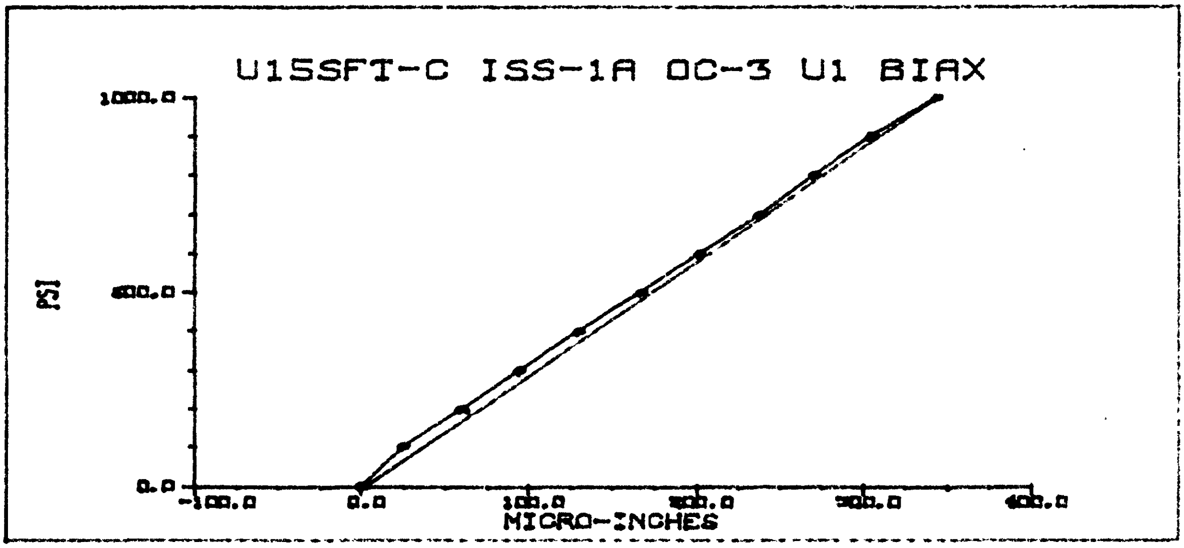
U15SFT-C ISS-1A OC-3 U1 BIAX
1000.0
500.0
0.0
PSI
-100.0
0.0
100.0
200.0
300.0
400.0
MICRO-INCHES

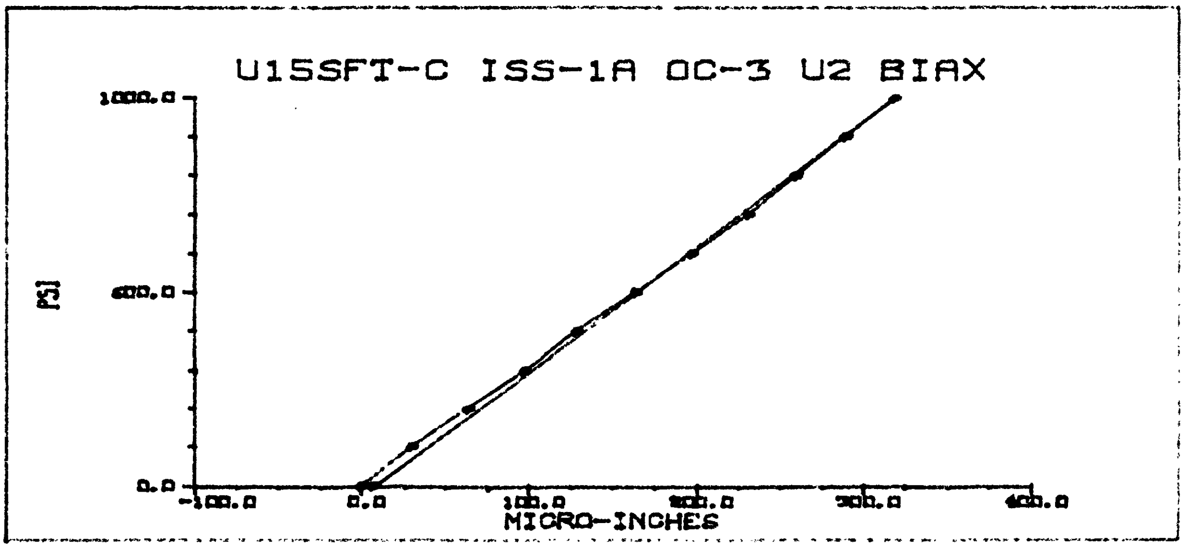
U15SFT-C ISS-1A OC-3 U2 BIAX
1000.0
500.0
0.0
PSI
-100.0
0.0
100.0
200.0
300.0
400.0
MICRO-INCHES

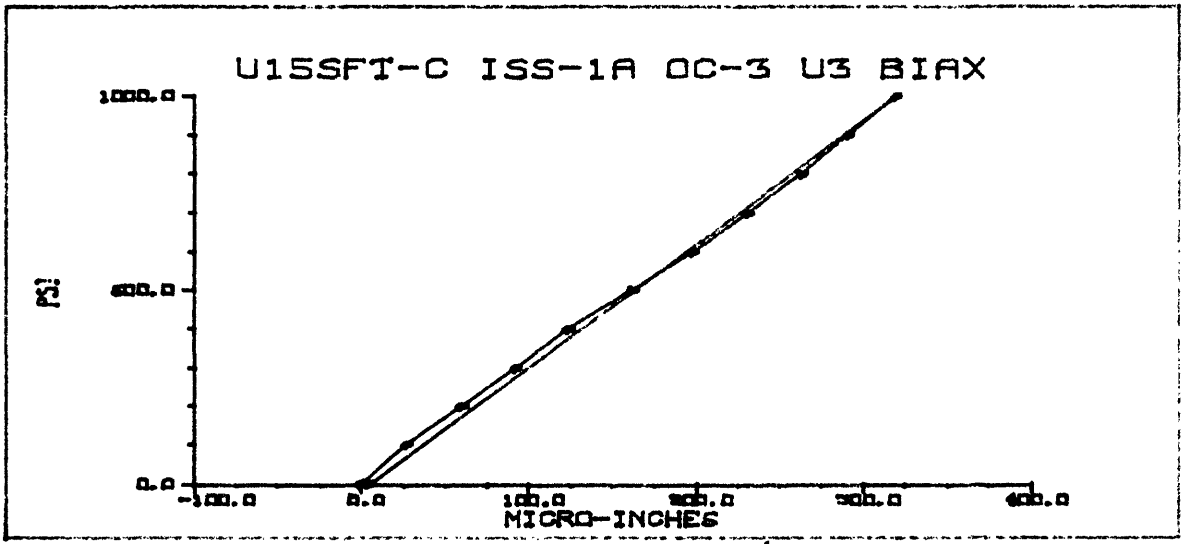
U15SFT-C ISS-1A OC-3 U3 BIAX
1000.0
500.0
0.0
PSI
-100.0
0.0
100.0
200.0
300.0
400.0
MICRO-INCHES

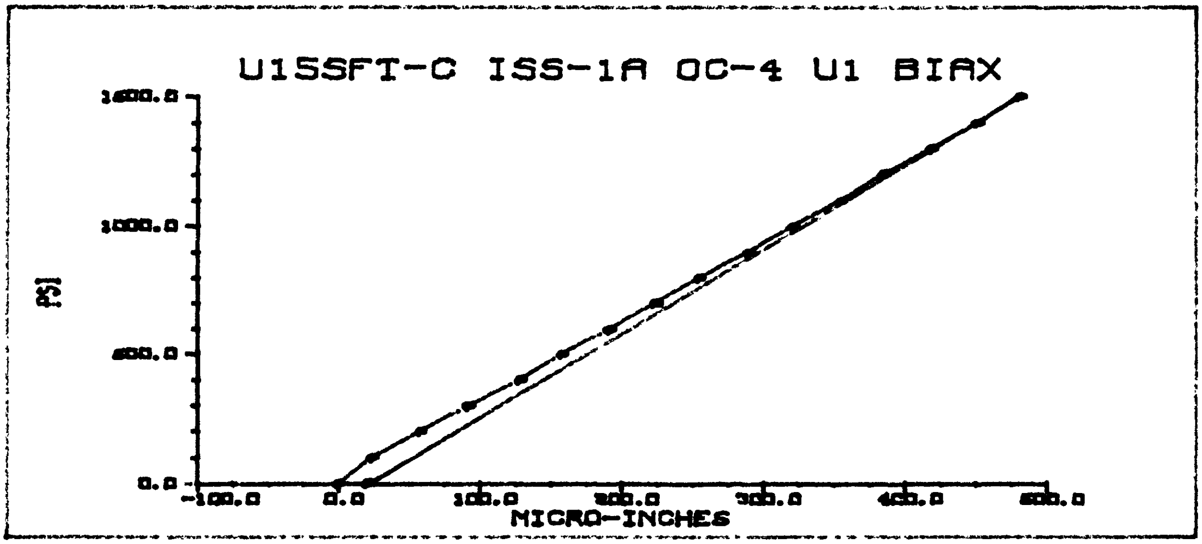
U1SSFT-C ISS-1A OC-4 U1 BIAX
PSI
MICRO-INCHES

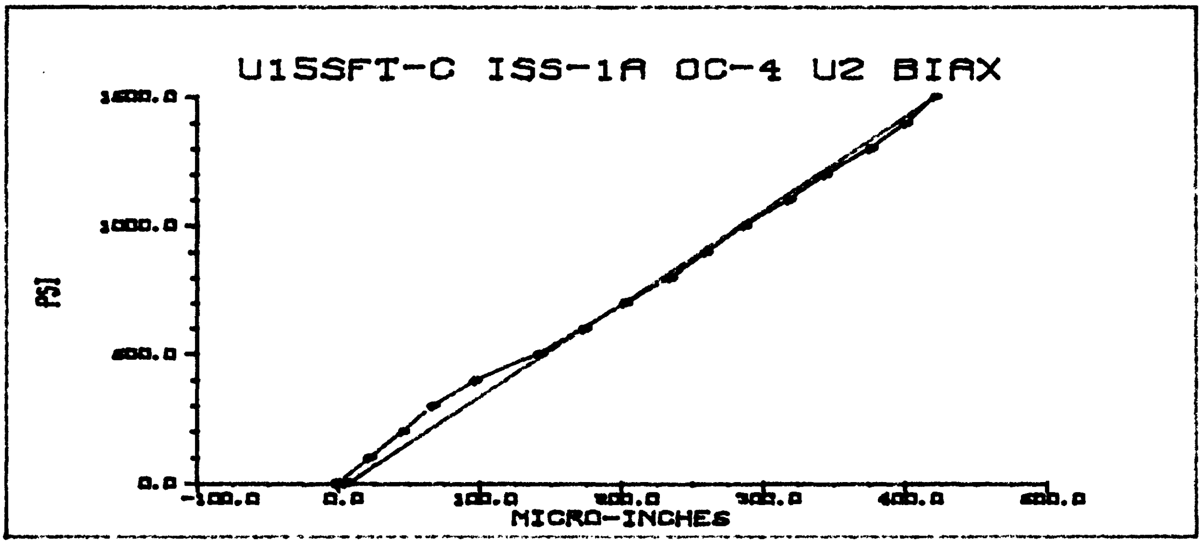
U1SSFT-C ISS-1A OC-4 U2 BIAX
PSI
MICRO-INCHES

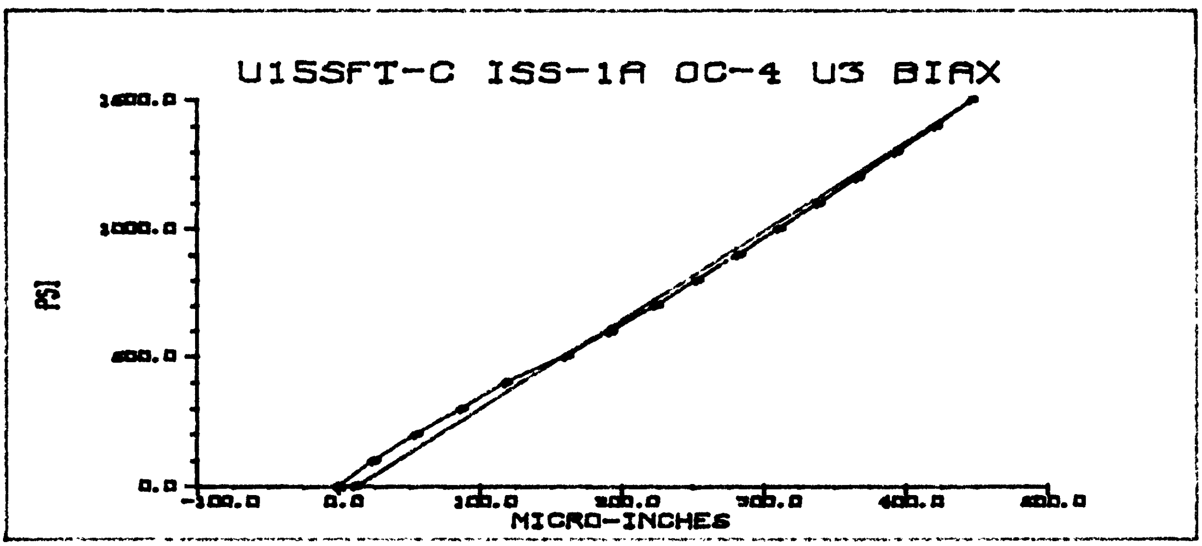
U1SSFT-C ISS-1A OC-4 U3 BIAX
PSI
MICRO-INCHES

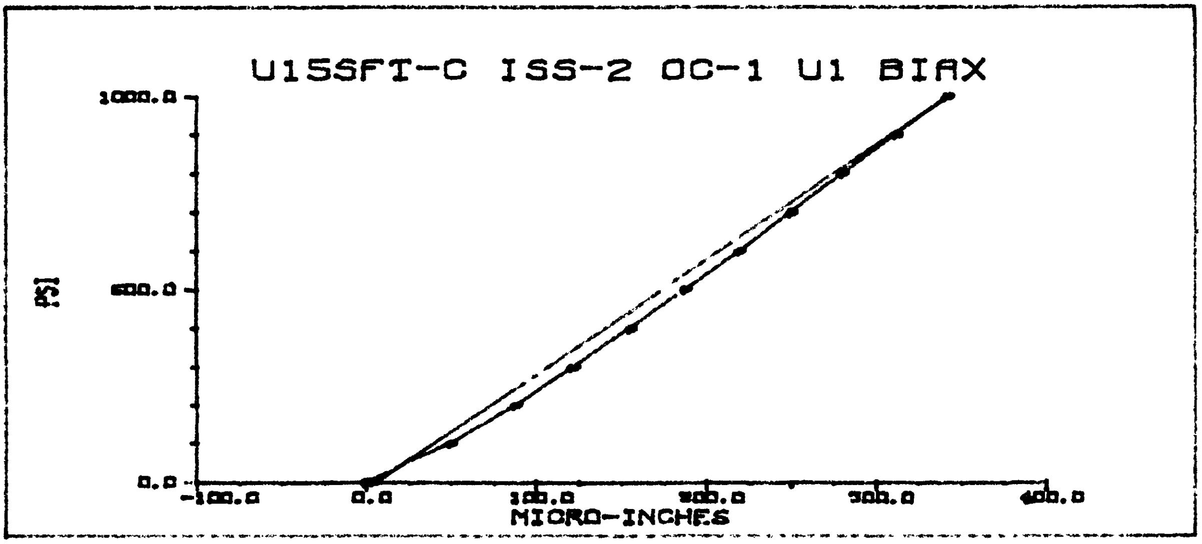
U15SFT-C ISS-2 OC-1 U1 BIAX
PSI
MICRO-INCHES

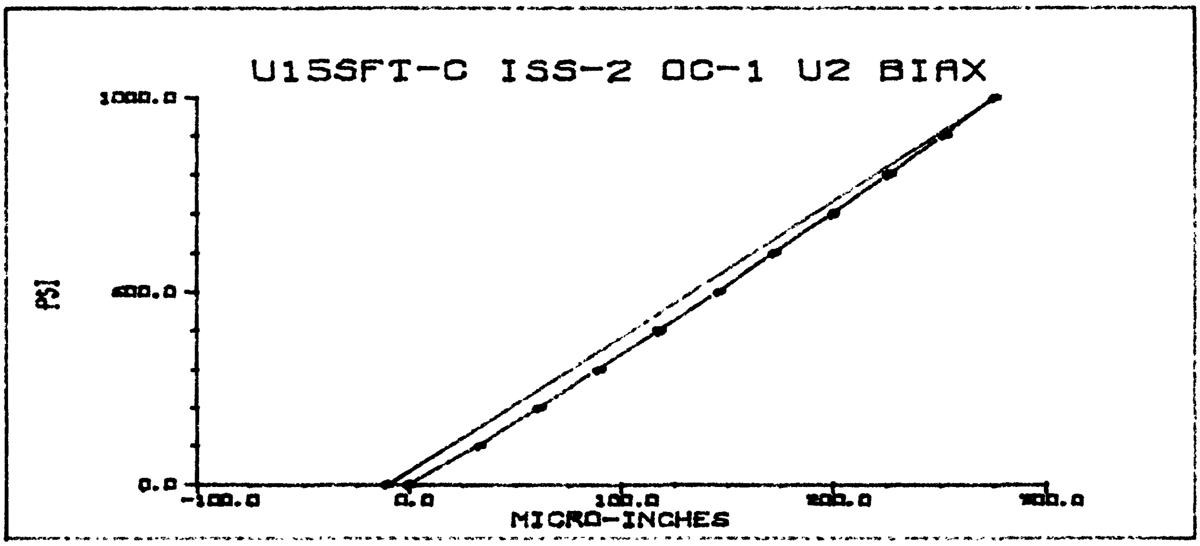
U15SFT-C ISS-2 OC-1 U2 BIAX
PSI
MICRO-INCHES

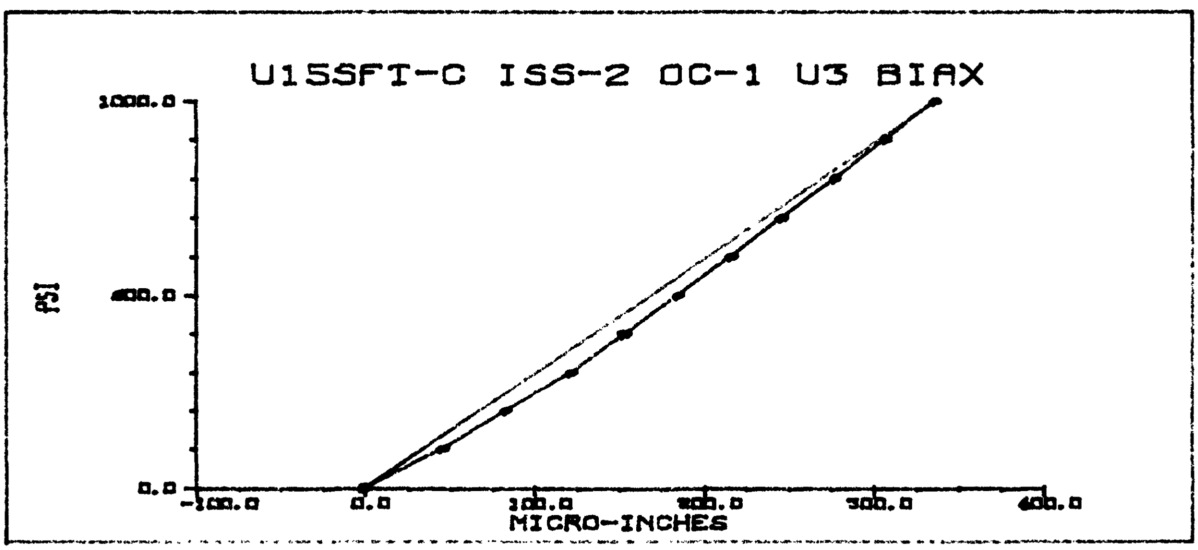
U15SFT-C ISS-2 OC-1 U3 BIAX
PSI
MICRO-INCHES

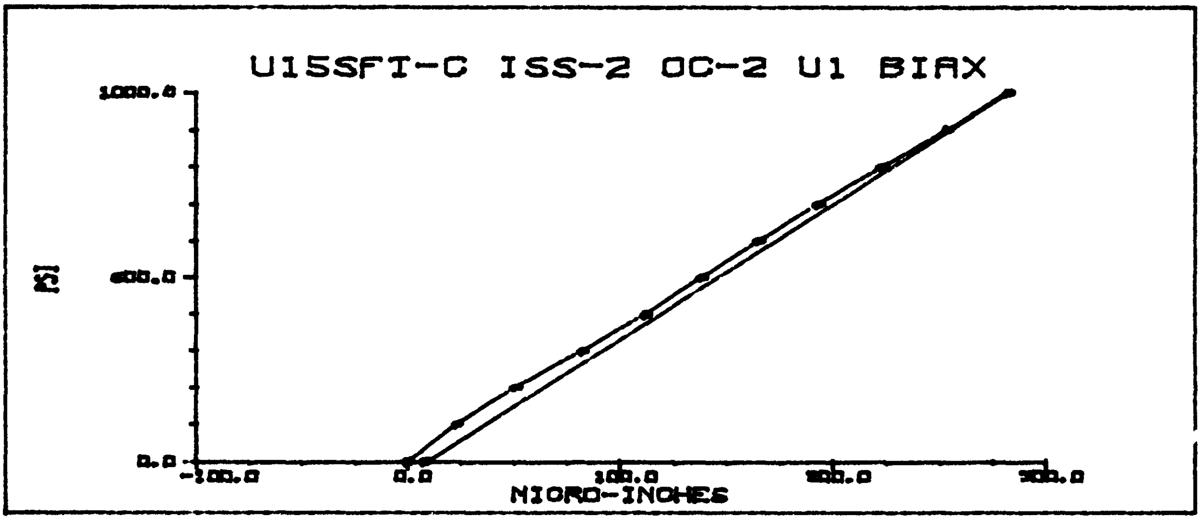
U15SFI-C ISS-2 OC-2 U1 BIAX
1000.0
0.0
-100.0
0.0
100.0
MICRO-INCHES

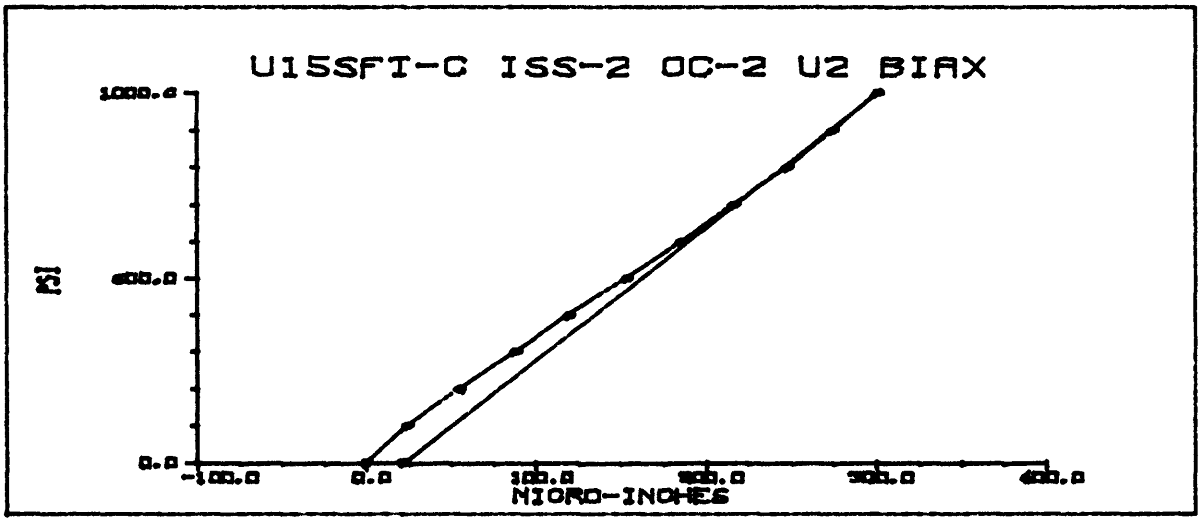
U15SFI-C ISS-2 OC-2 U2 BIAX
1000.0
0.0
-100.0
0.0
100.0
MICRO-INCHES

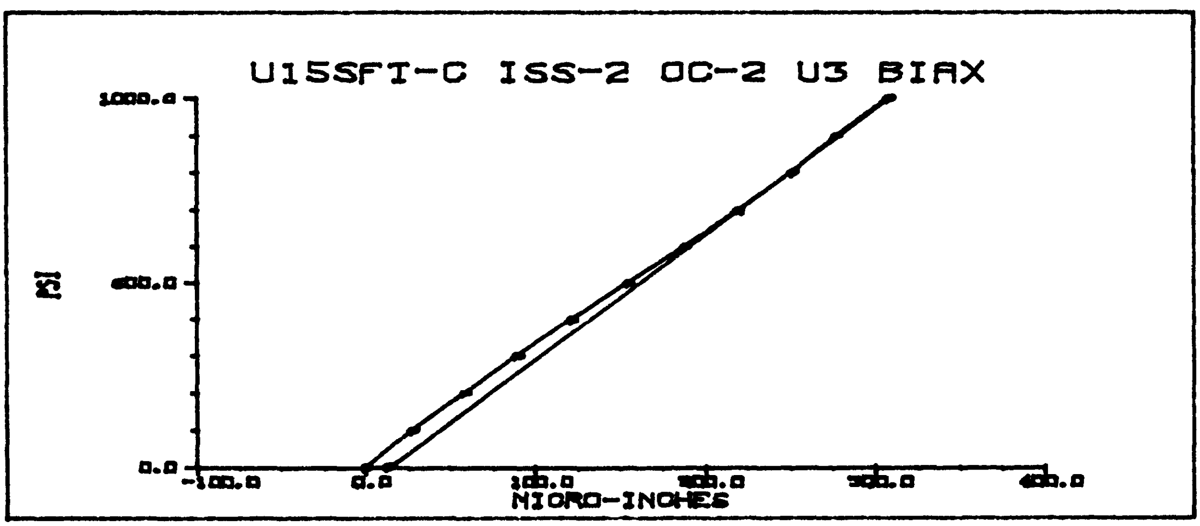
U15SFI-C ISS-2 OC-2 U3 BIAX
1000.0
0.0
-100.0
0.0
100.0
MICRO-INCHES

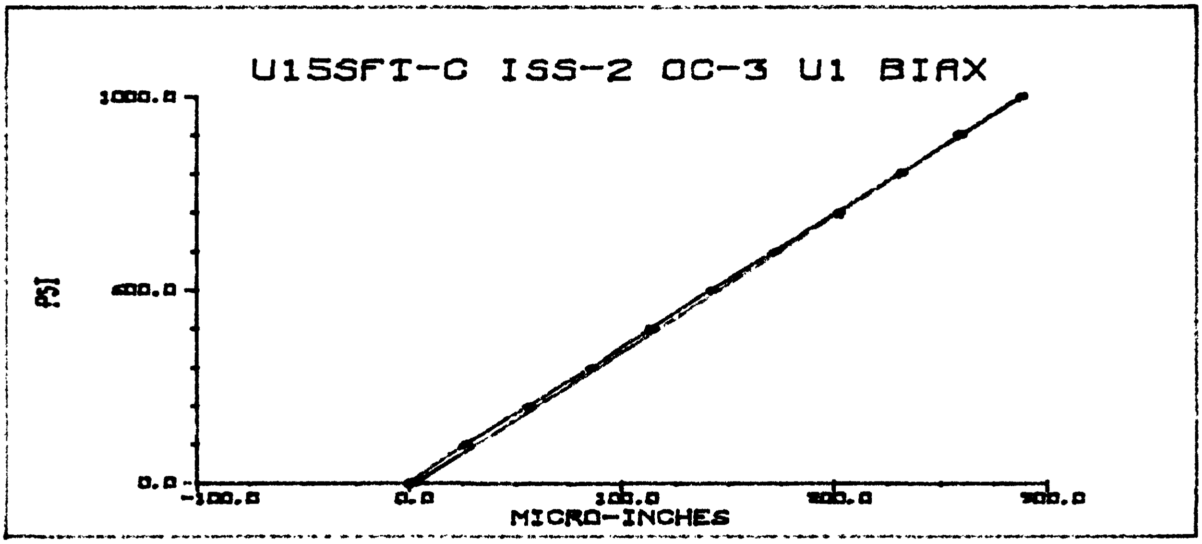
U15SFI-C ISS-2 OC-3 U1 BIAX
PSI
1000.0
500.0
0.0
-100.0
0.0
100.0
200.0
300.0
MICRO-INCHES

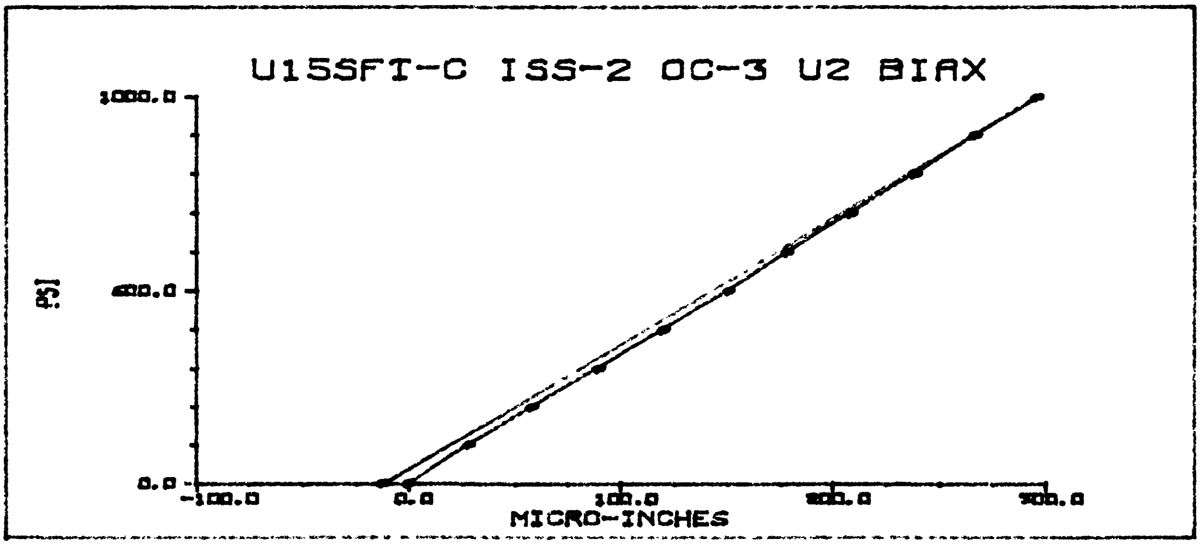
U15SFI-C ISS-2 OC-3 U2 BIAX
PSI
1000.0
500.0
0.0
-100.0
0.0
100.0
200.0
300.0
MICRO-INCHES

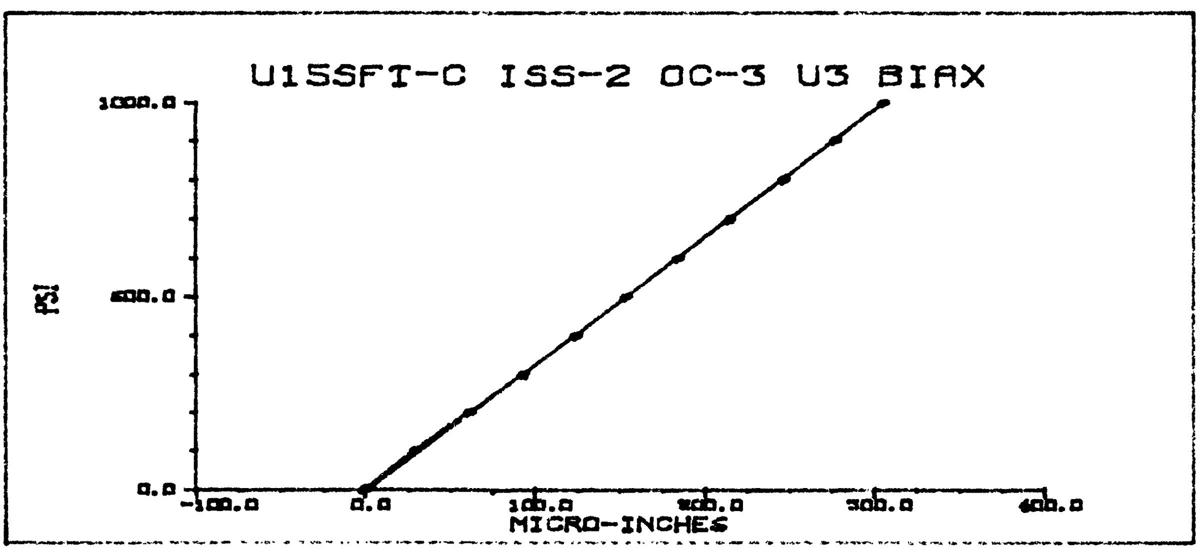
U15SFI-C ISS-2 OC-3 U3 BIAX
PSI
1000.0
500.0
0.0
-100.0
0.0
100.0
200.0
300.0
400.0
MICRO-INCHES

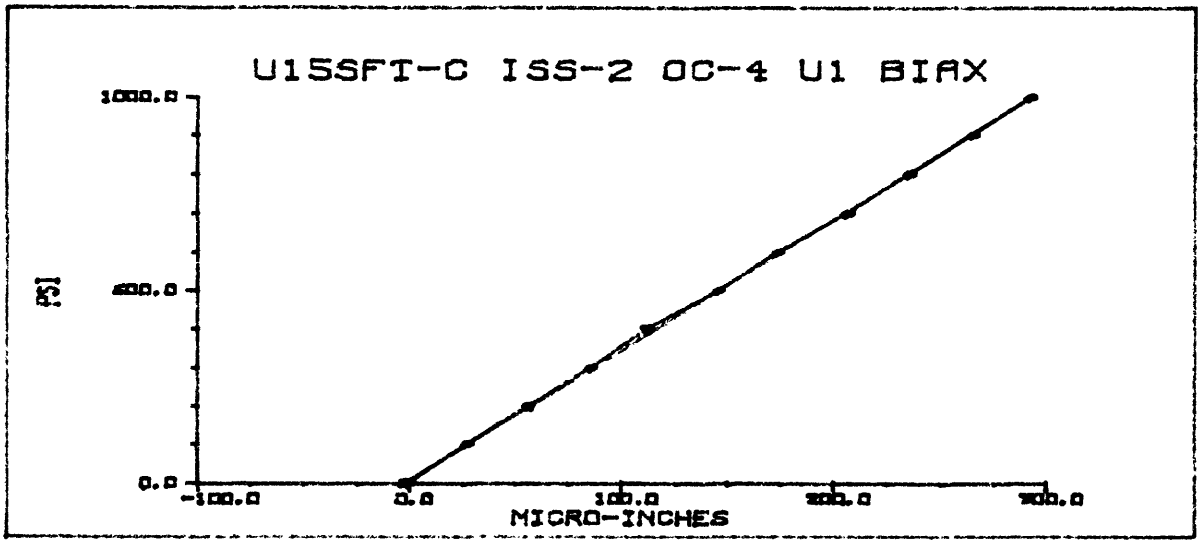
U15SFI-C ISS-2 OC-4 U1 BIAX
1000.0
500.0
0.0
PSI
-100.0
0.0
100.0
200.0
300.0
MICRO-INCHES

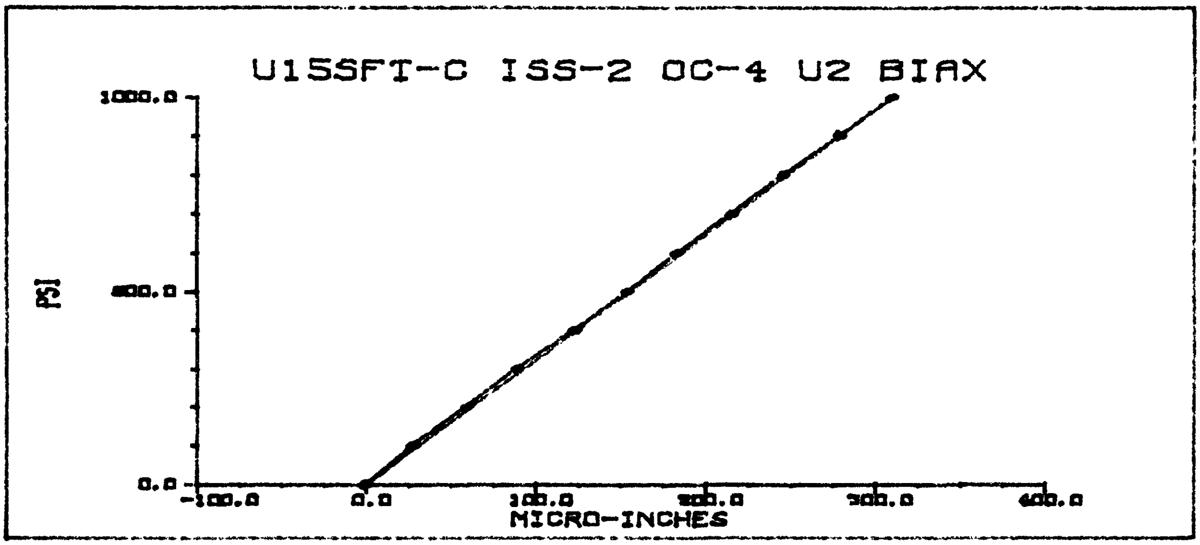
U15SFI-C ISS-2 OC-4 U2 BIAX
1000.0
500.0
0.0
PSI
-100.0
0.0
100.0
200.0
300.0
400.0
MICRO-INCHES

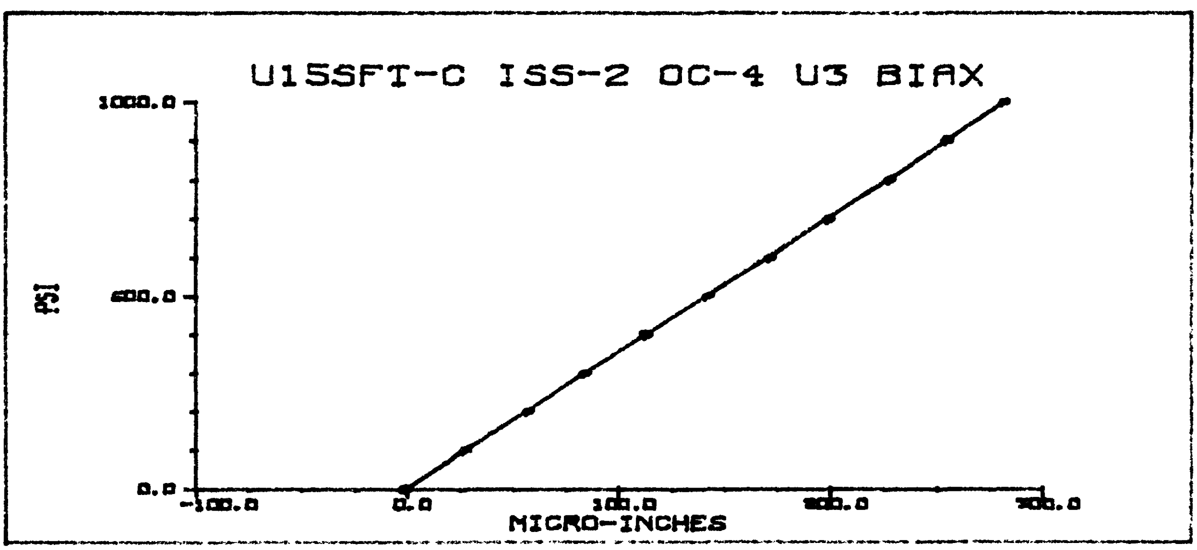
U15SFI-C ISS-2 OC-4 U3 BIAX
1000.0
500.0
0.0
PSI
-100.0
0.0
100.0
200.0
300.0
MICRO-INCHES

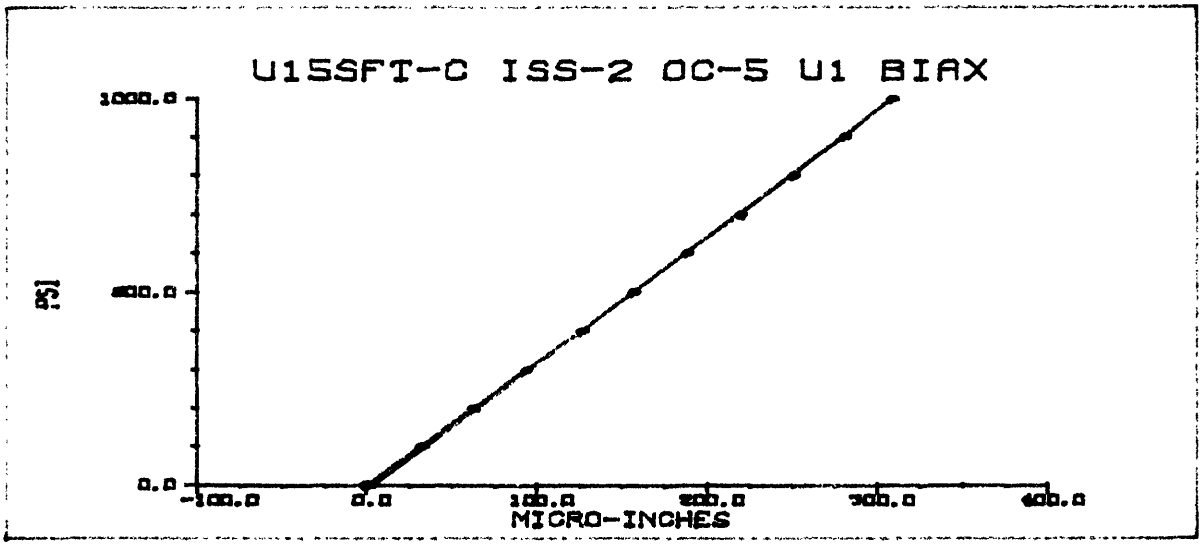
U15SFT-C ISS-2 OC-5 U1 BIAX
PSI
1000.0
500.0
0.0
-100.0
0.0
100.0
200.0
300.0
400.0
MICRO-INCHES

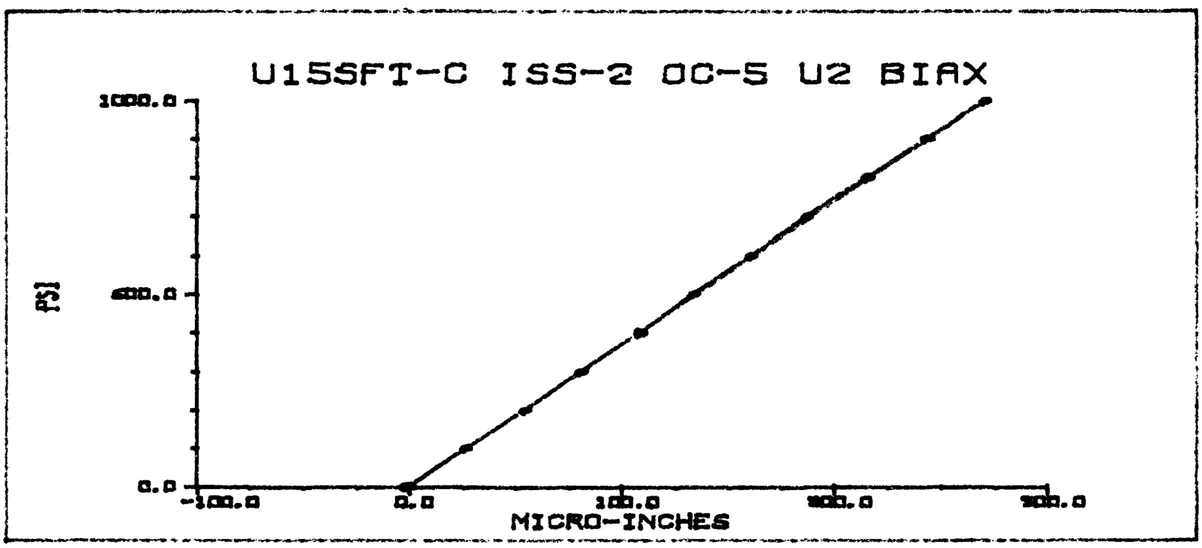
U15SFT-C ISS-2 OC-5 U2 BIAX
PSI
1000.0
500.0
0.0
-100.0
0.0
100.0
200.0
300.0
MICRO-INCHES

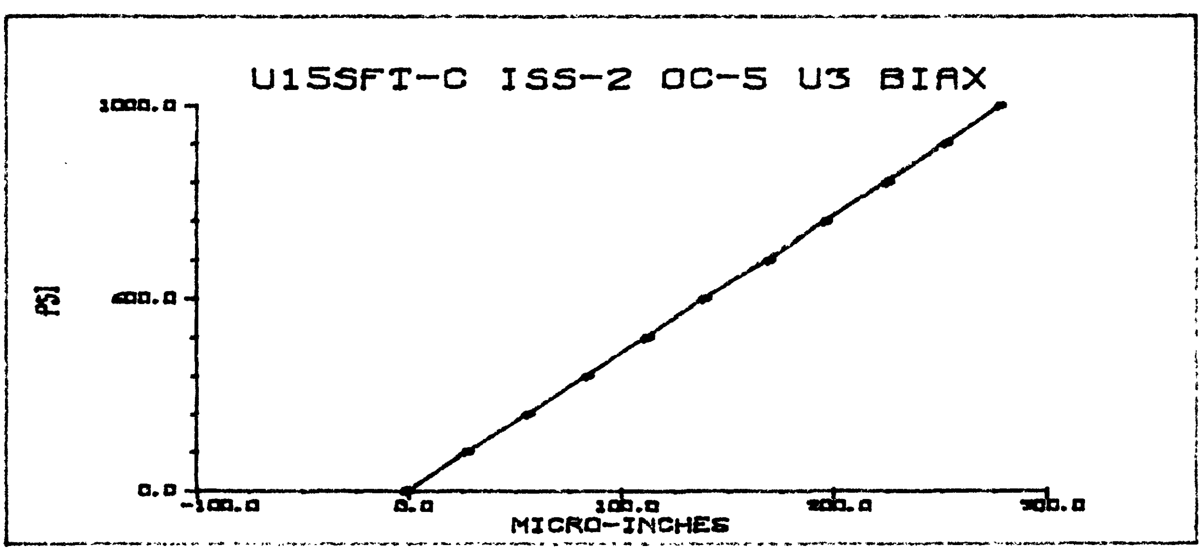
U15SFT-C ISS-2 OC-5 U3 BIAX
PSI
1000.0
500.0
0.0
-100.0
0.0
100.0
200.0
300.0
MICRO-INCHES

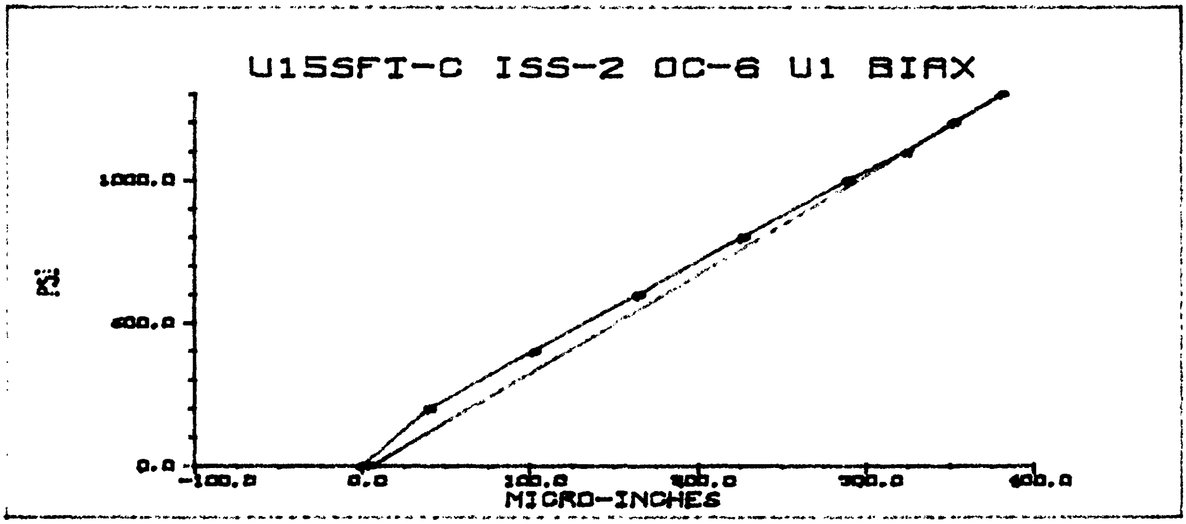
U15SFT-C ISS-2 OC-6 U1 BIAX
PSI
MICRO-INCHES
1000.0
600.0
0.0
-100.0
0.0
100.0
200.0
300.0
400.0

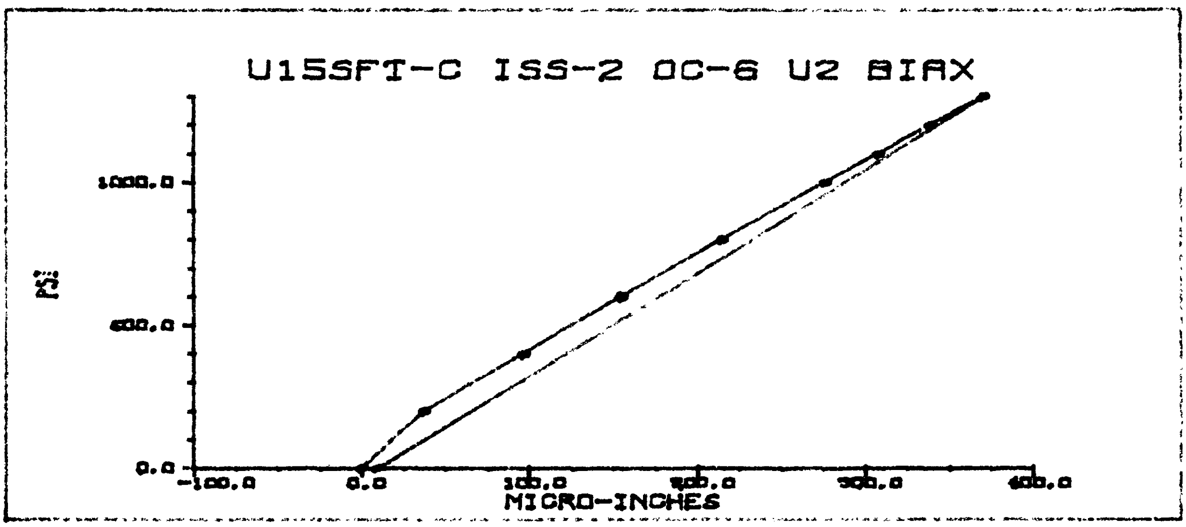
U15SFT-C ISS-2 OC-6 U2 BIAX
PSI
MICRO-INCHES
1000.0
600.0
0.0
-100.0
0.0
100.0
200.0
300.0
400.0

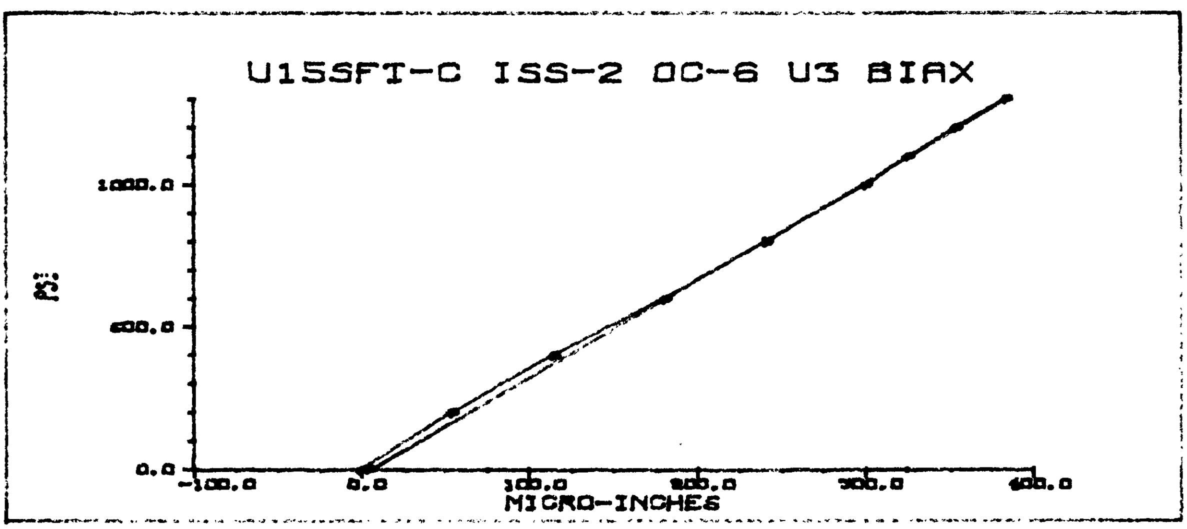
U15SFT-C ISS-2 OC-6 U3 BIAX
PSI
MICRO-INCHES
1000.0
600.0
0.0
-100.0
0.0
100.0
200.0
300.0
400.0

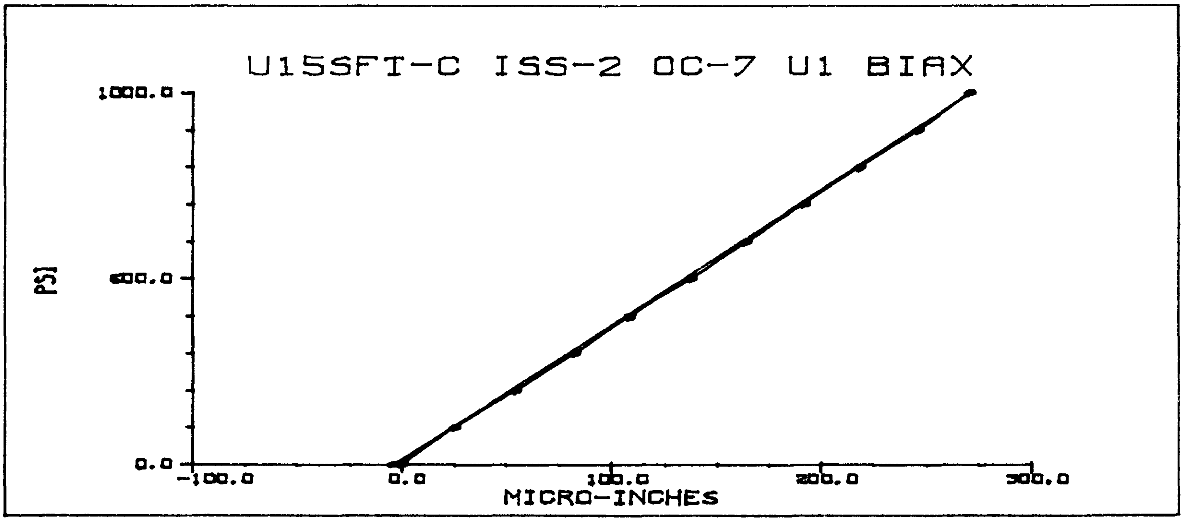
U15SFI-C ISS-2 OC-7 U1 BIAX
1000.0
500.0
0.0
PSI
-100.0
0.0
100.0
200.0
300.0
MICRO-INCHES

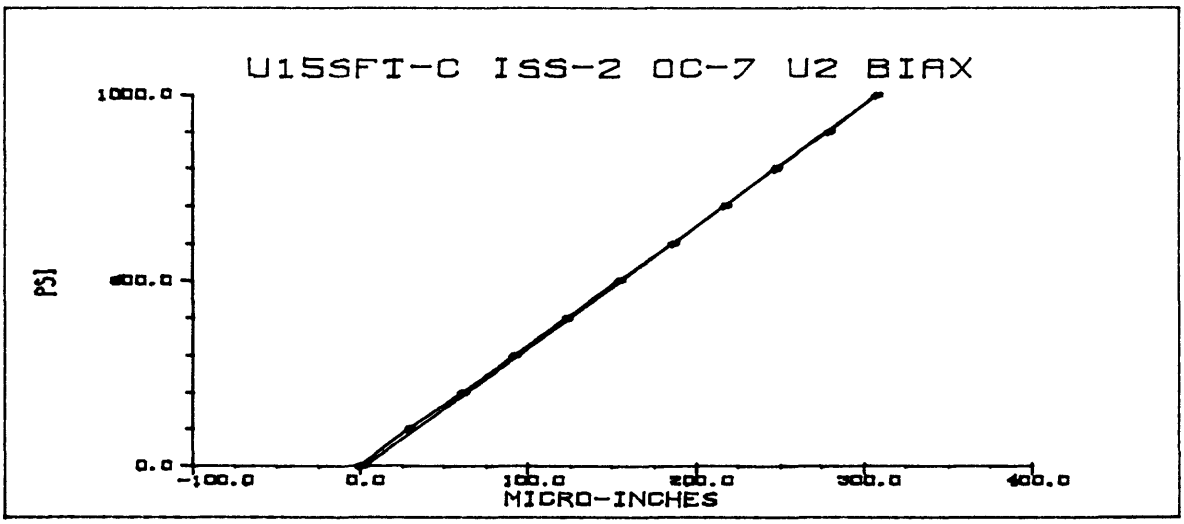
U15SFI-C ISS-2 OC-7 U2 BIAX
1000.0
500.0
0.0
PSI
-100.0
0.0
100.0
200.0
300.0
400.0
MICRO-INCHES

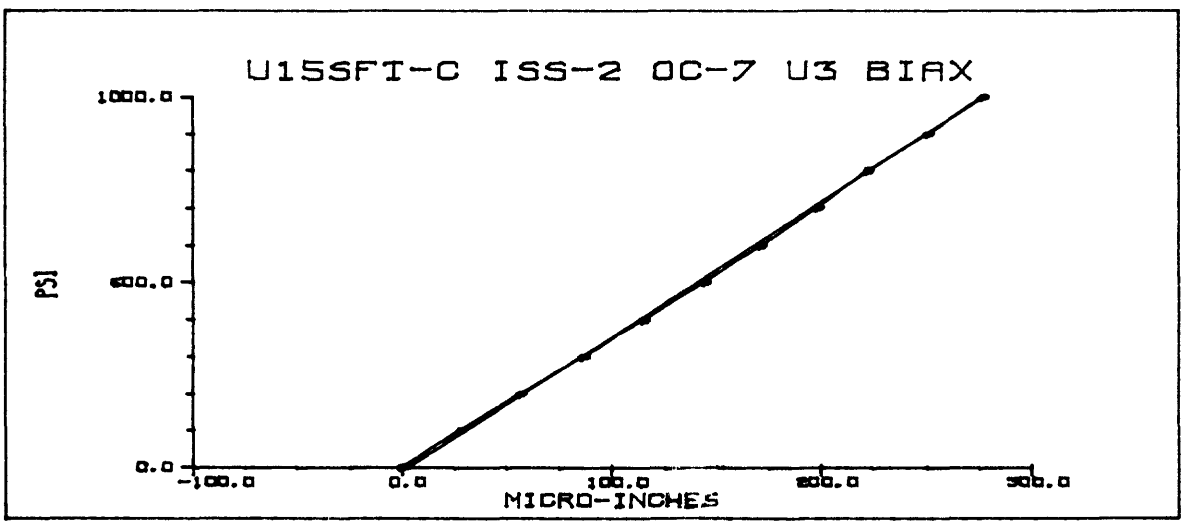
U15SFI-C ISS-2 OC-7 U3 BIAX
1000.0
500.0
0.0
PSI
-100.0
0.0
100.0
200.0
300.0
MICRO-INCHES

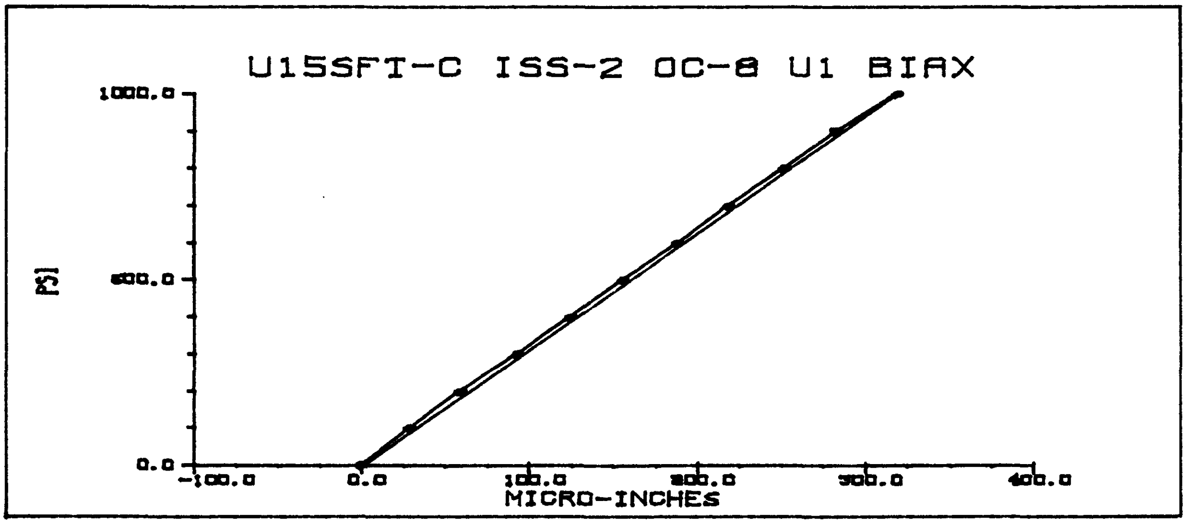
U15SFT-C ISS-2 OC-8 U1 BIAX
PSI
MICRO-INCHES

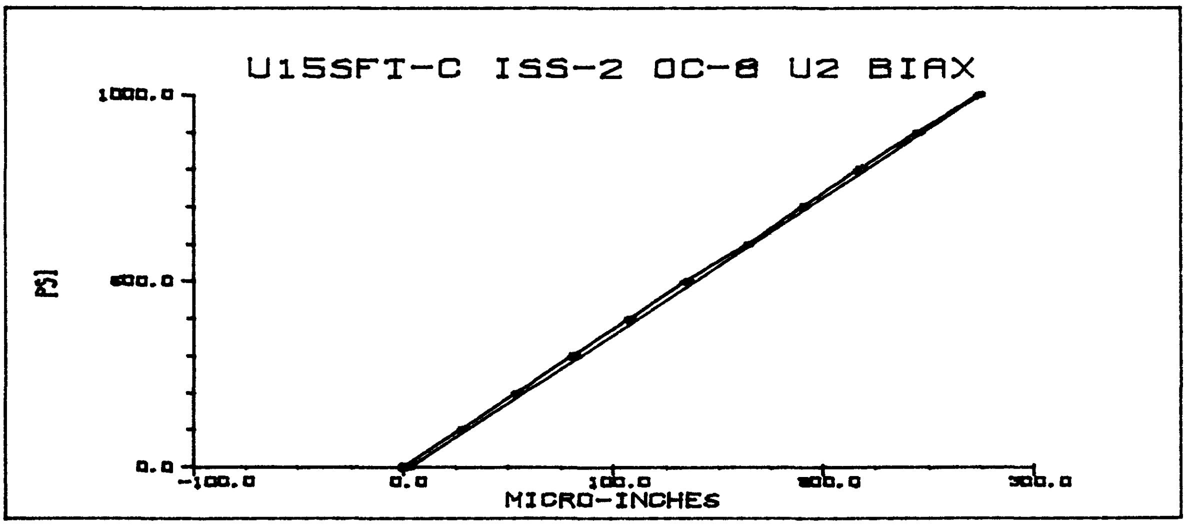
U15SFT-C ISS-2 OC-8 U2 BIAX
PSI
MICRO-INCHES

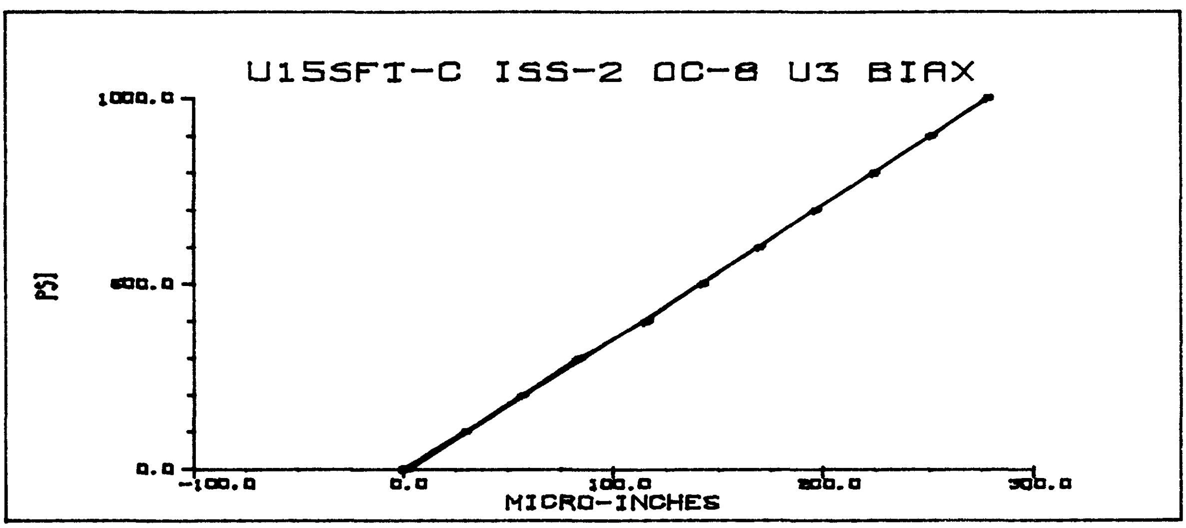
U15SFT-C ISS-2 OC-8 U3 BIAX
PSI
MICRO-INCHES

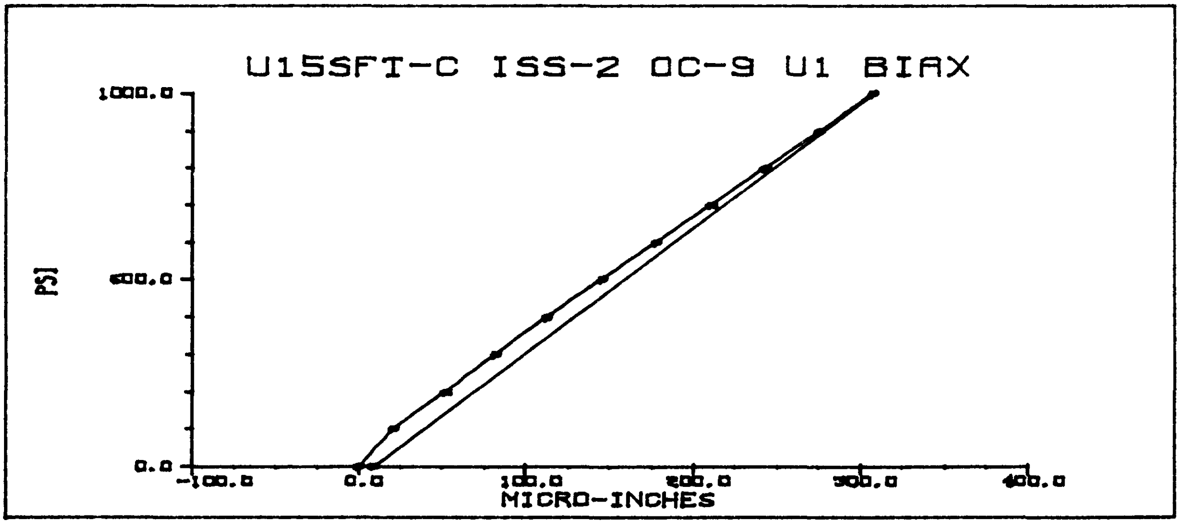
U15SFT-C ISS-2 OC-9 U1 BIAX
1000.0
500.0
0.0
PSI
-100.0
0.0
100.0
200.0
300.0
400.0
MICRO-INCHES

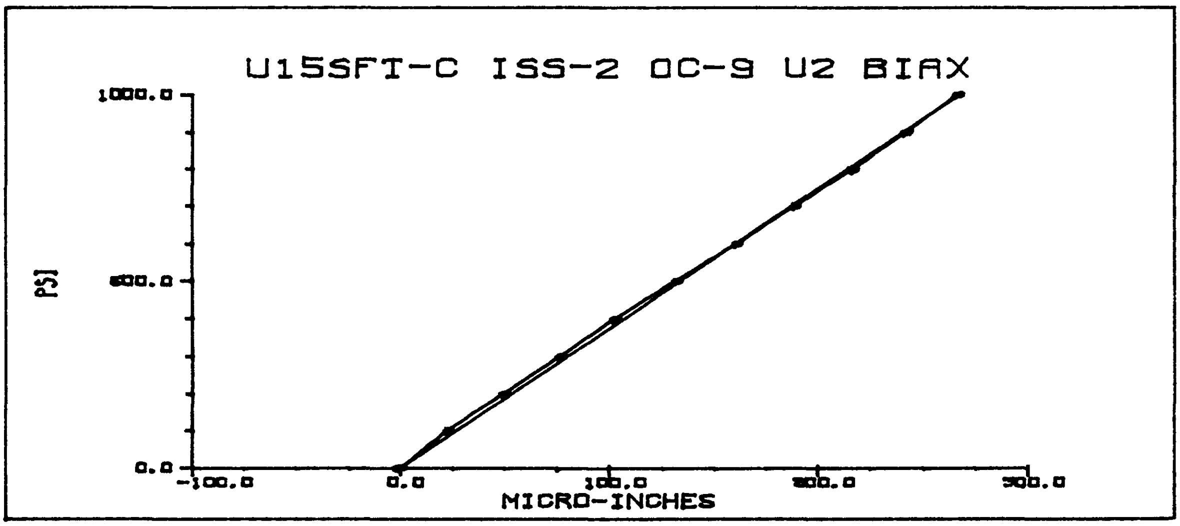
U15SFT-C ISS-2 OC-9 U2 BIAX
1000.0
500.0
0.0
PSI
-100.0
0.0
100.0
200.0
300.0
MICRO-INCHES

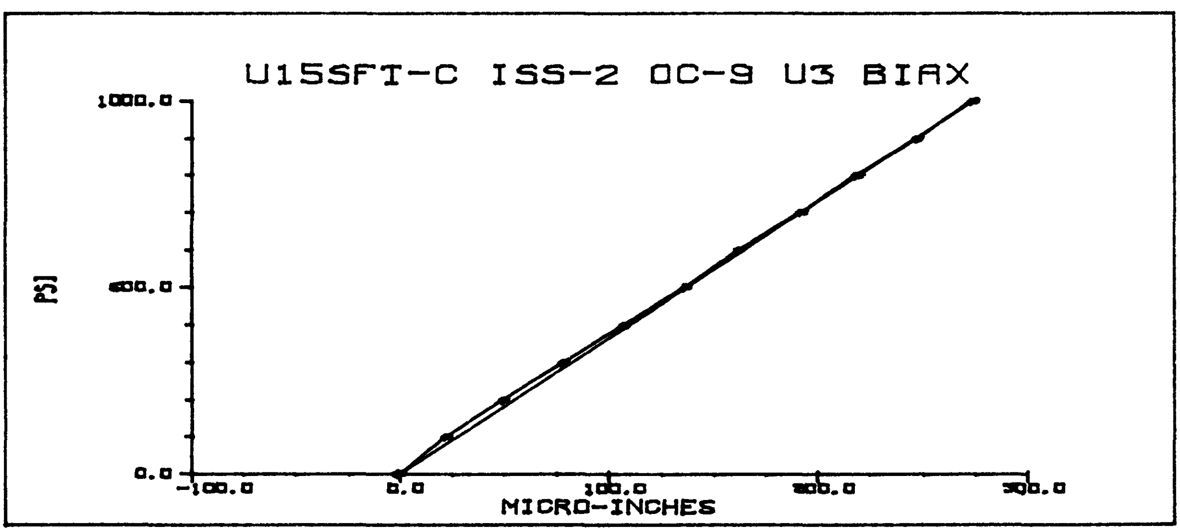
U15SFT-C ISS-2 OC-9 U3 BIAX
1000.0
500.0
0.0
PSI
-100.0
0.0
100.0
200.0
300.0
MICRO-INCHES

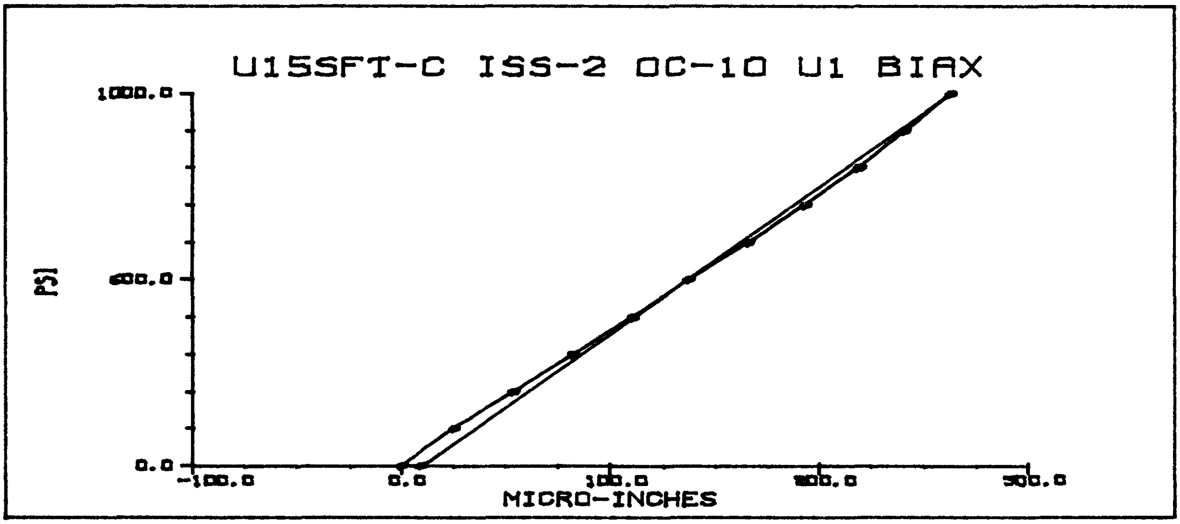
U15SFT-C ISS-2 OC-10 U1 BIAX
1000.0
500.0
0.0
PSI
-100.0
0.0
100.0
200.0
300.0
MICRO-INCHES

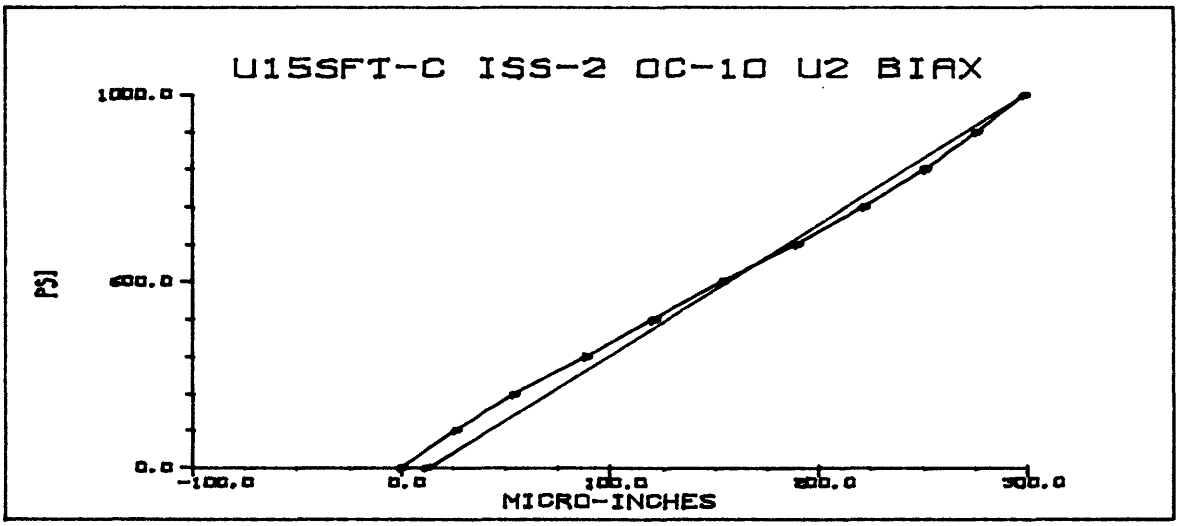
U15SFT-C ISS-2 OC-10 U2 BIAX
1000.0
500.0
0.0
PSI
-100.0
0.0
100.0
200.0
300.0
MICRO-INCHES

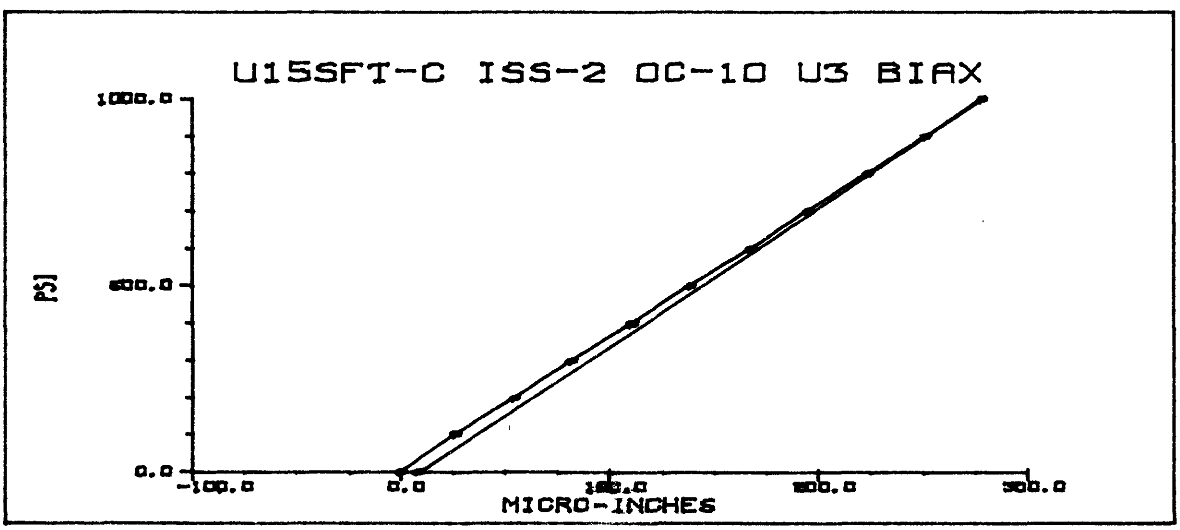
U15SFT-C ISS-2 OC-10 U3 BIAX
1000.0
500.0
0.0
PSI
-100.0
0.0
100.0
200.0
300.0
MICRO-INCHES

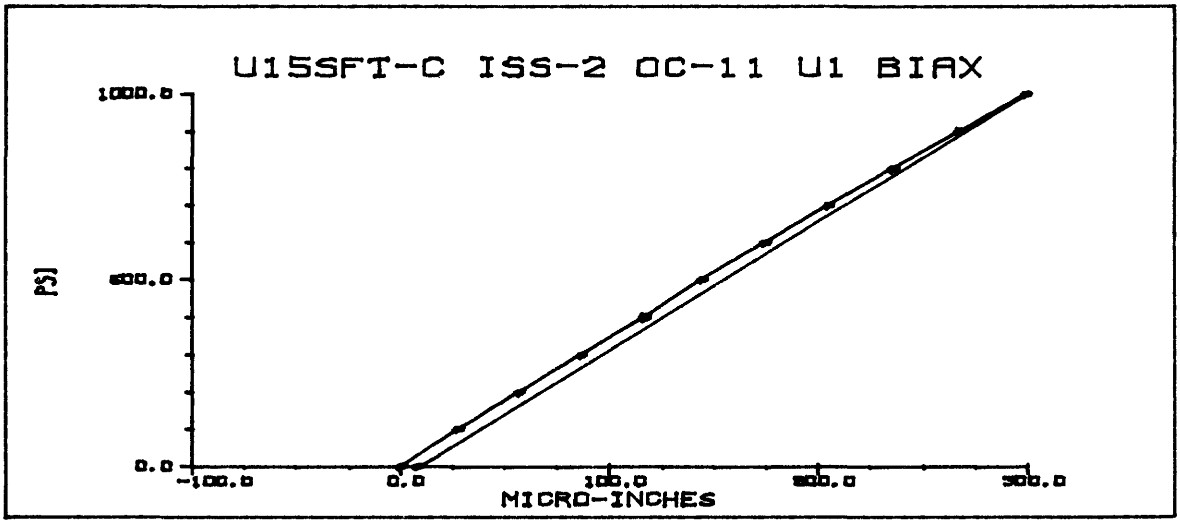
U15SFT-C ISS-2 OC-11 U1 BIAX
1000.0
500.0
0.0
PSI
-100.0
0.0
100.0
200.0
300.0
MICRO-INCHES

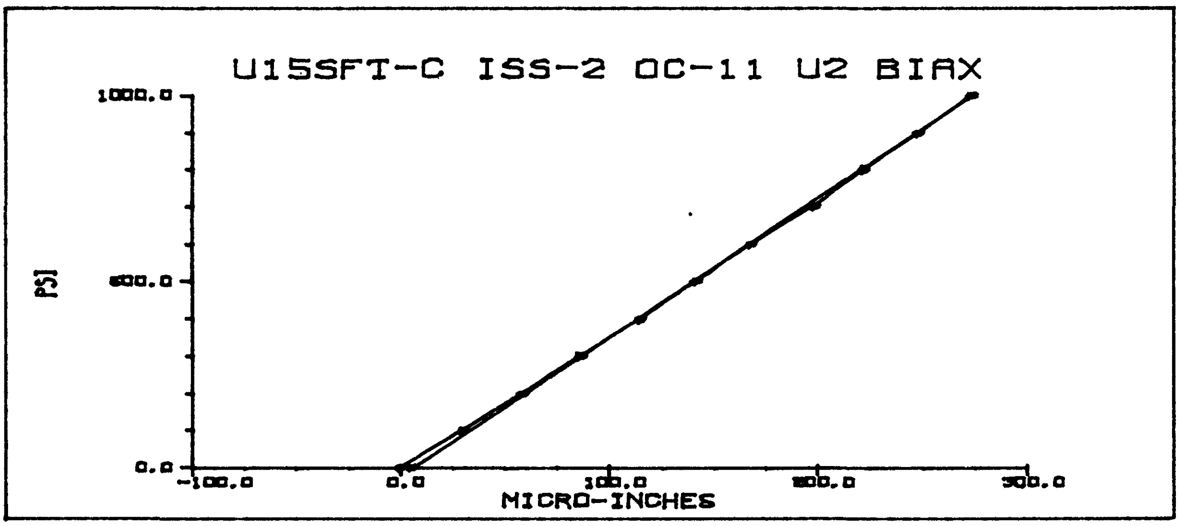
U15SFT-C ISS-2 OC-11 U2 BIAX
1000.0
500.0
0.0
PSI
-100.0
0.0
100.0
200.0
300.0
MICRO-INCHES

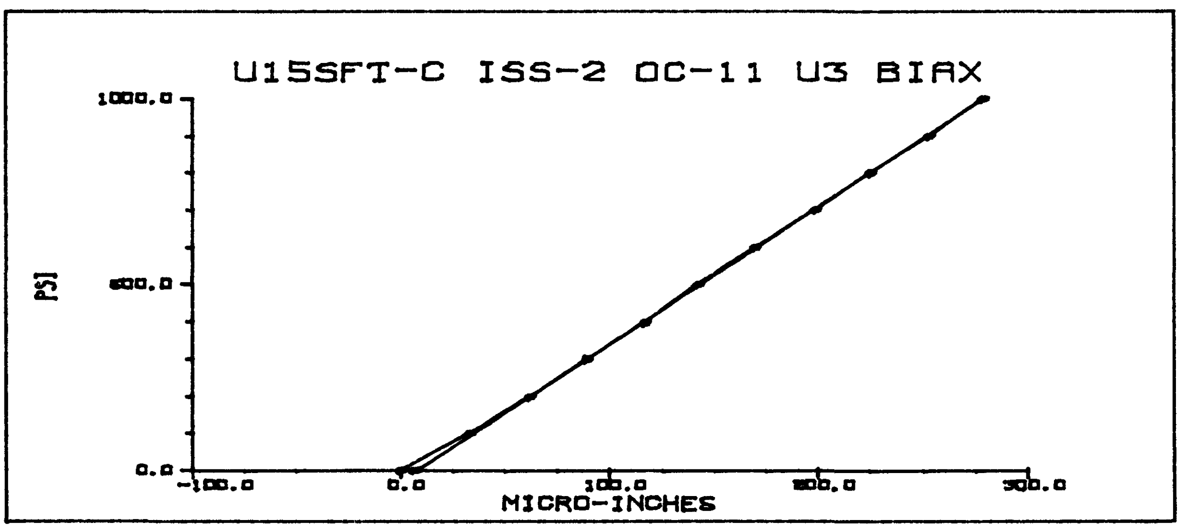
U15SFT-C ISS-2 OC-11 U3 BIAX
1000.0
500.0
0.0
PSI
-100.0
0.0
100.0
200.0
300.0
MICRO-INCHES

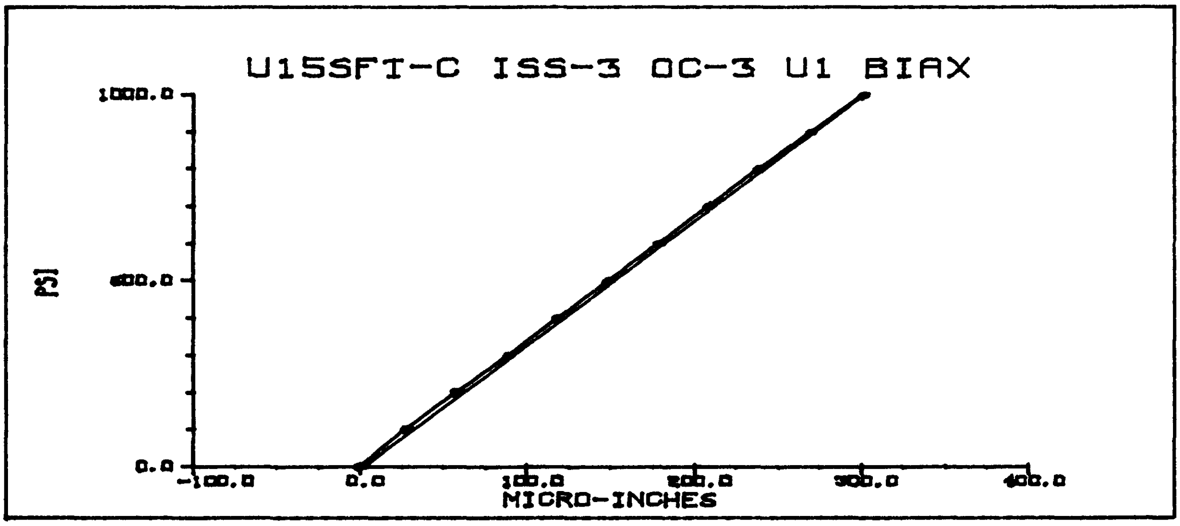
U15SFI-C ISS-3 OC-3 U1 BIAX
1000.0
500.0
0.0
PSI
-100.0
0.0
100.0
200.0
300.0
400.0
MICRO-INCHES

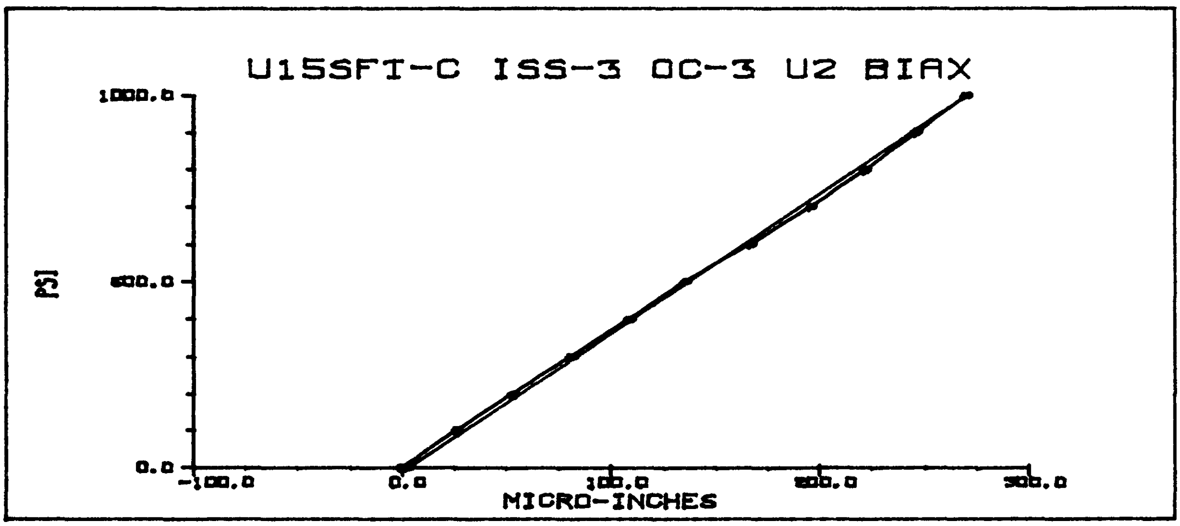
U15SFI-C ISS-3 OC-3 U2 BIAX
1000.0
500.0
0.0
PSI
-100.0
0.0
100.0
200.0
300.0
MICRO-INCHES

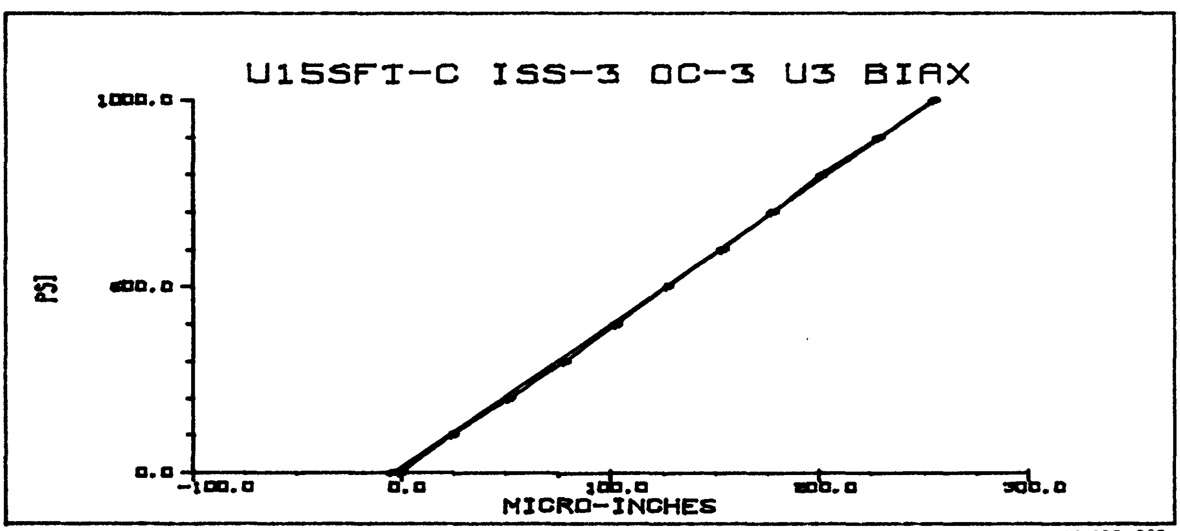
U15SFI-C ISS-3 OC-3 U3 BIAX
1000.0
500.0
0.0
PSI
-100.0
0.0
100.0
200.0
300.0
MICRO-INCHES